

**EVALUATION OF DAMPING CONTROLS OF A  
PERMANENT MAGNET SYNCHRONOUS  
GENERATOR WIND SYSTEM WITH STATCOM**

BY

**MIR SADAT ALI**

A Thesis Presented to the  
DEANSHIP OF GRADUATE STUDIES

**KING FAHD UNIVERSITY OF PETROLEUM & MINERALS**

DHAHRAN, SAUDI ARABIA

In Partial Fulfillment of the  
Requirements for the Degree of

**MASTER OF SCIENCE**

In

**ELECTRICAL ENGINEERING**

**APRIL 2012**

KING FAHD UNIVERSITY OF PETROLEUM AND MINERALS

DHAHRAN 31261, SAUDI ARABIA

DEANSHIP OF GRADUATE STUDIES

This thesis is written by MIR SADAT ALI under the direction of his Thesis Advisor and approved by his Thesis Committee members, has been presented to and accepted by the Dean of Graduate Studies, in partial fulfillment of the requirements for the degree of MASTER OF SCIENCE IN ELECTRICAL ENGINEERING.

Thesis Committee

A. H. Rahim

Dr. Abu Hamed M. Abdur-Rahim (Advisor)

Professor, EE Dept.

M. Kassas

Dr. Mahmood Kassas (Member)

Professor, EE Dept.

Z. Hamouz

Dr. Zakariya M. Al-Hamouz (Member)

Professor, EE Dept.

Ali Ahmad Al-Shaikhi  
8/9/12

Dr. Ali Ahmad Al-Shaikhi

Department Chairman

Salam A. Zummo  
8/9/12

Dr. Salam A. Zummo

Dean of Graduate Studies

8/9/12

Date



*Dedicated to*  
*My Father, Mother*  
*And*  
*My Brother,*

*(Whose Prayers and Perseverance*  
*led to this accomplishment)*

## ACKNOWLEDGEMENTS

*(IN THE NAME OF ALLAH, THE MOST COMPASSIONATE, THE MOST MERCIFUL)*

All praise and glory be to Almighty Allah who gave me the courage and patience to carry out this work and peace and blessings of Allah be upon his prophet Mohammed S.A.W.S.

I am deeply indebted to my thesis advisor Dr. Abu Hamed Abdur-Rahim for his constant support, guidance, encouragement and constructive criticism throughout the course of this research. I will always revere his patience, expert guidance and ability to solve intricate problems. At the later stages he helped me a lot in writing my thesis. I could not have imagined having a better advisor and mentor for my study.

I would also like to thank my committee members Dr. Mahmood Kassas and Dr. Zakariya M. Al-Hamouz for their co-operation and for spending their time reading my thesis and for their constructive comments and suggestions.

I would like to thank the electrical engineering department for being a great resource of knowledge and special thanks to Deanship of Graduate Studies for giving me this opportunity to fulfill my dream of graduating my masters from KFUPM. I would also like to thank all my friends in KFUPM, for always being very supportive and friendly.

I would like to thank my uncle Mr. Haqqani and my aunt Mrs. Tayyaba for their constant support, motivation and prayers during my master's program at KFUPM in Saudi Arabia.

Last but not the least; I would like to give my special thanks to my parents, brothers and friends for all their faith and confidence in me to pursue a Master's degree. Their love, knowledge and sacrifice have helped me achieve all my goals to date.

# TABLE OF CONTENTS

ACKNOWLEDGEMENTS .....	iv
TABLE OF CONTENTS.....	v
LIST OF FIGURES .....	viii
LIST OF TABLES.....	x
NOMENCLATURE .....	xi
ABBREVIATIONS .....	xiii
THESIS ABSTRACT (ENGLISH) .....	xiv
THESIS ABSTRACT (ARABIC) .....	xv
CHAPTER 1 .....	1
1.1 Renewables and Wind Energy .....	1
1.2 Wind Turbine Systems.....	2
1.2.1 Fixed Speed Concept .....	3
1.2.2 Variable Speed Fixed-Frequency Generators .....	5
1.3 Variable speed wind turbine PMSG control systems.....	7
1.4 Problem Statement .....	7
1.5 Thesis Objective.....	8
1.6 Thesis Organization.....	9
CHAPTER 2 .....	11
2.1 Wind Turbine Generators.....	11

2.2	Application of STATCOM in WECS .....	21
2.3	Control techniques of variable speed WT-PMSG system.....	22
CHAPTER 3 .....		25
3.1	The Wind Turbine and Wind System.....	26
3.2	The Variable Speed PMSG Model.....	29
3.3	Converter Models.....	33
3.4	The STATCOM Controller Model.....	37
3.5	Non Linear Model of the Composite System.....	40
3.6	Linearized Variable Speed PMSG System model.....	43
CHAPTER 4 .....		44
4.1	Small Signal Analysis .....	44
4.2	Evaluation of Damping Controls.....	48
4.2.1	Singular Value Decomposition.....	48
4.2.2	Hankel Singular Value Decomposition .....	52
4.2.3	Residue Method: .....	54
4.3	Stabilizing Controller Design.....	57
4.3.1	Pole Placement technique .....	60
4.3.2	PID Controller Design using Pole Placement technique .....	61
CHAPTER 5 .....		65
5.1	Simulation studies for a disturbance (15% torque pulse) on wind turbine .....	68

5.1.1	STATCOM connected at gen. side-converter using feedback control .....	68
5.1.2	STATCOM connected at grid side-converter using feedback control.....	72
5.2	Robustness of variable speed WT-PMSG system using feedback control .....	77
5.2.1	For 45% loading with / without STATCOM .....	78
5.2.2	For 85% loading with / without STATCOM .....	82
5.2.3	For change in STATCOM parameters.....	87
5.3	Simulation studies with disturbance (symmetrical 3 $\Phi$ fault) on grid bus .....	93
5.4	Simulation studies with disturbance (symmetrical 3 $\Phi$ fault) on load bus .....	98
CHAPTER 6 .....		104
6.1	Conclusion.....	104
6.2	Future Work .....	105
APPENDIX A.....		106
APPENDIX B .....		107
APPENDIX C .....		110
APPENDIX D.....		114
APPENDIX E .....		121
REFERENCES .....		129
VITAE.....		137

# LIST OF FIGURES

FIGURE 1.1 STRUCTURE OF FIXED SPEED WIND TURBINE. ....	4
FIGURE 2.1 STRUCTURES OF THE VARIABLE SPEED WIND TURBINE SYSTEMS .....	15
FIGURE 3.1 SCHEMATIC OF VARIABLE SPEED WT-PMSG CONNECTED TO GRID.....	25
FIGURE 3.2 POWER COEFFICIENT VS. TIP SPEED RATIO FOR DIFFERENT WIND SPEEDS.....	27
FIGURE 3.3 POWER OUTPUT VS. TURBINE SPEED CHARACTERISTICS OF A WIND TURBINE .....	28
FIGURE 3.4 POWER OUTPUT VS. TURBINE SPEED CHARACTERISTICS FOR WIND SPEED OF 11.95M/SEC .....	29
FIGURE 3.5 EQUIVALENT CIRCUIT OF PMSG .....	30
FIGURE 3.6 EQUIVALENT CIRCUIT OF PMSG IN D-Q AXES.....	31
FIGURE 3.7DRIVE TRAIN MODEL OF A TWO MASS SYSTEM .....	32
FIGURE 3.8 VARIABLE SPEED WT-PMSG CONNECTED TO GRID .....	33
FIGURE 3.9 PHASOR DIAGRAM OF PMSG.....	34
FIGURE 3.10 BASIC MODEL OF THE STATCOM CONTROLLER .....	38
FIGURE 3.11 VARIABLE SPEED WT-PMSG WITH STATCOM ON GENERATOR SIDE-CONVERTER .....	40
FIGURE 3.12 VARIABLE SPEED WT-PMSG WITH STATCOM ON GRID SIDE-CONVERTER.....	42
FIGURE 4.1 DOMINANT EIGEN VALUES OF VARIABLE SPEED PMSG SYSTEM FOR CASE (A), (B) & (C).....	47
FIGURE 4.2 MINIMUM SINGULAR VALUES FOR VARIOUS CONTROLS AS A FUNCTION OF GENERATOR OUTPUT, WHEN STATCOM IS CONNECTED AT GENERATOR SIDE-CONVERTER.....	50
FIGURE 4.3 MINIMUM SINGULAR VALUES FOR VARIOUS CONTROLS AS A FUNCTION OF GENERATOR OUTPUT, WHEN STATCOM IS CONNECTED AT GRID SIDE-CONVERTER .....	51
FIGURE 4.4 HANKEL SINGULAR VALUE INDICES FOR THE 5 CONVERTER CONTROLS WITH $\Delta\Omega_G$ AS OUTPUT WHEN STATCOM IS CONNECTED AT GENERATOR SIDE-CONVERTER.....	53
FIGURE 4.5 HANKEL SINGULAR VALUE INDICES FOR THE 5 CONVERTER CONTROLS WITH $\Delta\Omega_G$ AS OUTPUT WHEN STATCOM IS CONNECTED AT GRID SIDE-CONVERTER .....	54
FIGURE 4.6 LOCATION OF CONTROLLER IN THE PLANT .....	55
FIGURE 4.7 RESIDUES WHEN $\Delta\Omega_G$ IS TAKEN AS PLANT OUTPUT, WITH STATCOM ON GENERATOR SIDE-CONVERTER .....	56
FIGURE 4.8 RESIDUES WHEN $\Delta\Omega_G$ IS TAKEN AS PLANT OUTPUT, WITH STATCOM ON GRID SIDE-CONVERTER.....	57
FIGURE 4.9 FEEDBACK CONTROL SYSTEM .....	58
FIGURE 4.10 FEEDBACK CONTROL WITH PID CONTROLLER .....	61
FIGURE 5.1 TERMINAL VOLTAGE OF VARIABLE SPEED WIND TURBINE PMSG WITH AND WITHOUT STATCOM. ....	65
FIGURE 5.2 GENERATOR SPEED VARIATION FOR VARIABLE SPEED WIND TURBINE PMSG WITH & WITHOUT STATCOM.....	66
FIGURE 5.3 POWER ANGLE OF THE VARIABLE SPEED WIND TURBINE PMSG WITH AND WITHOUT STATCOM. ....	67
FIGURE 5.4 TERMINAL VOLTAGE OF VARIABLE SPEED WIND TURBINE PMSG SYSTEM WITH $\psi_{ST}$ CONTROL .....	69
FIGURE 5.5 STATCOM CONVERTER VOLTAGE OF VARIABLE SPEED WIND TURBINE PMSG SYSTEM WITH $\psi_{ST}$ CONTROL .....	69
FIGURE 5.6 STATCOM CURRENT OF VARIABLE SPEED WIND TURBINE PMSG SYSTEM WITH $\psi_{ST}$ CONTROL.....	70
FIGURE 5.7 INVERTER OUTPUT CURRENT OF VARIABLE SPEED WIND TURBINE PMSG SYSTEM WITH $\psi_{ST}$ CONTROL .....	70
FIGURE 5.8 CONVERTER DC VOLTAGE OF VARIABLE SPEED WIND TURBINE PMSG SYSTEM WITH $\psi_{ST}$ CONTROL.....	71
FIGURE 5.9 GENERATOR SPEED VARIATIONS OF VARIABLE SPEED WIND TURBINE PMSG SYSTEM WITH $\psi_{ST}$ CONTROL.....	71
FIGURE 5.10 POWER ANGLE OF VARIABLE SPEED WIND TURBINE PMSG SYSTEM WITH $\psi_{ST}$ CONTROL .....	72
FIGURE 5.11 TERMINAL VOLTAGE OF VARIABLE SPEED WIND TURBINE PMSG SYSTEM WITH $M_1$ CONTROL .....	73
FIGURE 5.12 STATCOM CONVERTER VOLTAGE OF VARIABLE SPEED WIND TURBINE PMSG SYSTEM WITH $M_1$ CONTROL .....	74
FIGURE 5.13 STATCOM CURRENT OF VARIABLE SPEED WIND TURBINE PMSG SYSTEM WITH $M_1$ CONTROL.....	74
FIGURE 5.14 INVERTER OUTPUT CURRENT OF VARIABLE SPEED WIND TURBINE PMSG SYSTEM WITH $M_1$ CONTROL .....	75
FIGURE 5.15 CONVERTER DC VOLTAGE OF VARIABLE SPEED WIND TURBINE PMSG SYSTEM WITH $M_1$ CONTROL.....	75
FIGURE 5.16 GENERATOR SPEED VARIATIONS OF VARIABLE SPEED WIND TURBINE PMSG SYSTEM WITH $M_1$ CONTROL.....	76
FIGURE 5.17 POWER ANGLE OF VARIABLE SPEED WIND TURBINE PMSG SYSTEM WITH $M_1$ CONTROL .....	77
FIGURE 5.18 TERMINAL VOLTAGE OF VARIABLE SPEED WIND TURBINE PMSG SYSTEM AT 45% LOADING .....	79
FIGURE 5.19 STATCOM CONVERTER VOLTAGE OF VARIABLE SPEED WIND TURBINE PMSG SYSTEM AT 45% LOADING .....	79
FIGURE 5.20 STATCOM CURRENT OF VARIABLE SPEED WIND TURBINE PMSG SYSTEM AT 45% LOADING .....	80
FIGURE 5.21 INVERTER OUTPUT CURRENT OF VARIABLE SPEED WIND TURBINE PMSG SYSTEM AT 45% LOADING.....	80
FIGURE 5.22 DC LINK VOLTAGE OF VARIABLE SPEED WIND TURBINE PMSG SYSTEM AT 45% LOADING .....	81



FIGURE 5.23 GENERATOR SPEED VARIATION OF VARIABLE SPEED WIND TURBINE PMSG SYSTEM AT 45% LOADING .....	81
FIGURE 5.24 POWER ANGLE VARIATION OF VARIABLE SPEED WIND TURBINE PMSG SYSTEM AT 45% LOADING .....	82
FIGURE 5.25 TERMINAL VOLTAGE OF VARIABLE SPEED WIND TURBINE PMSG SYSTEM AT 85% LOADING .....	83
FIGURE 5.26 STATCOM CONVERTER VOLTAGE OF VARIABLE SPEED WIND TURBINE PMSG SYSTEM AT 85% LOADING .....	84
FIGURE 5.27 STATCOM CURRENT OF VARIABLE SPEED WIND TURBINE PMSG SYSTEM AT 85% LOADING .....	84
FIGURE 5.28 INVERTER OUTPUT CURRENT OF VARIABLE SPEED WIND TURBINE PMSG SYSTEM AT 85% LOADING.....	85
FIGURE 5.29 DC LINK VOLTAGE OF VARIABLE SPEED WIND TURBINE PMSG SYSTEM AT 85% LOADING .....	85
FIGURE 5.30 GENERATOR SPEED VARIATION OF VARIABLE SPEED WIND TURBINE PMSG SYSTEM AT 85% LOADING.....	86
FIGURE 5.31 POWER ANGLE VARIATION OF VARIABLE SPEED WIND TURBINE PMSG SYSTEM AT 85% LOADING .....	87
FIGURE 5.32 TERMINAL VOLTAGE OF VARIABLE SPEED WIND TURBINE PMSG AT DIFFERENT $R_{ST}$ & $L_{ST}$ .....	88
FIGURE 5.33 STATCOM CONV. VOLTAGE OF VARIABLE SPEED WIND TURBINE PMSG AT DIFFERENT $R_{ST}$ & $L_{ST}$ .....	89
FIGURE 5.34 STATCOM CURRENT OF VARIABLE SPEED WIND TURBINE PMSG AT DIFFERENT $R_{ST}$ & $L_{ST}$ .....	89
FIGURE 5.35 INVERTER OUTPUT CURRENT OF VARIABLE SPEED WIND TURBINE PMSG AT DIFFERENT $R_{ST}$ & $L_{ST}$ .....	90
FIGURE 5.36 DC LINK VOLTAGE OF VARIABLE SPEED WIND TURBINE PMSG AT DIFFERENT $R_{ST}$ & $L_{ST}$ .....	90
FIGURE 5.37 GENERATOR SPEED VARIATION OF VARIABLE SPEED WIND TURBINE PMSG AT DIFFERENT $R_{ST}$ & $L_{ST}$ .....	91
FIGURE 5.38 POWER ANGLE VARIATION OF VARIABLE SPEED WIND TURBINE PMSG AT DIFFERENT $R_{ST}$ & $L_{ST}$ .....	92
FIGURE 5.39 GRID POWER OF VARIABLE SPEED WIND TURBINE PMSG WITH AND WITHOUT STATCOM FOR A 3-PHASE FAULT ON GRID BUS .....	94
FIGURE 5.40 GENERATOR POWER OF VARIABLE SPEED WIND TURBINE PMSG WITH AND WITHOUT STATCOM FOR A 3-PHASE FAULT ON GRID BUS .....	94
FIGURE 5.41 TERMINAL VOLTAGE OF VARIABLE SPEED WIND TURBINE PMSG WITH AND WITHOUT STATCOM FOR A 3-PHASE FAULT ON GRID BUS .....	95
FIGURE 5.42 INVERTER OUTPUT CURRENT OF VARIABLE SPEED WIND TURBINE PMSG WITH AND WITHOUT STATCOM FOR A 3- PHASE FAULT ON GRID BUS .....	95
FIGURE 5.43 DC LINK VOLTAGE OF VARIABLE SPEED WIND TURBINE PMSG WITH AND WITHOUT STATCOM FOR A 3-PHASE FAULT ON GRID BUS .....	96
FIGURE 5.44 GENERATOR SPEED VARIATIONS OF THE VARIABLE SPEED WIND TURBINE PMSG WITH AND WITHOUT STATCOM FOR A 3-PHASE FAULT ON GRID BUS .....	97
FIGURE 5.45 POWER ANGLE OF THE VARIABLE SPEED WIND TURBINE PMSG WITH AND WITHOUT STATCOM FOR A 3-PHASE FAULT ON GRID BUS .....	97
FIGURE 5.46 GRID POWER OF VARIABLE SPEED WIND TURBINE PMSG WITH AND WITHOUT STATCOM FOR A 3-PHASE FAULT ON LOAD BUS .....	99
FIGURE 5.47 GENERATOR POWER OF VARIABLE SPEED WIND TURBINE PMSG WITH AND WITHOUT STATCOM FOR A 3-PHASE FAULT ON LOAD BUS .....	99
FIGURE 5.48 TERMINAL VOLTAGE OF VARIABLE SPEED WIND TURBINE PMSG WITH AND WITHOUT STATCOM FOR A 3-PHASE FAULT ON LOAD BUS .....	100
FIGURE 5.49 INVERTER OUTPUT CURRENT OF VARIABLE SPEED WIND TURBINE PMSG WITH AND WITHOUT STATCOM FOR A 3- PHASE FAULT ON LOAD BUS .....	100
FIGURE 5.50 DC LINK VOLTAGE OF VARIABLE SPEED WIND TURBINE PMSG WITH AND WITHOUT STATCOM FOR A 3-PHASE FAULT ON LOAD BUS .....	101
FIGURE 5.51 GENERATOR SPEED VARIATIONS OF THE VARIABLE SPEED WIND TURBINE PMSG WITH AND WITHOUT STATCOM FOR A 3-PHASE FAULT ON LOAD BUS .....	102
FIGURE 5.52 POWER ANGLE OF THE VARIABLE SPEED WIND TURBINE PMSG WITH AND WITHOUT STATCOM FOR A 3-PHASE FAULT ON LOAD BUS .....	102

## LIST OF TABLES

TABLE 2.1 TYPES OF WIND TURBINES PRODUCED BY VARIOUS WIND GENERATOR MANUFACTURERS .....	12
TABLE 4.1 EIGEN VALUES OF THE VARIABLE SPEED PMSG SYSTEM WITHOUT STATCOM.....	45
TABLE 4.2 EIGEN VALUES OF THE VARIABLE SPEED PMSG WITH STATCOM ON GENERATOR SIDE-CONVERTER. ....	45
TABLE 4.3 EIGEN VALUES OF THE VARIABLE SPEED PMSG WITH STATCOM ON GRID SIDE-CONVERTER.....	46
TABLE 4.4 CRITICAL MODES FOR A NOMINAL LOADING OF 0.65 P.U. ....	46
TABLE 4.5 PI CONTROLLER GAINS WHEN $\Delta\Omega_g$ IS TAKEN AS PLANT OUTPUT .....	63
TABLE 4.6 PID CONTROLLER GAINS WHEN $\Delta\Omega_g$ IS TAKEN AS PLANT OUTPUT .....	64

## NOMENCLATURE

- $\omega_o$  : Synchronous speed in rad/sec
- $\omega_t, \omega_g$  : Angular speed of wind turbine, PMSG in rad/sec
- $n_t$  : Mechanical Speed of wind turbine in rpm
- $\delta$  : Load angle of PMSG in radians.
- $P_m, P_e$  : Mechanical input of wind turbine, Electrical output of PMSG in p.u.
- $H_t, H_g$  : Inertia constant of wind turbine, PMSG in sec
- $K_s$  : Stiffness co-efficient of the shaft in p.u.
- $\theta_s$  : Shaft angle in radians.
- $V_g$  : PMSG terminal voltage reference in p.u.
- $V_c$  : DC link Capacitor voltage in p.u.
- $V_i$  : Internal voltage of grid side-converter (inverter) system in p.u.
- $V_t$  : Load Terminal voltage of the PMSG in p.u.
- $V_{st}$  : STATCOM terminal voltage in p.u.
- $V_{dc}$  : STATCOM DC link capacitor voltage in p.u.
- $V_b$  : Grid voltage referenced along the direct-axis in p.u.
- $R_a$  : Armature Resistance of PMSG in p.u.
- $X_d, X_q$  : d-axis, q-axis synchronous reactance of PMSG in p.u.
- $\Psi_o$  : Residual Flux linkage of PMSG in p.u.
- $R_i, X_i$  : Internal Resistance, Reactance of grid side-converter (inverter) system.
- $R_L, X_L$  : Resistance, Reactance of the load at bus 't'.
- $g_{11}, b_{11}$  : Conductance, Susceptance of the load at bus 't'.
- $R_{st}, L_{st}$  : Resistance, Inductance of the STATCOM transmission line.

$R, X$  : Resistance, Reactance of the transmission line.

$g_{12}, b_{12}$  : Conductance, Susceptance of the transmission line.

$i_{gd}, i_{gq}$  : d-q axes currents of PMSG in p.u.

$V_{gd}, V_{gq}$  : d-q axes voltages of PMSG in p.u.

$i_{id}, i_{iq}$  : d-q axes currents of grid side-converter (inverter) system in p.u.

$V_{id}, V_{iq}$  : d-q axes voltages of grid side-converter (inverter) system in p.u.

$i_{std}, i_{stq}$  : d-q axes currents of STATCOM controller in p.u.

$V_{std}, V_{stq}$  : d-q axes voltages of STATCOM controller in p.u.

$m_1, \alpha_1$  : modulation index, firing angle of generator side converter (rectifier).

$m_2, \alpha_2$  : modulation index, extinction angle of grid side converter (inverter).

$m_{st}, \psi_{st}$  : modulation index, firing angle of STATCOM controller.

## ABBREVIATIONS

AC	Alternating Current
BESS	Battery Energy Storage System
CCSG	Converter Connected Asynchronous Generator
CHP	Combined Heat and Power
DFIG	Doubly Fed Induction Generator
ECS	Energy Capacitor System
EDLC	Electric Double Layer Capacitor
EESG	Electrically Excited Synchronous Generator
ESS	Energy Storage System
FACT	Flexible AC Transmission System Device
FRT	Fault Ride Through
LVRT	Low Voltage Ride Through
HSV	Hankel Singular Value
HVAC	High voltage AC
HVDC	High voltage DC
IGBT	Insulated Gate Bipolar Transistor
LCC	Line Commutated Converter
MPPT	Maximum Power Point Tracking
MVAR	Mega Volt Ampere Reactive
MW	Megawatt
MWh	Megawatt hour
NREL	National Renewable Energy Laboratory (Boulder, USA)
NRMSE	Normalised Root Mean Square Error
NTC	Net Transfer Capacity
PI	Proportional plus Integral
PID	Proportional plus Integral plus Differential
PMSG	Permanent Magnet Synchronous Generator
PSS	Power System Stabilizer
SCADA	Supervisory Control and Data Acquisition
SCIG	Squirrel Cage Induction Generator
STATCOM	Static Synchronous Compensator
SVC	Static Var Compensator
SVD	Singular Value Decomposition
TW	Terawatt
TWh	Terawatt hour
VFC	Variable Frequency Converter
VSC	Voltage Source Converter
VSWT	Variable Speed Wind Turbine
WECS	Wind Energy Conversion System
WEPP	Wind Energy Power Plant
WRIG	Wound Rotor Induction Generator
WT	Wind Turbine
WTGS	Wind Turbine Generating System

## **THESIS ABSTRACT (ENGLISH)**

**Name:** MIR SADAT ALI

**Title:** EVALUATION OF DAMPING CONTROLS OF A PERMANENT MAGNET SYNCHRONOUS GENERATOR WIND SYSTEM WITH STATCOM

**Degree:** MASTER OF SCIENCE

**Major Field:** ELECTRICAL ENGINEERING

**Date of Degree:** APRIL, 2012

*Large wind farms may pose stability and control issues when integrated to the power system. Although integration of large penetration of wind power into an existing transmission system does not require a major redesign, it necessitates additional control and compensating equipment to enable recovery from severe system disturbances. A variable speed permanent magnet synchronous generator (PMSG) wind generator system is considered in this study. This thesis develops a model of a variable speed wind turbine permanent magnet synchronous generator (PMSG) system including the detailed dynamics of the converter circuitry. The static converters used in PMSG systems decouple the mechanical frequency of the rotor and the electrical frequency of the grid, and are modeled as current controlled voltage sources. A STATCOM device is used to control the system performance in transient as well as in steady state.*

*The impacts of the location of the STATCOM device on the generator as well as grid side of the converter were investigated and best possible location is examined through small signal analysis. To enhance the operation of the PMSG system, the damping capabilities of the generator and grid side converter controls were investigated using various decomposition techniques through small signal analysis and control design is carried out with the best stabilizing signal for the control input identified. Non-linear time domain simulations have been carried out to validate the findings of the small signal model and also to assess the controller performance in terms of enhancing system operation. It was observed that the modulation index of the generator side-converter has the higher controllability to damp the oscillatory modes of the system when the STATCOM is located at the grid side converter. A PI/PID controller is designed to improve the performance of the wind turbine grid connected system. The controller gains were tuned through a frequency based optimization procedure.*

**MASTER OF SCIENCE DEGREE**

**KING FAHD UNIVERSITY OF PETROLEUM & MINERALS**

**Dhahran, Saudi Arabia**

## THESIS ABSTRACT (ARABIC)

الاسم: مير سادات على

العنوان: تقييم التخميد ضوابط نظام الرياح مولد المغناطيس الدائم المتزامن مع ستاتكوم

درجة: ماجستير في العلوم

الميدانية الرئيسية: الهندسة الكهربائية

التاريخ لدرجة: نيسان/أبريل، 2012

مزارع الرياح كبيرة قد تثير قضايا الاستقرار والسيطرة عند دمجها بنظام الطاقة. على الرغم من أن تكامل اختراق كبير لطاقة الرياح في نظام إرسال موجود لا تتطلب إعادة تصميم رئيسية، فإنه يستلزم مراقبة إضافية ومعدات تعويضية لتمكين التعافي من اضطرابات نظام شديد. ويعتبر نظام مولد رياح مولد متزامن (PMSG) مغناطيس دائم متغيرة سرعة في هذه الدراسة. هذه الأطروحة يطور نموذج لمغناطيس دائم عنفه الرياح متغيرة السرعة مولد متزامن (PMSG) نظام بما في ذلك ديناميات مفصلة من الدوائر المحول. ثابتة المحولات المستخدمة في نظم PMSG فصل تواتر الميكانيكية للدوار وتردد الشبكة الكهربائية، وهي على غرار كمصادر التيار الكهربائي التي تسيطر عليها حالياً. يتم استخدام جهاز STATCOM مراقبة أداء النظام في عابرة، وكذلك كما هو الحال في حالة مستقرة.

وتم التحقيق في آثار موقع الجهاز STATCOM على المولدات الكهربائية، فضلا عن الجانب الشبكة للمحول وهو بحث أفضل مكان ممكن من خلال تحليل الإشارات الصغيرة. لتحسين تشغيل نظام PMSG، تم التحقيق قدرات التخميد الضوابط تحويل الجانب المولد والشبكة باستخدام تقنيات مختلفة من التحلل من خلال تحليل الإشارات الصغيرة وجتصميم يتم الاضطلاع بها مع أفضل الاستقرار إشارة لعنصر التحكم الإدخال المحددة. نالمحاكاة على خطي الوقت المجال أجريت للتحقق من صحة نتائج نموذج إشارة صغيرة، وأيضا لتقييم أداء المراقب المالي فيما يتعلق بتعزيز نظام التشغيل. فقد لوحظ أن الفهرس التحوير لمولد الجانب-المحول قد التحكم أعلى رطوبة أوضاع متذبذبة من النظام عند STATCOM يقع في الجانب الشبكة المحول. وحدة تحكم PI/PID يهدف إلى تحسين أداء نظام الشبكة متصل التوربينات الريحية. المكاسب التي تحكم تم ضبطها من خلال تردد على أساس إجراء تحسين.

درجة الماجستير في العلوم

جامعة الملك فهد للبترول والمعادن

الظهران، المملكة العربية السعودية

# CHAPTER 1

## INTRODUCTION

### 1.1 Renewables and Wind Energy

In traditional power systems a few large centralized power generation plants produce bulk of the power. The generated power is then transferred to consumers over long transmission lines. Today, the world is much more concerned about the environmental issues and energy security; thus governments around the world are relying on renewable energy for reducing the environmental problems caused by the conventional energy sources. As energy demand around the world increase, the need for renewable energy source that will not harm the environment has also been increased. Some projections indicate that the global energy demand will almost triple by 2050. One such example, to improve unfavorable earth environment in the field of the generation of electricity is wind farm, which are installed at an increasing tempo. Wind turbine technology has being undergoing a dramatic development and now is the world's fastest growing energy [1-4]. Wind power growth with a 20% annual rate has experienced the fastest growth among all renewable energy sources since five years ago. It is predicted that by 2020 up to 12% of the world's electricity will have been supplied by wind power[1].

When compared to other renewable energy sources, such as photovoltaic, wave and tidal power, wind power is a relatively cheap source of renewable energy. Therefore, the promotion of renewable energy by a number of governments has led to a strong growth of wind power in the respective countries. The countries with the highest total installed



capacity are Germany (20 622 MW), Spain (11 615 MW), USA (11 603 MW), India (6270 MW) and Denmark (3136 MW)[1]. According to global wind energy council report, Europe continues to lead the market with 48 545 MW of installed capacity at the end of 2006, representing 65% of the global total, and the European wind energy association has set a target of satisfying 23% European electricity needs with wind energy by 2030[4]. It is clear that the global market for the electrical power produced by wind turbine generators has been increasing steadily, which directly pushes the wind technology into a more competitive area.

## **1.2 Wind Turbine Systems**

The development of modern wind power conversion technology has been going on since 1970s, and the rapid development has been seen from 1990s. The worldwide market for the electrical power generated by the wind system generator has been rising progressively, which promptly impels the wind technology into a highly competitive environment. Various wind turbine concepts have been developed and different wind generators have been built that are generally of two types: Fixed Speed and Variable Speed. Fixed speed generators are induction generators with capacitor bank for self-excitation or two-pole pairs or those which use rotor resistance control. Variable speed wind turbines are connected to the grid using power electronic technology and maximize effective turbine speed control. Variable speed generators are either DFIG (which is a round rotor machine) or full power converters such as permanent magnet synchronous generators, or externally magnetized synchronous generators[4].

Additionally, a variety of innovative concepts of wind turbines appear, for example, an interesting alternative may be a mixed solution with a gearbox and a smaller low speed permanent magnet synchronous generator (PMSG), because direct-drive wind generators are becoming larger and even more expensive for increasing power levels and decreasing rotor speeds.

### **1.2.1 Fixed Speed Concept**

Historically induction generator (IG) has been extensively used in commercial wind turbine units. Asynchronous operation of induction generators is considered an advantage for application in wind turbine systems, because it provides some degree of flexibility when the wind speed is fluctuating. There are two main types of induction machines: squirrel cage and wound rotor[3, 4]. The induction generator based on Squirrel-Cage rotor (SCIG) is a very popular machine because of its low price, mechanical simplicity, robust structure, and resistance against disturbance and vibration. The wound-rotor is suitable for speed control purposes. By changing the rotor resistance, the output of the generator can be controlled and also speed control of the generator is possible. Although wound rotor induction generator has the advantage described above, it is more expensive than a squirrel-cage rotor. Its rotation speed can only vary slightly which is almost “fixed speed” in comparison with the other wind turbine concepts.

In the early 1990’s, almost every wind turbine installed was operated at fixed speed, irrespective of wind speed[5]. The rotor speed of the turbine is fixed to the speed defined

by the normal frequency of the power grid to which the turbine is connected. The gear ratio and the design of generator permit the rotor to rotate at this fixed speed for variable wind speeds[6]. The standard electrical system for fixed speed wind turbine is the squirrel-cage induction generator (SCIG) connected to grid as shown in Figure 1.1. To compensate for the no-load current of the generator, a capacitor bank is installed which reduces the reactive power demand. Moreover, a thyristor based soft starter is employed to reduce the inrush current.

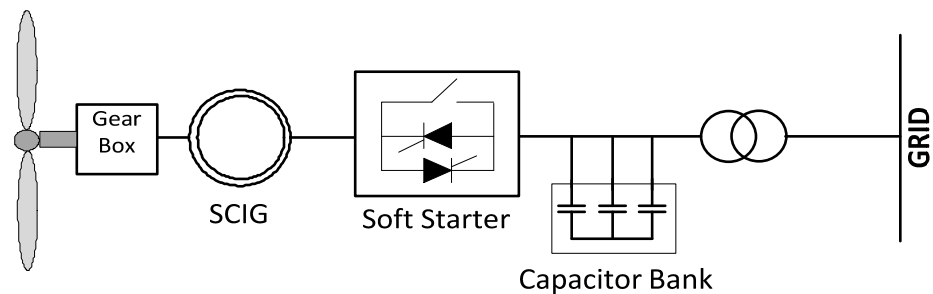


**Figure 1.1 Structure of Fixed Speed Wind Turbine.**

The well-known advantages of SCIG are their robustness, ease and relatively lower cost for mass production. In addition, SCIG enables stall-regulated machines to operate at a constant speed when it is connected to a large grid, which provides a stable control frequency.

The disadvantages of SCIG for the fixed speed wind turbine concept are that only speeds higher than the synchronous are possible for generator operation. Additionally, the fixed speed concept means that wind speed fluctuations are directly translated into electromechanical torque variations, this causes high mechanical and fatigue stresses on the system (turbine blades, gearbox and generator) and may result in swing oscillations

between turbine and generator shaft. Also the periodical torque dips because of the tower shadow and shear effect are not damped by speed variations and result in higher flicker.

### **1.2.2 Variable Speed Fixed-Frequency Generators**

A variable speed wind turbine runs at a certain speed relative to the current wind speed, defined by the optimal tip-speed ratio, in order to produce maximum power [4, 5]. The energy captured can be increased by using an active pitch, which adjusts the pitch angle instantaneously to the wind speed. Unfortunately, this advantage can be utilized only at low or medium wind speeds as the bandwidth of the pitch control results in overload due to large wind power fluctuations at high wind speed. The stall-controlled wind turbine can be designed to manage power overload but this increases the cost of the electrical system.

Variable-speed operation of wind turbines offers certain advantages: mechanical stress is reduced, torque oscillations are not transmitted to the grid; can operate below rated wind speed, and the rotor speed is controlled to achieve maximum aerodynamic efficiency. To improve their efficiency, many modern wind generators adopt a variable speed operation in one of two ways: direct AC to AC frequency converters, such as the cyclo-converters; or using voltage controlled inverters (AC-DC-AC), which convert power at varying frequencies at the variable-speed generator to DC, and then use some form of power electronics to convert the DC power back to AC at a fixed frequency appropriate for the grid connection. The two most interesting configurations in variable speed operation of

wind turbines are DFIG (Doubly Fed Induction Generator) with partially 30% back to back converters and the direct driven PMSG with full scale power converters[2, 3]. Many papers have proven that the direct driven PMSG is a good choice due to the elimination of gearbox, the advances in power electronics technology, the higher efficiency of PMSG and the wide range of speed control in the PMSG[4, 5, 7]. The full scale power converters are divided into generator and grid side converters. The generator side converter is used mainly to control the electrical torque of the generator to obtain the optimum power. The grid side converter is used mainly to control the dc bus voltage and the reactive power flow to the grid. The behavior of the variable frequency control and the associated wind turbine generator system relies on the performance of its control system. With well-designed controllers, it is possible to increase the chance of the wind turbine generating system (WTGS) to remain in service during grid disturbances.

In the last decade, various modern control techniques such as adaptive control, variable structure control and intelligent control have been studied for controlling the nonlinear components in power systems. However, these control techniques have few real applications probably due to their complicated structures or the lack of confidence in their stability. Therefore, in this research the conventional PI controllers, because of their simple structures, will be utilized for control of the wind turbines equipped with PMSG [8-12]. Hence, it can be concluded that Permanent magnet wind generators are used in variable speed, direct-driven wind energy conversion systems (WECS), whilst induction generators are used in constant, semi-constant speed and geared systems. If speed of generator varies with wind speed, the wind generator may be used at the peak power and

received the maximum power from the wind. Eliminating the gear-box between the generator shaft and wind turbine such varying speed generator is possible[7, 13].

### **1.3 Variable speed wind turbine PMSG control systems**

Though wind power is considered as a prospective energy source, wind power fluctuation due to randomly varying wind speed is still a serious problem for power grid companies or transmission system owners (TSOs). Therefore, it is essential to emphasize the research on the smoothening of wind power fluctuation by using some control scheme at the generator side or the load side. It is possible to smoothen the wind power fluctuation up to a certain range by the blade pitch angle control of the wind turbine[14]. The load side controls are generally converter or energy storage based. In some reports, a battery energy storage system (BESS) or static synchronous compensator (STATCOM) integrated with BESS [15, 16] has also been proposed to smoothen wind power fluctuation. Another relatively new energy storage technology is energy capacitor storage (ECS), which is composed of power electronic devices and electric double layer capacitor (EDLC)[17].

### **1.4 Problem Statement**

Some of the major concerns of variable speed wind generating systems are the stability issues, power quality and voltage instability problems occurring in a power system that are not able to meet the reactive power demand during faults and heavy loading

conditions. Low voltage ride through (LVRT) is a recently introduced requirement that transmission operators demand from wind farms.

Among the energy storage elements STATCOM is a relatively popular device. The main motivation for choosing STATCOM in wind farms is its ability to provide voltage support either by supplying / absorbing reactive power into the system[18, 19]. A STATCOM is reported to be effective in providing LVRT for wind turbines in a wind farm but its application in terms of PMSG system are not fully explored. For example, the ideal location of the device needs careful investigation. Stability studies in variable speed wind turbine generating systems are required to ensure a safe operation with good performance.

## **1.5 Thesis Objective**

A major objective of this research is to study the impact of a variable-speed wind turbine-PMSG system in terms of transient performance for the power system and to design controllers so that the transients are adequately controlled [11, 20]. The design should be robust to perform well for a reasonable set of operating conditions. A STATCOM is proposed to be used as a control device, and its ideal location in terms of transient performance will be investigated. Damping properties of the various input signals will be explored. The suggested steps to achieve the aims of the thesis are as follows:

1. Developing a non-linear model of wind turbine connected to PMSG two-mass system for a single machine modeling including STATCOM controller.

2. Developing a linearized model of wind turbine connected PMSG two-mass system for a single machine infinite bus system decoupled through static-converters along with STATCOM controller. This is required for control design.
3. Carrying out nonlinear and linearized time-domain simulations and comparison of the responses for STATCOM on both generator and grid sides.
4. Evaluation of damping properties of various controls through decomposition techniques such as SVD, Hankel etc.
5. Design of the PI/PID controllers through frequency response methods.
6. Investigation of the uncontrolled & controlled system response and identify the proper control including the location of the STATCOM controller.

## **1.6 Thesis Organization**

The organization of the thesis is as follows: In chapter 2, a literature survey of the wind turbine generators, variable speed operation techniques and application of FACTS devices in WECS are discussed. The recent studies on hybrid models, stability issues and their solutions and various control techniques are included.

Chapter 3 presents the detailed nonlinear and linear models of variable speed PMSG wind generation systems along with STATCOM controller.

In Chapter 4 small signal analysis is done to verify the damping properties of the composite system with and without STATCOM device. Also the best possible location of the STATCOM controller for stability enhancement will be examined and establishes the



hierarchies of controls in terms of dynamic performance enhancement through minimum singular value decomposition, Hankel singular value decomposition and residue principles. Control design is carried out with the best stabilizing signal for the control input identified.

In Chapter 5 non-linear time domain simulations have been carried out to validate the findings of the small signal model and also to assess the controller performance in terms of enhancing system operation. Simulation studies are carried out with and without STATCOM device for various disturbances in the system.

Finally, conclusion and suggested future work are presented in chapter 6.

## CHAPTER 2

### LITERATURE REVIEW

The literature review on this subject is divided into three sections. In the first section, types of wind turbine generators and the recent studies on permanent magnet synchronous generator (PMSG), wind system and the application of power electronics for variable speed operation are documented. In the second section, application of FACTS devices for variable speed operation of PMSG, connected to grid will be discussed. In the last section, several control techniques and decomposition methods which help in improving the performance of variable speed operation of PMSG WECS have been discussed.

#### 2.1 Wind Turbine Generators

The common types of AC generator [4, 13, 21] that are possible candidates in modern wind turbine systems are as follows:

- 1) Squirrel-Cage rotor Induction Generator (SCIG),
- 2) Wound-Rotor Induction Generator (WRIG),
- 3) Doubly-Fed Induction Generator (DFIG),
- 4) Synchronous Generator (With external field excitation)and,
- 5) Permanent Magnet Synchronous Generator (PMSG).

There are many wind turbine manufacturers who produce different wind turbine technologies. Table 2.1 gives a list of all the MW range WTs manufactured by various producers and their technical specifications[4].

Table 2.1 Types of wind turbines produced by various wind generator manufacturers

<b>Wind Turbine</b>	<b>Rated Speed</b>	<b>Cut out speed</b>	<b>Generator</b>	<b>Power Control</b>
GE 1.5 MW	13 m/s	25 m/s	DFIG	Active blade pitch
GE 2.5 MW	12.5 m/s	25 m/s	PM generator	Active blade pitch
GE 3.6 MW	14 m/s	27 m/s	DFIG	Active blade pitch
VESTAS 1.65 MW	13 m/s	20 m/s	Asynchronous	Active Stall
VESTAS 1.8 MW	15 m/s	25 m/s	Asynchronous with Optislip	OptiSlip / Pitch
VESTAS 3 MW	15 m/s	25 m/s	Asynchronous with Optispeed	OptiSpeed and OptiTip Pitch regulation
NORDEX 2.5 MW	15 m/s	25 m/s	DFIG	Pitch
NORDEX 3 MW	13 m/s	25 m/s	DFIG	Pitch
SUZLON 0.95 MW	11 m/s	25 m/s	Asynchronous	Pitch
SUZLON 1.25 MW	13 m/s	25 m/s	Asynchronous	Pitch

A conventional wind turbine rotating at fixed speed connected to the normal utility grid is modeled in[22]. Utilizing this model, the detailed short circuit analysis is done. A three-phase fault is applied in proximity to wind turbine generator, and detached immediately by disconnecting the faulted line. The base case is also used to analyze and discuss the effect of various mechanical, electrical and operating parameters for the certain critical fault-clearing time. The parameters examined are the wind speed, the power output, the short-circuit power at the connection bus, the distance to the fault, the reactive power

compensation, the hub-generator resonant frequency, the distance between generator and faulted point, the rotor inertia etc. The proposed methodology is very well organized to analyze the transient stability performance in fixed speed wind system.

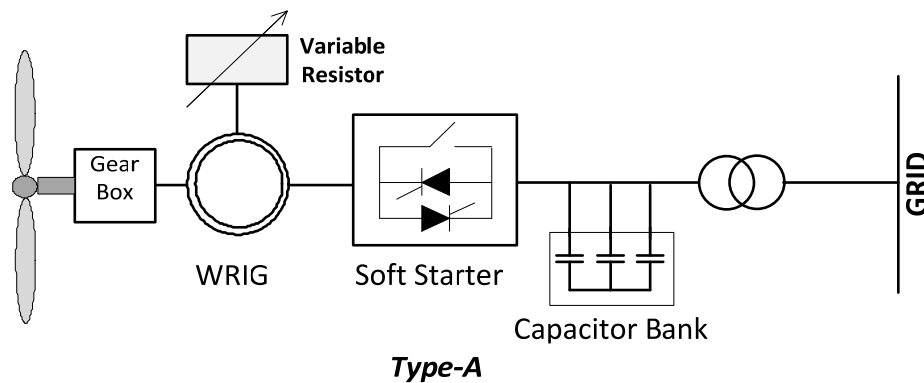
Equivalent wind system models operating at fixed speed are proposed in[23] by accumulating the wind turbines into an approximate equivalent wind turbine which can operate on an equivalent wind system electric network. Two effective equivalent wind turbines have been designed. The first equivalent model for accumulated wind turbines operated efficiently for identical winds, the other equivalent model is extended to operate with different incoming winds.

Various dynamic models of fixed speed wind turbine, comprising of a comprehensive model and reduced third order equivalent model of wind systems with fixed speed wind turbine generators is presented in[24]. The power system stability studies were also presented with the stator flux transient incorporated. The fault ride through capability of the generator has been investigated for a symmetrical three phase fault on the grid bus.

The concept has been continuously further developed, for example in the so-called active stall designs, where the blade pitch angle can be changed towards stall by the control system. This is the conventional concept applied by many Danish wind turbine manufacturers during the 1980s and 1990s. The upwind, stall-regulated, three-bladed wind turbine concept using a SCIG is also referred to as 'Danish concept'. Since the SCIG always draws reactive power from the grid, during the 1980s this concept was

extended with a capacitor bank for reactive power compensation. Smoother grid connection was also achieved by incorporating a soft-starter[25]. Furthermore, a pole-changeable SCIG has been used, which leads two rotation speeds.

For variable speed wind turbines, many different arrangements of electrical systems are possible. Three types of configurations are shown in Figure 2.1. *Type-A* corresponds to a limited variable speed wind turbine generator with variable rotor resistance. *Type-B* is a limited variable speed doubly fed induction generator wind turbine connected with a partial frequency converter to the utility network. These two configurations of wind systems cannot be operated in standalone mode as the induction generator consumes reactive power from the grid or power electronic systems to generate its exciting current in the rotor. Therefore when isolated from the utility network, lack of excitation current may cause induction generator to stop. Aerodynamic control combined with *Type-A* concept is mostly passive stall, and as a consequence there are few active control options, besides connecting and disconnecting, especially if there is no blade pitch change mechanism.



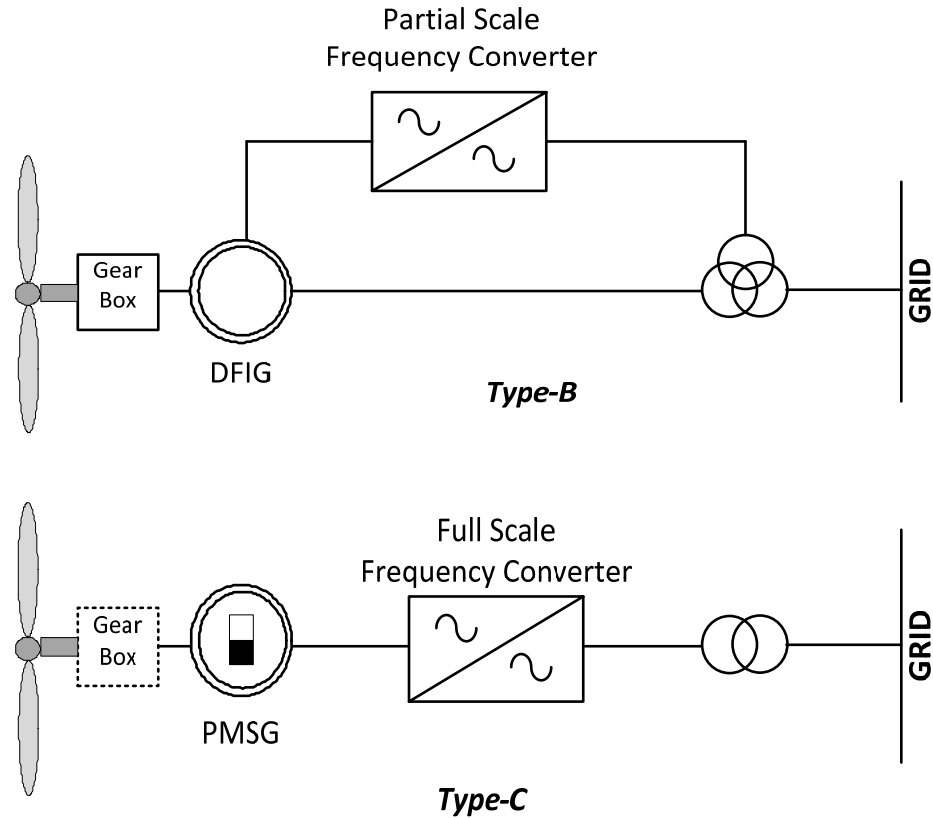


**Figure 2.1 Structures of the variable speed wind turbine systems**

*Type-C* is a permanent magnet synchronous generator connected to the main grid through a full frequency converter. PMSG wind turbine has several benefits. There are no field windings; external excitation is provided by the permanent magnet instead of the coils hence they can be operated without providing external excitation. The PMSG has the capability of variable speed control due to its change in rotor speed in a large range which makes the maximum power point tracking function easier. Due to the low rotational speed of PMSG wind turbine, gear box can be omitted and thus reducing the cost. In a recent research, the most critical component in wind system is found to be the gear box due to its high downtime per failure in comparison with other system components.

In terms of wind power generation technology, as a result of numerous technical benefits (higher energy yield, reducing power fluctuations and improving var supply) the modern MW-size wind turbines always use variable speed operation which is achieved by power electronics converters[4, 13, 21]. These converters are typically associated with individual generators and they contribute significantly to the costs of wind turbines. Between variable speed wind turbine generators doubly fed induction generators (DFIGs) and permanent magnet synchronous generators (PMSGs) with primary converters are emerging as the preferred technologies[4]. An important aspect to be considered in modeling variable speed wind generation systems is the behavior of the static converters, which are invariably present in this type of technology. The models utilized to these components must adhere to the general simplifying assumptions that must be done to consider the interconnection of the wind generation to the electrical power system. Amongst many variable speed concepts, the DFIG equipped wind turbine has many advantages over others. When compared with conventional induction generators, the DFIG may have several advantages which depend on how the frequency converter control is arranged, as [26]:

1. An ability to control reactive power and support grid voltage
2. Decoupled control of active and reactive power that means independent control of torque and rotor excitation current.

During the last decade, the concept of the variable-speed wind turbine (VSWT) equipped with a doubly fed induction generator (DFIG) has received increasing attention due to its noticeable advantages over other wind turbine concepts[2, 4]. In the DFIG concept, the

induction generator is grid-connected at the stator terminals, but the rotor terminals are connected to the grid via a partial-load variable frequency AC-DC-AC converter (VFC) and a transformer. The VFC only needs to handle a fraction (25-30%) of the total power to achieve full control of the generator. Compared to the fixed-speed wind turbine with induction generator, the VSWT with DFIG can provide decoupled control of active and reactive power of the generator, more efficient energy production, improved power quality, and improved dynamic performance during power system disturbances such as network voltage sags and short circuits[13, 27]. Compared to the VSWT equipped with a synchronous generator, in which a full load VFC is connected directly between the generator stator and the grid, the VFC of the DFIG is smaller in size and therefore much cheaper. The small-signal stability of the DFIG has been examined in papers, either for open-loop [28] or with control loops [29]. The impact of variable-speed wind turbines on power system oscillations has been treated in [30]with a constant power model for variable-speed wind turbines. Modeling with back to back PWM converters and their applications to variable speed wind-energy generation has been observed in [31]. An optimal tuning procedure for rotor side converter controllers for DFIG used for power system stability study is also presented in [28]. It is particularly observed that both the stator and rotor dynamics should be incorporated for optimally tuning controller parameters. Hence, it can be said that with VSWTs becoming more popular, DFIGs are preferred over conventional induction generators.

As far as variable-speed generation is concerned, it is necessary to produce constant-frequency electric power from a variable-speed source. Another type of generator that has



been proposed for wind turbines in several research articles is synchronous generator. This type of generator has the capability of direct connection (direct-drive) to wind turbines, with no gearbox [7-13]. This advantage is favorable with respect to lifetime and maintenance. Synchronous machines can use either electrically excited or permanent magnet (PM) rotor [32]. The PM and electrically-excited synchronous generators (EESG) differ from the induction generator in that the magnetization is provided by a Permanent Magnet pole system or a dc supply on the rotor, featuring providing self-excitation property. Self-excitation allows operation at high power factors and high efficiencies for the PM synchronous generators. Advantages of the PM generators include simple design of rotor, lack of slip rings and generator excitation, lower temperature rise and consequently improvement of the efficiency [33].

PM generators are classified into four groups: radial flux, axial flux, tooth pole and cross-field. It has been proved that most wind turbine PM generators are radial flux and axial flux types. The inner rotor, radial flux PM generators are more popular due to their low cost and easy construction. In [7], Three 500 kW wind generators consists of; (i) a 4-pole, fixed speed induction generators with gear-box, (ii) a fixed speed synchronous generator with gear-box, frequency converter, (iii) a variable speed PM generator with no gear-box with frequency converter have been studied and it has been shown that gearless PM generator has higher efficiency over all speeds and loads because of lower core losses, rotational losses and gear losses over low speeds. This thesis plays a significant role in this concept, where the gear-box is replaced by using high efficiency low speed PMSG as shown in Fig. 2.1. The PMSG can be connected directly to the wind turbine, which results

in a simple mechanical system. Many disadvantages can also be avoided in gearless WTG. The noise caused mainly at high rotational speed can be reduced and also high overall efficiency and reliability are achieved in addition to reduced weight and diminished need for maintenance. However, the WTG can extract maximum power at different wind speeds. In the variable speed operation, there is a reduction of the drive train noise, reduction in mechanical stresses, and the increased energy capture [4, 7, 13].

Moreover, relatively small size generators can be built based on their power ratings. PMSG machines have comparatively larger air gaps which hamper the flux linkage even in the multi-pole machine[34]. The dynamic model with pitch angle and stability control schemes of a variable speed wind turbine with permanent magnet synchronous generator (PMSG) is created in[35]. The model comprises of a PMSG, the pitch angle controlled wind turbine and a drive train model. The drive train model employs single mass model to represent the generator mechanical characteristics. The control strategy development involves the pitch angle control for wind turbine and a speed control block for PMSG.

The comprehensive model and control strategy development of variable speed wind generator is also very well depicted in[36]. In order to find out the gain in energy obtained from one methodology over the other, many models of off-grid wind generator systems have been designed in matlab/simulink [37]. All methodologies under consideration have the same parameters and components. A new technique is proposed to track the maximum energy from a 20kW PMSG and a fair comparison is done with the results of previous control schemes. In [16, 38]stand-alone wind energy systems (i.e.,

systems not connected to the utility grid) are presented, that is considered as an effective way to provide continuous power to electrical loads.

In [8-10, 12], detailed modeling and control system of variable speed PMSG wind generator system are presented, but the steady state and dynamic performances are not analyzed sufficiently. In [39], the transient characteristic of variable speed wind turbine PMSG is discussed for a step change of generator speed, but no fault condition is considered there. In [11], the transient stability of VSWT-PMSG is analyzed in detail. For the maximum power point tracking (MPPT) operation, rotor speed is used as a controller input instead of wind speed, because the rotor speed can be measured precisely and more easily than the wind speed. Different types of symmetrical and unsymmetrical faults were considered to be occurred at several locations. It was found that by controlling the power converters of PMSG in proper way, the transient stability of VSWT-PMSG can be enhanced.

In order to solve the problem with short circuit faults, some measures are proposed about the low voltage ride through capability of the wind turbine with PMSG. FACTS/energy storage system (ESS) have recently emerged as more promising devices for power system applications, which have the ability to improve both voltage and power quality of wind generator as it can control both active and reactive power which is very well depicted in [40]. Besides, a braking resistor may be inserted into the dc circuit of the frequency converter, in parallel with the capacitor. It is used to dissipate the excessive energy during grid faults [41]. In [42] low-voltage ride-through (LVRT) capability of a 2MW-level

variable speed wind turbine with a PMSG was investigated. A new control scheme was designed and simulated for the wind turbine that allows it to be connected to the grid during transient grid faults. This control scheme emphasizes the regulation of dc-link voltage so as to protect the power electronic system under faults.

## **2.2 Application of STATCOM in WECS**

Only recently, after the increase in wind power penetration, have some stringent interconnection rules, known as “grid codes” with which these wind plants have to conform been developed. These grid codes require that wind turbine generators are treated more like conventional generating units and participate in grid voltage and frequency regulation[43]. To facilitate WT participation in frequency control there are two major controls: turbine-based control and substation-based control. In turbine-based control systems, each turbine has to have some specific control capabilities, such as power factor or reactive power (Q) control. In substation-based control, some kind of reactive power compensation is either provided by switched capacitors (manual or static compensation) or FACTS devices[44].

Power control is necessary for all connection requirements for wind turbines, which vary widely according to the short circuit capacity of the system. The relative impedance for weak grids is high, so the impact of Q support is usually significant. If wind turbines are connected to a weak system, more power control is required to keep the system stable during and after a fault[18, 19, 45, 46].

A turbine's low voltage ride through (LVRT) capability is its ability to survive a transient voltage dip without tripping. Wind turbines' LVRT capability is vital for wind farm interconnection because the tripping of a wind farm due to a fault on a nearby power line results in the loss of two major system components (the line and the wind farm). It is important to modify the performance of the wind energy systems by modifying the design of mechanical and electrical systems. One such modification can be done by employing STATCOM which act as a central controller to the grid connected wind turbine system [18, 19, 46]. The STATCOM is from the family of FACTS devices that can be used effectively in wind farms to provide transient voltage support to prevent system collapse. The STATCOM can also contribute to the low voltage ride through requirement because it can operate at full capacity even at lower voltages. In this thesis, a voltage source converter (VSC) PWM technique based STATCOM is proposed to stabilize grid connected PMSG based variable speed wind turbine.

The rating of the STATCOM also decides the maximum reactive power that can be supplied, but usually they have some extra capability called the transient capability which is available to the system for a short period of time. The reactive power supplied is also dependent on the immediate reactive power sources in the system. The size of the wind turbine and the synchronous machine also influences on the reactive power capability.

### **2.3 Control techniques of variable speed WT-PMSG system**

Large participation of electronically interfaced power sources with rapid variations disturbs the power system stability and can cause critical problems. This difficulty can be

overcome by employing static synchronous compensator (STATCOM) which can act as a central controller to the variable speed WT-PMSG system.

The paper describes the design of a variable speed wind turbine PMSG system. Oscillatory modes have been identified in simulation studies. There are some modes which are responsible for instabilities in the system at some operating conditions.

These critical modes dictate the initiation of control action to improve the performance of the variable speed wind turbine PMSG system. In the design and evaluation of the controllers, the properties of linear models such as the controllability and observability are employed. It is always important to know how difficult is to control the dominant mode from an input of the system. A theoretical explanation of the basics of singular value decomposition(SVD) used to measure the ability of inputs to control a mode is given in[47] - An investigation of the significance of singular value decomposition in power system dynamics.

Generally, it is observed that variable speed wind turbine PMSG parameters change with generation and system loading making the system behavior quite different for different operating conditions. Whenever there is a drastic change in the power system operation parameters, the controller parameter which stabilize the system under normal operating condition, may no longer yield appropriate results due to the change of controller parameters in a complex manner. To maintain the required control performance and power quality during changing operating conditions, a fine tuning of controller parameters is required. A method for shifting the complex open loop poles to any desired

position while preserving the imaginary parts is presented in [48] - Optimal pole shifting for power system stabilization. In every step of this technique, it is required to solve a first-order linear matrix Lyapunov equation for shifting one real pole and a second order equation for shifting two complex poles. The solution obtained using this approach is optimal with respect to quadratic performance index. In [49] power system stabilizer based on optimal pole shifting is proposed. An approach for shifting the real parts of the open-loop poles to any desired positions while preserving the imaginary parts is presented where the PSS is based on Riccati equation approach.

In this thesis, nonlinear time-domain based as well as eigen-value based objective functions are proposed to minimize the error in the measured power and to enhance the damping characteristics, respectively. Also the nonlinear time-domain simulation has been done to evaluate the usefulness of the designed controllers under various loading and disturbance conditions.

## CHAPTER 3

### DYNAMIC MODELING OF PMSG WIND SYSTEM

The dynamic model of the permanent magnet synchronous generator (PMSG) connected to wind turbine along with the power electronics converter circuits is developed in this chapter. A schematic diagram of the wind turbine-PMSG system connected to the power system grid is shown in Figure 3.1. The permanent magnet synchronous generator is driven by a horizontal axis wind turbine. The converters are located in between the generator terminals and the grid. The system model, given in the following, includes that of the wind turbine, the wind system, the PMSG, the converter circuits, the load and transmission line connected at grid side.

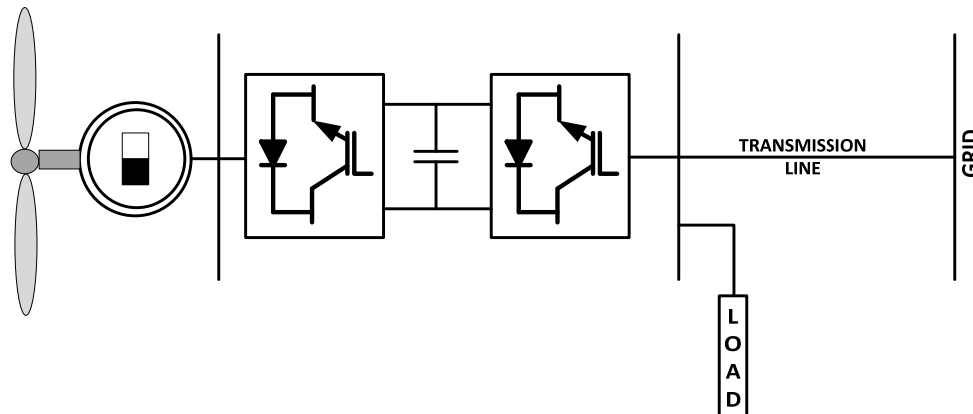


Figure 3.1 Schematic of Variable Speed WT-PMSG connected to grid

The stator of the PMSG is directly connected to the power electronics converter which is controlled by controlling the IGBT switches. The power electronics converter is a back-to-back converter system consisting of two voltage source converters (VSC) connected through a DC link. The stator circuit of the generator feeds the generator side-converter (rectifier) system. The grid side-converter (inverter) system maximizes the power



injected into the DC link of the back-to-back converter with the active power exchanged with the grid. The power electronics frequency converter provides a connection between the stator circuit operating at variable frequency and the power grid being at the fixed frequency. The linearized model of each component is derived from their corresponding non-linear dynamics.

### 3.1 The Wind Turbine and Wind System

The mechanical power output in (Watt) of a wind turbine is related to the wind speed  $V_\omega$  in (m/sec) by [13, 33, 50]

$$P_m = \frac{1}{2} \rho A C_p(\lambda, \beta) V_\omega^3 \quad (3.1)$$

Here,  $\rho$  is the air density and A is the swept area by the turbine blades. The power coefficient  $C_p$  is a function of both tip speed ratio,  $\lambda$  and the blade pitch angle  $\beta$ . The tip speed ratio  $\lambda$ , which is the ratio of linear speed at the tip of blades to the speed of wind, is expressed as,

$$\lambda = \frac{\omega_t R}{V_\omega} \quad (3.2)$$

where R and  $\omega_t$  are the radius and the mechanical angular velocity of the wind turbine.

Analytical expressions for  $C_p$  as a function of  $\lambda$  and  $\beta$  employed in [13, 33, 50] are,

$$C_p(\lambda, \beta) = 0.5176 \left( \frac{116}{\lambda_i} - 0.4\beta - 5 \right) e^{\frac{-21}{\lambda_i}} + 0.0068\lambda$$

$$\frac{1}{\lambda_i} = \frac{1}{\lambda + 0.08\beta} - \frac{0.035}{\beta^3 + 1}$$
(3.3)

Figure 3.2 & 3.3 shows the power co-efficient vs. tip speed ratio and mechanical power vs. turbine speed characteristics curves of a typical 2MW wind turbine for various wind velocities. Wind turbine data is given in Appendix A.



Figure 3.2 Power coefficient vs. tip speed ratio for different wind speeds

From figure 3.2 it is clear that in variable speed wind turbine system, power coefficient is almost same for same pitch angle and different wind speeds. Whereas from figure 3.3, it is clear that the mechanical power  $P_m$  is having large variations in power output at different values of turbine speed and wind speed. To achieve MPPT, the variable speed wind turbine shall be operated at optimum value of turbine speed below the rated turbine speed for a given wind speed as shown in figure 3.3.

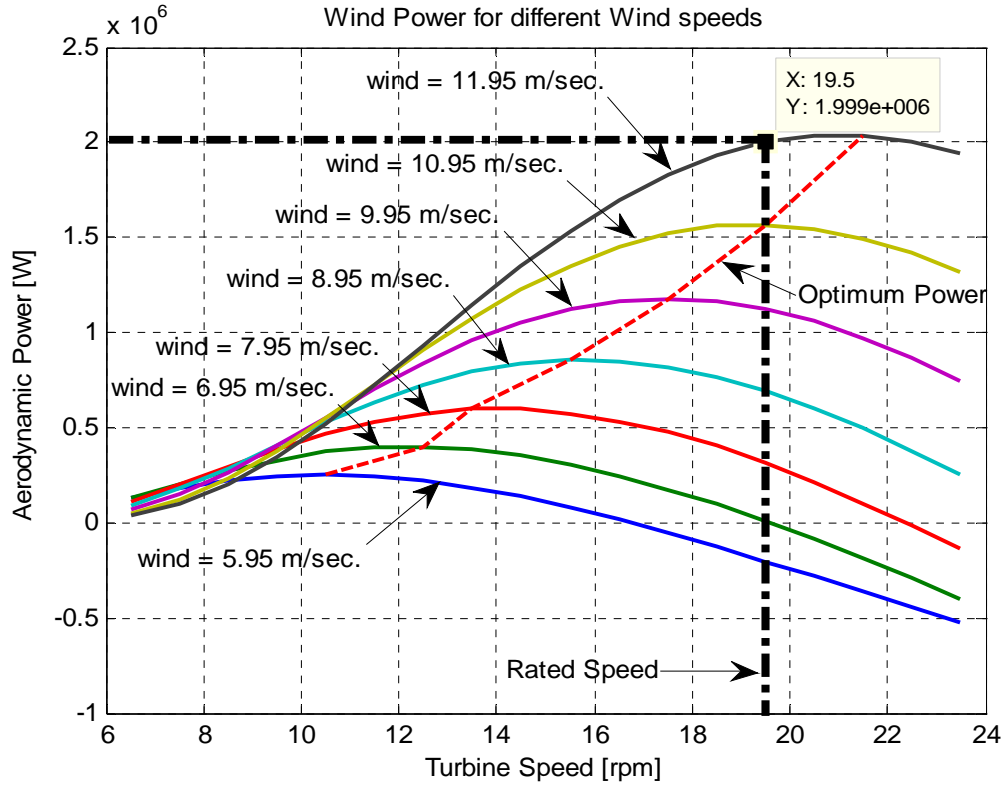


Figure 3.3 Power output vs. turbine speed characteristics of a wind turbine

For closed form dynamic representation, the turbine power output given in figure 3.3 is expressed through an analytical expression in terms of wind turbine speed ( $n_t$ ). For example, for a wind velocity of 11.95m/s the expression for the power output as a function of speed  $n_t$  (rpm) is obtained, by using Matlab function polyfit as,

$$P_m = -2.102 \times 10^{-13} n_t^6 + 1.305 \times 10^{-9} n_t^5 - 2.965 \times 10^{-6} n_t^4 + 28.750 \times 10^{-4} n_t^3 - 1.030 n_t^2 + 143.348 n_t - 4033.626$$

In general, it can be written as;

$$P_m = C_1 n_t^6 + C_2 n_t^5 + C_3 n_t^4 + C_4 n_t^3 + C_5 n_t^2 + C_6 n_t + C_7 \quad (3.4)$$

To extract maximum power, pitch angle control can also be applied at lower wind speed. Since, the power co-efficient  $C_p$  and the mechanical power  $P_m$  are function of blade pitch angle  $\beta$ , therefore by varying the pitch angle, mechanical power output can be varied as shown in figure 3.4. In this thesis pitch angle control is not considered therefore the value of angle  $\beta=0$  for the complete analysis.

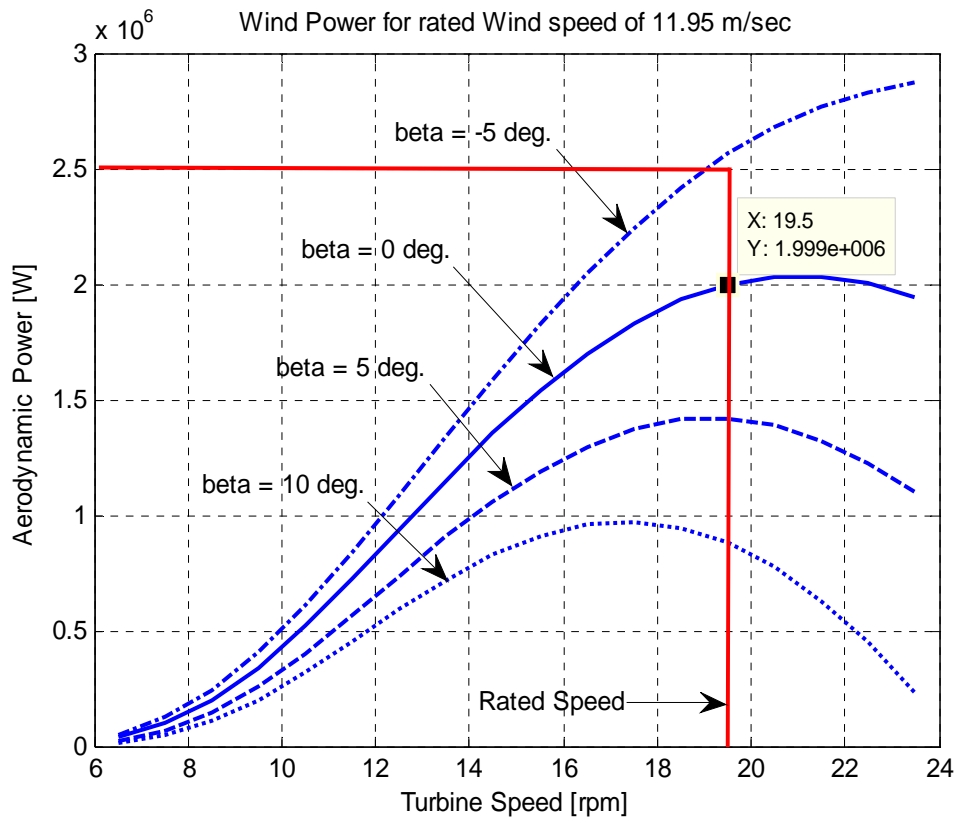


Figure 3.4 Power output vs. turbine speed characteristics for wind speed of 11.95m/sec

### 3.2 The Variable Speed PMSG Model

In this section, a non-linear model of the variable speed wind turbine-PMSG system is developed. The PMSG system model contains that of the permanent magnet generator

and its drive train system. The voltage-current-flux relationships of permanent magnet synchronous generator are written as;

$$\begin{aligned}\psi_d &= -X_d i_{gd} + X_{afd} i_{fd} \\ \psi_q &= -X_q i_{gq} \\ \psi_{fd} &= -X_{afd} i_{gd} + X_{ffd} i_{fd}\end{aligned}\tag{3.5}$$

$$\begin{aligned}V_{gd} &= -R_a i_{gd} - \omega_g \psi_q + \frac{1}{\omega_o} p(\psi_d) \\ V_{gq} &= -R_a i_{gq} + \omega_g \psi_d + \frac{1}{\omega_o} p(\psi_q)\end{aligned}\tag{3.6}$$

Here, the term  $X_{afd} i_{fd} = \psi_o$  (constant), where,  $\psi_o$  is the residual flux linkage of permanent magnet rotor. Hence, equations (3.5) & (3.6) gets modified for permanent magnet rotor as,

$$\begin{aligned}\psi_d &= -X_d i_{gd} + \psi_o \\ \psi_q &= -X_q i_{gq}\end{aligned}\tag{3.7}$$

$$\begin{aligned}V_{gd} &= -R_a i_{gd} - \omega_g \psi_q + \frac{1}{\omega_o} p(\psi_d) \\ V_{gq} &= -R_a i_{gq} + \omega_g \psi_d + \frac{1}{\omega_o} p(\psi_q)\end{aligned}\tag{3.8}$$

The equivalent circuit of a three phase permanent magnet synchronous generator considering sinusoidal flux distribution is as shown in Figure 3.5.

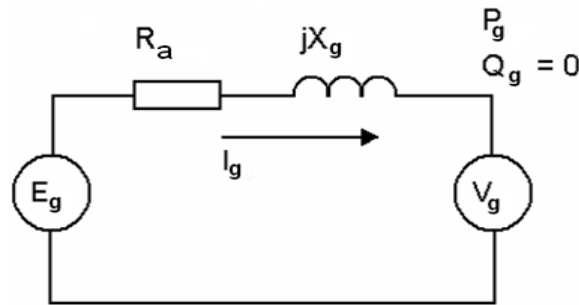


Figure 3.5 Equivalent circuit of PMSG

Substituting equation (3.7) in (3.8), we get;

$$V_{gd} = -R_a i_{gd} + \omega_g X_q i_{gq} - \frac{X_d}{\omega_o} p(i_{gd}) \quad (3.9)$$

$$V_{gq} = -\omega_g X_d i_{gd} - R_a i_{gq} + \omega_g \psi_o - \frac{X_q}{\omega_o} p(i_{gq})$$

The above can be expressed in terms of the following 2 equivalent circuits in terms of d-q quantities [7-13].

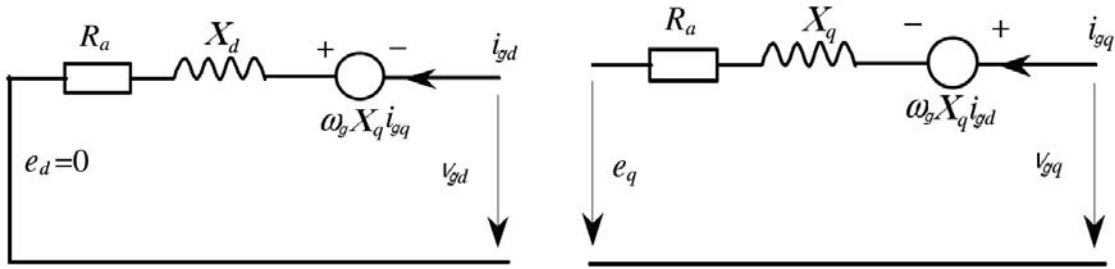


Figure 3.6 Equivalent circuit of PMSG in d-q axes.

The differential equations relating voltage and current finally are;

$$p(i_{gd}) = \frac{\omega_o}{X_d} [-R_a i_{gd} + X_q i_{gq} \omega_g - V_{gd}]$$

$$p(i_{gq}) = \frac{\omega_o}{X_q} [-X_d i_{gd} \omega_g - R_a i_{gq} + \psi_o \omega_g - V_{gq}] \quad (3.10)$$

### Drive Train Model of a Two Mass System:

The wind energy conversion system (WECS) consists of wind turbine and PMSG with their respective inertias as  $H_t$  and  $H_g$ . Both the systems are connected through the shaft having stiffness co-efficient  $K_s$  and damping coefficients  $D_t$  and  $D_g$  for turbine and generator with respect to shaft system as shown in the figure 3.7.

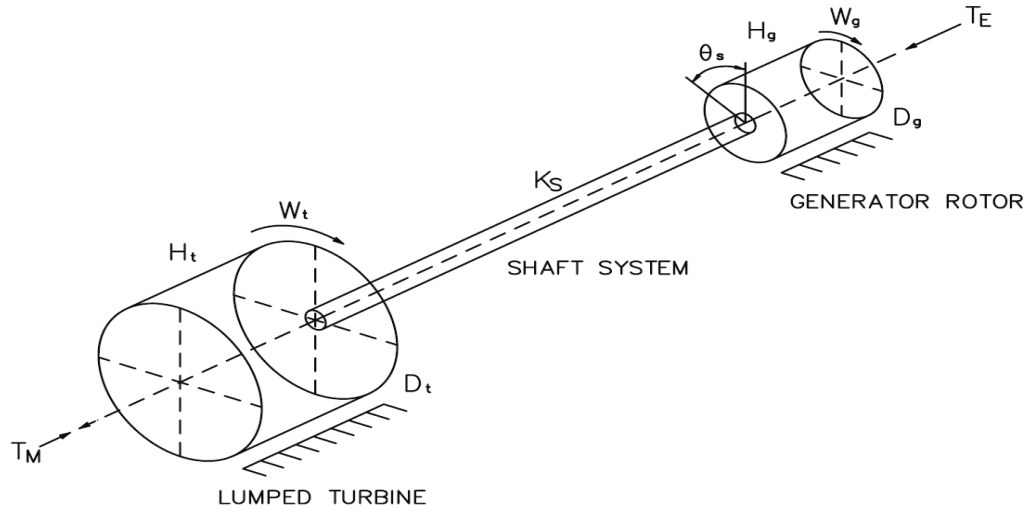


Figure 3.7 Drive train model of a two mass system

The electromechanical equation for the drive train model can be derived as 4-first order differential equations [13];

$$p(\delta) = \omega_o (\omega_g - 1) \quad (3.11)$$

$$p(\omega_g) = \frac{1}{2H_g} (K_s \theta_s - P_{ag} - D_g (\omega_g - 1))$$

$$p(\theta_s) = \omega_o (\omega_t - \omega_g) \quad (3.12)$$

$$p(\omega_t) = \frac{1}{2H_t} (P_m - K_s \theta_s - D_t (\omega_t - 1))$$

Here,  $\delta$  and  $\omega_g$  are the load angle and rotor speed of the PMSG,  $\theta_s$  is the stiffness coefficient of the shaft and  $\omega_t$  is the turbine speed.  $P_m$  is the mechanical power of wind turbine (3.4), and  $P_{ag}$  is the electrical air-gap power given as;

$$P_{ag} = (\psi_o i_{gq} + (X_q - X_d) i_{gd} i_{gq}) \omega_g \quad (3.13)$$

This can also be written as;

$$P_{ag} = V_{gd} i_{gd} + V_{gq} i_{gq} + R_a (i_{gd}^2 + i_{gq}^2) \quad (3.14)$$

### 3.3 Converter Models

The configuration of the converters in the PMSG system is shown in Figure 3.8.

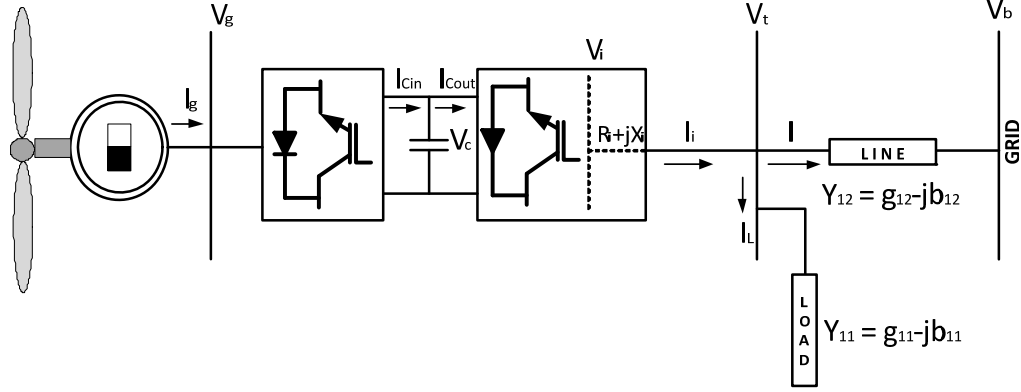


Figure 3.8 Variable Speed WT-PMSG connected to grid

Since the PMSG is directly connected to the generator side-converter system, the voltage equation can be written as;

$$V_g = m_1 V_c \alpha_1 \quad (3.15)$$

written in d-q frames, this is

$$\begin{aligned} V_{gd} &= m_1 V_c \cos \alpha_1 \\ V_{gq} &= m_1 V_c \sin \alpha_1 \end{aligned} \quad (3.16)$$

where,  $m_1$  is the modulation index of the generator side-converter system,  $\alpha_1$  is the firing angle and  $V_c$  is the DC link capacitor voltage. The equation (3.16) can be modified by replacing the firing angle ( $\alpha_1$ ) with  $(90^\circ - \delta)$  using phasor diagram as shown in Figure 3.9.

$$\begin{aligned} V_{gd} &= m_1 V_c \sin \delta \\ V_{gq} &= m_1 V_c \cos \delta \end{aligned} \quad (3.17)$$

Substituting equation (3.17) in equation (3.10), we get;



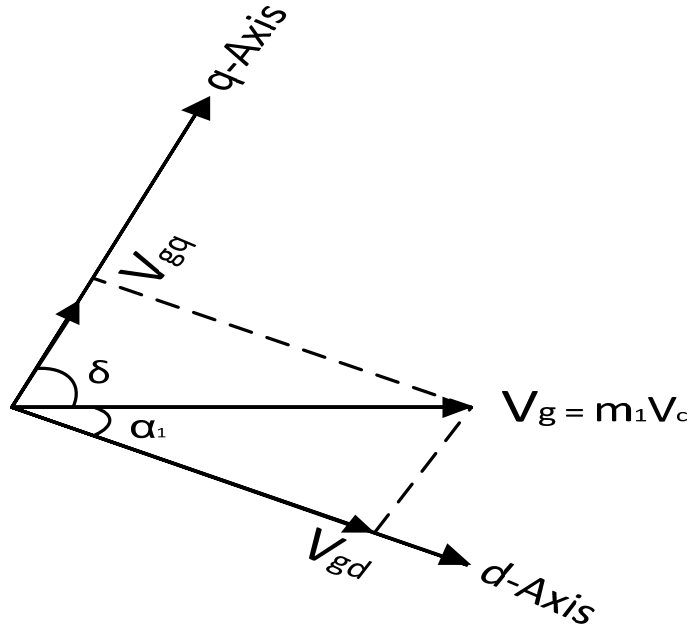


Figure 3.9 Phasor diagram of PMSG

$$p(i_{gd}) = \frac{\omega_o}{X_d} [-R_a i_{gd} + X_q i_{gq} \omega_g - m_1 V_c \sin \delta] \quad (3.18)$$

$$p(i_{gq}) = \frac{\omega_o}{X_q} [-X_d i_{gd} \omega_g - R_a i_{gq} + \psi_o \omega_g - m_1 V_c \cos \delta]$$

Now applying KVL, on the grid side-converter (inverter) system at bus  $V_i$ , as shown in figure 3.8, we get;

$$V_i = V_t + R_i I_i + \frac{X_i}{\omega_o} \cdot \frac{d}{dt}(I_i) \quad (3.19)$$

Breaking  $V_i$ ,  $V_t$ ,  $I_i$  along d-q axes rotating with synchronous frequency  $\omega_e$  at the grid side, the differential equations relating the inverter currents can be written as;

$$\begin{aligned} p(i_{id}) &= \frac{\omega_o}{X_i} [-R_i i_{id} + \omega_e X_i i_{iq} - V_{id} - V_{td}] \\ p(i_{iq}) &= \frac{\omega_o}{X_i} [-\omega_e X_i i_{id} - R_i i_{iq} + V_{iq} - V_{tq}] \end{aligned} \quad (3.20)$$

$$\text{here, } V_i = -V_{id} + jV_{iq}, \quad I_i = I_{id} + jI_{iq} \text{ and } V_t = V_{td} + jV_{tq} \quad (3.21)$$

Expressing the grid-side converter (inverter) system as,

$$V_i = m_2 V_c \alpha_2 \quad (3.22)$$

The d-q components are,

$$\begin{aligned} V_{id} &= m_2 V_c \cos \alpha_2 \\ V_{iq} &= m_2 V_c \sin \alpha_2 \end{aligned} \quad (3.23)$$

where,  $m_2$  is the modulation index of the grid side-converter (inverter) system,  $\alpha_2$  is the extinction angle of the inverter and  $V_c$  is DC link capacitor voltage.

Finally, applying KCL at the terminal voltage bus  $V_t$  of Figure 3.6, we get;

$$I_i = I_L + I = V_t \cdot Y_{11} + (V_t - V_b) \cdot Y_{12}$$

Here,  $Y_{11} = g_{11} - jb_{11}$  is the load admittance, and  $Y_{12} = g_{12} - jb_{12}$  is the transmission line admittance. Considering that the grid bus voltage is along the d-axis, the d-q components of  $V_t$  can be expressed as;

$$\begin{aligned} v_{td} &= k_1 i_{id} + k_2 i_{iq} + V_b (k_1 \cdot g_{12} - k_2 \cdot b_{12}) \\ v_{tq} &= k_3 i_{id} + k_4 i_{iq} + V_b (k_3 \cdot g_{12} - k_4 \cdot b_{12}) \end{aligned} \quad (3.24)$$

Substitution of equation (3.23) and (3.24) in equation (3.20), gives;

$$\begin{aligned} p(i_{id}) &= \frac{\omega_o}{X_i} \left[ -(R_i + k_1) i_{id} + (\omega_e X_i - k_2) i_{iq} - m_2 V_c \cos \alpha_2 - V_b (k_1 g_{12} - k_2 b_{12}) \right] \\ p(i_{iq}) &= \frac{\omega_o}{X_i} \left[ -(\omega_e X_i + k_3) i_{id} - (R_i + k_4) i_{iq} + m_2 V_c \sin \alpha_2 - V_b (k_3 g_{12} - k_4 b_{12}) \right] \end{aligned} \quad (3.25)$$

The expressions for  $k_1$ ,  $k_2$ ,  $k_3$  &  $k_4$  and derivation of equation (3.24) are presented in detail in Appendix B.

### DC Link Capacitor:

The transfer of real power from the generator into the grid can be realized through the DC-link by keeping its voltage constant. The current in the DC-link is discontinuous as it is switched on or off with respect to the switching frequency of the converter. This process induces voltage ripples in the DC-link capacitor which can be made small to the extent that the voltage appears virtually constant during switching period by selecting a large value of capacitor. On the other hand a small capacitor enables fast control of the DC-link voltage. Hence the selection of the size of the capacitor has to be a trade-off between the voltage ripples and fast changes in DC voltage. From the Figure 3.8, it can be seen that the dc power through the capacitor is,

$$P_{DC} = V_c \left[ C \frac{d}{dt} (V_c) \right] \quad (3.26)$$

If the converters are assumed to be lossless, we can write,

$$P_{DC} = P_{C_{in}} + P_{C_{out}} \quad (3.27)$$

where;

$$\begin{aligned} P_{cin} &= V_{gd} i_{gd} + V_{gq} i_{gq} \\ P_{cout} &= -V_{id} i_{id} + V_{iq} i_{iq} \end{aligned} \quad (3.28)$$

Substituting equation (3.26) and (3.28) in (3.27), we get;

$$V_c C p(V_c) = [V_{gd} i_{gd} + V_{gq} i_{gq} - V_{id} i_{id} + V_{iq} i_{iq}]$$

Substituting the expressions for  $V_{gd}$ ,  $V_{gq}$  and  $V_{id}$ ,  $V_{iq}$  in the above equation yields;

$$p(V_c) = \frac{1}{C} [m_1 i_{gd} \sin \delta + m_1 i_{gq} \cos \delta - m_2 i_{id} \cos \alpha_2 + m_2 i_{iq} \sin \alpha_2] \quad (3.29)$$

### 3.4 The STATCOM Controller Model

Static Synchronous Compensator (STATCOM), was proposed by Gyugi [44] in 1998, which use turn off devices like GTOs. STATCOM, previously known as STATCON or static condenser, is an advanced Static Var Compensator (SVC) using voltage source converters which in general, converts an input dc voltage into a three phase ac output voltage at fundamental frequency, with rapidly controllable amplitude and phase angle. In addition to this, the controller has a coupling transformer and dc capacitor. The control system can be designed to maintain the magnitude of the bus voltage constant by controlling the amplitude and / or the phase shift of the VSC output voltage [51-53]. The general arrangement of STATCOM is shown in Fig 3.10. As compared to conventional SVC, STATCOM does not require expensive large inductors, moreover it can also operate as reactive power sink or source flexibly, which makes STATCOM more attractive [18, 19, 45].

This research includes a STATCOM voltage source controller for control of transients arising out of electrical or mechanical phenomenon. Modelings were made with the STATCOM controller located on the generator side-converter and also on the grid side-converter independently as depicted in the Figures 3.11 and 3.12 respectively.

In general, the connection of the STATCOM to the PMSG system at bus having voltage  $V_x \angle \Theta_x$ , is shown in Figure 3.10. Here,  $V_x$  can either be the generator terminal voltage  $V_g$  or the load bus voltage  $V_t$ . The STATCOM is modeled as a controllable voltage source which supplies the reactive power by varying the modulation index ( $m_{st}$ ) of the

VSC. The storage capacitor can cater for limited real power through the variation of the phase angle ( $\psi_{st}$ ). Hence, the general expression for the two cases will be;

$$V_x = |V_x| \angle \Theta_x \quad (3.30)$$

The output voltage of the voltage source converter in terms of modulation index and phase angle can be written as;

$$V_{st} = m_{st} V_{dc} \angle \psi_{st} \quad (3.31)$$

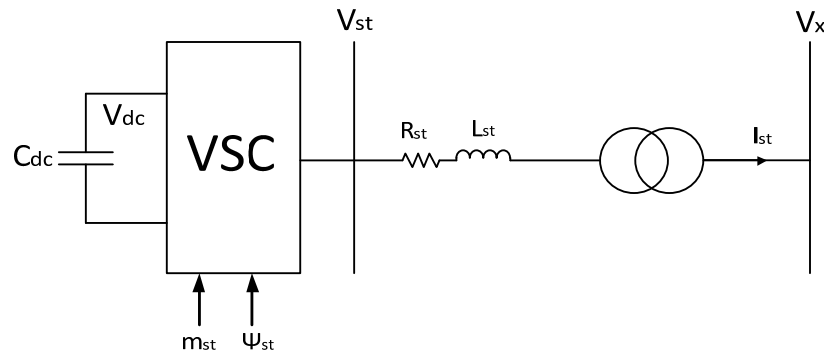


Figure 3.10 Basic Model of the STATCOM Controller

Breaking the voltage in d-q components, we get;

$$\begin{aligned} \therefore V_{std} &= m_{st} V_{dc} \cos \psi_{st} \\ V_{stq} &= m_{st} V_{dc} \sin \psi_{st} \end{aligned} \quad (3.32)$$

Applying KVL at the terminal of the VSC gives;

$$V_{st} = V_x + R_{st} I_{st} + \frac{L_{st}}{\omega_o} \cdot \frac{d}{dt} (I_{st}) \quad (3.33)$$

$$\text{Where, } V_{st} = V_{std} + jV_{stq}, \quad I_{st} = i_{std} + ji_{stq} \quad \text{and} \quad V_x = V_{xd} + jV_{xq} \quad (3.34)$$

Here,  $R_{st}$  and  $L_{st}$  are the resistance and inductance of the STATCOM;  $V_{st}$  and  $I_{st}$  are the STATCOM output voltage and output current respectively.

Breaking the voltages and currents into d-q components and normalizing we can get,

$$\begin{aligned} V_{std} &= R_{st} i_{std} - \omega_x L_{st} i_{stq} + \frac{L_{st}}{\omega_o} p(i_{std}) + V_{xd} \\ V_{stq} &= \omega_x L_{st} i_{std} + R_{st} i_{stq} + \frac{L_{st}}{\omega_o} p(i_{stq}) + V_{xq} \end{aligned} \quad (3.35)$$

Substituting the expression for  $V_{std}$  and  $V_{stq}$  from (3.32) in equation (3.35), we get;

$$\begin{aligned} p(i_{std}) &= \frac{\omega_o}{L_{st}} \left[ -R_{st} i_{std} + \omega_x L_{st} i_{stq} + m_{st} V_{dc} \cos(\psi_{st}) - V_{xd} \right] \\ p(i_{stq}) &= \frac{\omega_o}{L_{st}} \left[ -\omega_x L_{st} i_{std} - R_{st} i_{stq} + m_{st} V_{dc} \sin(\psi_{st}) - V_{xq} \right] \end{aligned} \quad (3.36)$$

If the STATCOM is located on the generator side  $V_{xd}$  and  $V_{xq}$  will be replaced by  $V_{gd}$  and  $V_{gq}$  respectively, and equation (3.36) will be written as;

$$\begin{aligned} p(i_{std}) &= \frac{\omega_o}{L_{st}} \left[ -R_{st} i_{std} + \omega_g L_{st} i_{stq} + m_{st} V_{dc} \cos(\psi_{st}) - m_l V_c \sin \delta \right] \\ p(i_{stq}) &= \frac{\omega_o}{L_{st}} \left[ -\omega_g L_{st} i_{std} - R_{st} i_{stq} + m_{st} V_{dc} \sin(\psi_{st}) - m_l V_c \cos \delta \right] \end{aligned} \quad (3.37)$$

Similarly, if the STATCOM is located at the load side, state equation (3.36) will take the form,

$$\begin{aligned} p(i_{std}) &= \frac{\omega_o}{L_{st}} \left[ -k_1 i_{id} - k_2 i_{iq} - R_{st} i_{std} + \omega_e L_{st} i_{stq} + m_{st} V_{dc} \cos(\psi_{st}) - V_b (k_1 g_{12} - k_2 b_{12}) \right] \\ p(i_{stq}) &= \frac{\omega_o}{L_{st}} \left[ -k_3 i_{id} - k_4 i_{iq} - \omega_e L_{st} i_{std} - R_{st} i_{stq} + m_{st} V_{dc} \sin(\psi_{st}) - V_b (k_3 g_{12} - k_4 b_{12}) \right] \end{aligned} \quad (3.38)$$

Note that here angular frequency is given as  $\omega_e$  (grid frequency) instead of  $\omega_t$  from the definition given above, because  $\omega_t$  is denoted as another state variable (turbine speed).

Proceeding in a similar way as the PMSG converter DC link voltage equation, the Power balance on the STATCOM DC link capacitor gives,

$$V_{dc} \left[ C_{dc} \frac{d}{dt} (V_{dc}) \right] = - \left[ V_{std} i_{std} + V_{stq} i_{stq} \right]$$

this can be simplified as;

$$p(V_{dc}) = -\frac{m_{st}}{C_{dc}} [\cos\psi_{st} i_{std} + \sin\psi_{st} i_{stq}] \quad (3.39)$$

### 3.5 Non Linear Model of the Composite System

From the component models developed, the composite dynamic model of the PMSG wind turbine including the wind system, the permanent magnet generator, the drive train system, the PMSG converters, the load, transmission line and STATCOM controller can

be written as,  $\dot{x} = f[x, u]$  (3.40)

where, x is the state vector,  $[i_{gd} \ i_{gq} \ \delta \ \omega_g \ \theta_s \ \omega_t \ V_c \ i_{id} \ i_{iq} \ i_{std} \ i_{stq} \ V_{dc}]$

And u is the vector of converter controls  $[m_1 \ m_2 \ \alpha_2 \ m_{st} \ \psi_{st}]$

The non-linear model with STATCOM on the generator side-converter as shown in figure 3.9, is obtained by combining differential equations (3.11 - 3.14); (3.18); (3.25); (3.29); (3.37) & (3.39), forming the 12<sup>th</sup> order model.

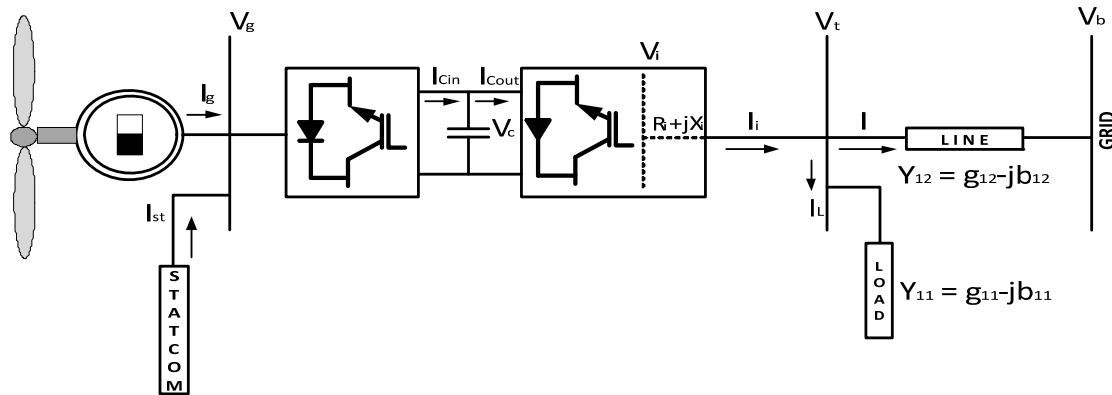


Figure 3.11 Variable Speed WT-PMSG with STATCOM on generator side-converter

The complete model is reproduced as;

$$\begin{aligned}
p(i_{gd}) &= \frac{\omega_o}{X_d} [-R_a i_{gd} + X_q i_{gq} \omega_g - m_1 V_c \sin \delta] \\
p(i_{gq}) &= \frac{\omega_o}{X_q} [-X_d i_{gd} \omega_g - R_a i_{gq} + \psi_o \omega_g - m_1 V_c \cos \delta] \\
p(\delta) &= \omega_o (\omega_g - 1) \\
p(\omega_g) &= \frac{1}{2H_g} [K_s \theta_s - P_{ag} - D_g (\omega_g - 1)] \\
p(\theta_s) &= \omega_o (\omega_t - \omega_g) \\
p(\omega_t) &= \frac{1}{2H_t} [P_m - K_s \theta_s - D_t (\omega_t - 1)] \\
p(V_c) &= \frac{1}{C} [m_1 (i_{gd} + i_{std}) \sin \delta + m_1 (i_{gq} + i_{stq}) \cos \delta - m_2 i_{id} \cos \alpha_2 + m_2 i_{iq} \sin \alpha_2] \\
p(i_{id}) &= \frac{\omega_o}{X_i} [-(R_i + k_1) i_{id} + (\omega_e X_i - k_2) i_{iq} - m_2 V_c \cos \alpha_2 - V_b (k_1 g_{12} - k_2 b_{12})] \\
p(i_{iq}) &= \frac{\omega_o}{X_i} [-(\omega_e X_i + k_3) i_{id} - (R_i + k_4) i_{iq} + m_2 V_c \sin \alpha_2 - V_b (k_3 g_{12} - k_4 b_{12})] \\
p(i_{std}) &= \frac{\omega_o}{L_{st}} [-R_{st} i_{std} + \omega_g L_{st} i_{stq} + m_{st} V_{dc} \cos \psi_{st} - m_1 V_c \sin \delta] \\
p(i_{stq}) &= \frac{\omega_o}{L_{st}} [-\omega_g L_{st} i_{std} - R_{st} i_{stq} + m_{st} V_{dc} \sin \psi_{st} - m_1 V_c \cos \delta] \\
p(V_{dc}) &= -\frac{m_{st}}{C_{dc}} [\cos \psi_{st} i_{std} + \sin \psi_{st} i_{stq}] \tag{3.41}
\end{aligned}$$

The Non-linear model with the STATCOM on the load side-converter as shown in figure 3.10 is obtained by combining differential equations (3.11 – 3.14); (3.18); (3.25); (3.29); (3.38)& (3.39), forming the 12<sup>th</sup> order model to give the closed form state equations as;



$$p(i_{gd}) = \frac{\omega_o}{X_d} [-R_a i_{gd} + X_q i_{gq} \omega_g - m_1 V_c \sin \delta]$$

$$p(i_{gq}) = \frac{\omega_o}{X_q} [-X_d i_{gd} \omega_g - R_a i_{gq} + \psi_o \omega_g - m_1 V_c \cos \delta]$$

$$p(\delta) = \omega_o (\omega_g - 1)$$

$$p(\omega_g) = \frac{1}{2H_g} [K_s \theta_s - P_{ag} - D_g (\omega_g - 1)]$$

$$p(\theta_s) = \omega_o (\omega_t - \omega_g)$$

$$p(\omega_t) = \frac{1}{2H_t} [P_m - K_s \theta_s - D_t (\omega_t - 1)]$$

$$p(V_c) = \frac{1}{C} [m_1 i_{gd} \sin \delta + m_1 i_{gq} \cos \delta - m_2 i_{id} \cos \alpha_2 + m_2 i_{iq} \sin \alpha_2]$$

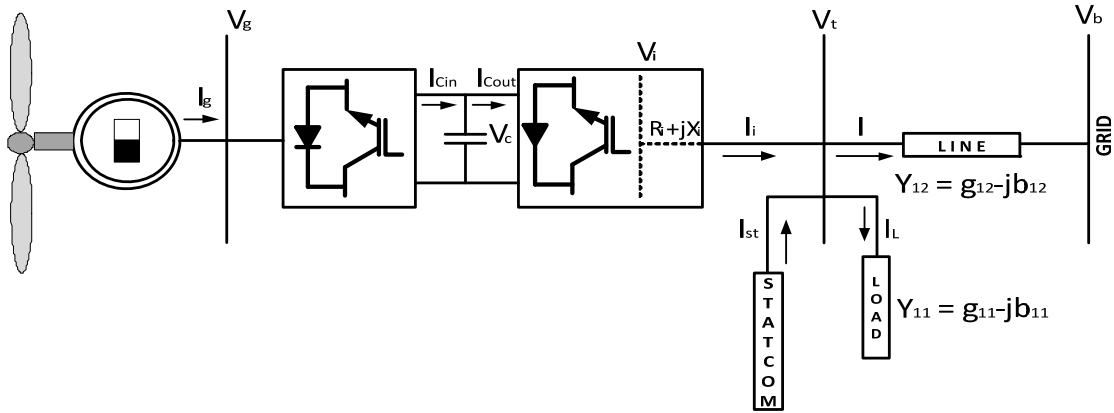


Figure 3.12 Variable Speed WT-PMSG with STATCOM on grid side-converter

$$p(i_{id}) = \frac{\omega_o}{X_i} [- (R_i + k_1) i_{id} + (\omega_e X_i - k_2) i_{iq} - m_2 V_c \cos \alpha_2 - k_1 i_{std} - k_2 i_{stq} - V_b (k_1 g_{12} - k_2 b_{12})]$$

$$p(i_{iq}) = \frac{\omega_o}{X_i} [- (\omega_e X_i + k_3) i_{id} - (R_i + k_4) i_{iq} + m_2 V_c \sin \alpha_2 - k_3 i_{std} - k_4 i_{stq} - V_b (k_3 g_{12} - k_4 b_{12})]$$

$$p(i_{std}) = \frac{\omega_o}{L_{st}} [-k_1 i_{id} - k_2 i_{iq} - R_{st} i_{std} + \omega_e L_{st} i_{stq} + m_{st} V_{dc} \cos \psi_{st} - V_b (k_1 \cdot g_{12} - k_2 \cdot b_{12})]$$

$$p(i_{stq}) = \frac{\omega_o}{L_{st}} [-k_3 i_{id} - k_4 i_{iq} - \omega_e L_{st} i_{std} - R_{st} i_{stq} + m_{st} V_{dc} \sin \psi_{st} - V_b (k_3 \cdot g_{12} - k_4 \cdot b_{12})]$$

$$p(V_{dc}) = -\frac{m_{st}}{C_{dc}} [\cos \psi_{st} i_{std} + \sin \psi_{st} i_{stq}] \quad (3.42)$$

### 3.6 Linearized Variable Speed PMSG System model

The linear model of the PMSG-STATCOM system is required for control design purposes as will be shown in the following chapters. The system equations of the linearized model are written as

$$\Delta \dot{\mathbf{x}} = \mathbf{A} \Delta \mathbf{x} + \mathbf{B} \Delta \mathbf{u}; \quad ( 3.43 )$$

where,  $\Delta \mathbf{x}$  is the perturbation or change in the original state variable  $\mathbf{X}$ . Note the matrices  $\mathbf{A}$ ,  $\mathbf{B}$  will be different depending on the location of the STATCOM controller. Appendix C to E gives the details of the derivation of the  $\mathbf{A}$  &  $\mathbf{B}$  matrices for the STATCOM located at the generator as well as grid side of the PMSG system.

## CHAPTER 4

### SMALL SIGNAL ANALYSIS AND CONTROL DESIGN

This chapter identifies the various available controls of the PMSG system including the converters and STATCOM device in terms of their damping behavior. A small signal analysis is carried out to find out the stability behavior of the system as the system output changes. Control design is carried out with the best stabilizing signal for the control input identified.

#### 4.1 Small Signal Analysis

The small signal analysis starts with the linearized system equations (3.43). For an appropriate output variable  $y$ , the linearized system equations are expressed in the form,

$$\begin{aligned} \dot{x} &= Ax + Bu \\ y &= Cx + Du \end{aligned} \quad (4.1)$$

Small signal analysis is used to determine the frequency response of the system for control design and identifies damping characteristics associated with them, if any. In the previous chapter of section 3.5, non-linear model of the composite system for two different configurations were developed as shown in figure 3.11 & 3.12. In this section we will use the linearized model of the composite system given in appendix C to E, for performing small signal analysis. Eigen values will be obtained for three cases;

- (a) Without STATCOM
- (b) With STATCOM on generator side-converter and
- (c) With STATCOM on grid side-converter.

For the study analysis nominal loading of the variable speed wind turbine PMSG system is taken as 65% for a nominal wind velocity of 11.95 m/sec with a load of 100% operating at a steady state grid bus voltage of 1.03 p.u. All the system parameters for the composite system are given in Appendix A. The Eigen values of the variable speed PMSG system with / without STATCOM are presented in Tables (4.1- 4.3).

Table 4.1 Eigen values of the variable speed PMSG system without STATCOM.

<i>PMSG</i>	<i>Real part</i>	<i>Imaginary Part</i>
	-316.46	$\pm 886.91i$
	+0.00	$\pm 28.48i$
	-0.05	$\pm 3.73i$
	-1.57	0
	-5.21	$\pm 315.05i$

Table 4.2 Eigen values of the variable speed PMSG with STATCOM on generator side-converter.

<i>PMSG</i>	<i>Real part</i>	<i>Imaginary Part</i>
	-316.46	$\pm 886.92i$
	+0.33	$\pm 53.74i$
	-0.08	$\pm 3.9i$
	-1.68	0
	-5.19	$\pm 315.06i$
<i>STATCOM</i>	-21.21	$\pm 314.09i$
	-0.01	

Table 4.3 Eigen values of the variable speed PMSG with STATCOM on grid side-converter.

<b><i>PMSG</i></b>	<b><i>Real part</i></b>	<b><i>Imaginary Part</i></b>
	-503	$\pm 1266.8i$
	-0.0	$\pm 28.5i$
	-0.10	$\pm 3.7i$
	-1.3	0
	-5.3	$\pm 315i$
<b><i>STATCOM</i></b>	-24.9	$\pm 316.2i$
	-0.0	

The Eigen values identified as critical in terms of their location from  $j\omega$  axis for a nominal loading of 0.65 p.u. are given in Table 4.4 as shown below.

Table 4.4 Critical Modes for a nominal loading of 0.65 p.u.

<b>Eigen value values</b>	<b>Component</b>	<b>Modes</b>
$+0.00 \pm 28.48i$	PMSG, WITHOUT STATCOM	Electromechanical modes
$+0.33 \pm 53.74i$	PMSG, WITH STATCOM on generator side-converter	Electromechanical modes
$-0.0 \pm 28.5i$	PMSG, WITH STATCOM on grid side- converter	Electromechanical modes

Figure 4.1 shows the variation of the real part of the dominant eigen value of the variable speed wind turbine PMSG system, when the power output is varied from 0.1 to 1.2 p.u. and wind power contribution is changed by a disturbance of 0.15 p.u. respectively. This is done for three cases as mentioned below;

(a) Without STATCOM;

(b) With STATCOM on generator side-converter and

(c) With STATCOM on grid side-converter.

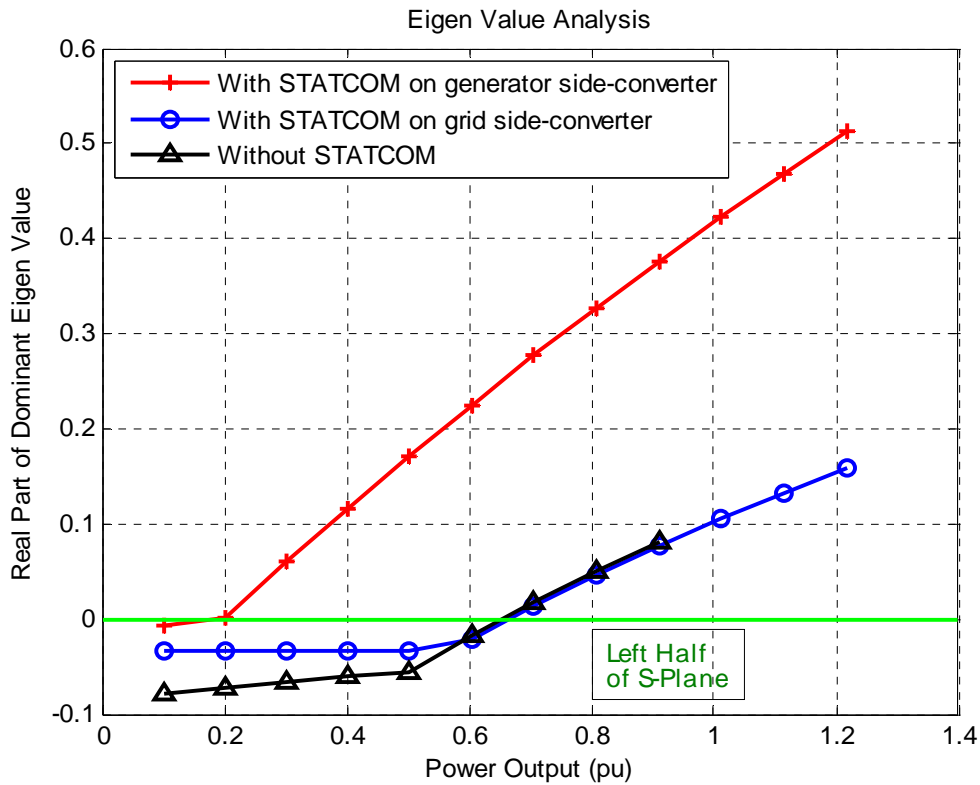


Figure 4.1 Dominant Eigen values of Variable Speed PMSG system for case (a), (b) & (c).

Hence, from this section we conclude that;

- Variable speed wind turbine PMSG system without STATCOM controller is within the stability limit up to 0.6 p.u loading and marginally stable at a nominal loading of 0.65 p.u. as shown figure 4.1 and Table 4.4.

- When STATCOM controller is located at grid side-converter (inverter) the system is within the stability limit up to nominal loading of 0.65 p.u. as shown in figure 4.1 and Table 4.4.
- When STATCOM controller is located at generator side-converter (rectifier) the system is unstable from 0.1p.u.onwards, as shown in figure 4.1 and Table 4.4.

Since for low power outputs the STATCOM on the grid side-converter show better stability behavior, it is ideal to locate on this side. The ideality of the location is further explored through decomposition techniques given below.

## 4.2 Evaluation of Damping Controls

The 5 converter control variables  $[m_1 \ m_2 \ \alpha_2 \ m_{st} \ \psi_{st}]$  identified in previous chapter are evaluated in terms of their effectiveness in providing damping to the PMSG system. The methods employed for the evaluation processes are *singular value decomposition* (SVD), *Hankel singular value* (HSV), and the *residue* method. The analysis also suggests the prospective signals which can be employed in the damping controller. These are briefly outlined below followed by simulation results.

### 4.2.1 Singular Value Decomposition

For an  $m \times n$  matrix  $G$ , the singular value decomposition (SVD) of  $G$  is the factorization,

$$G = U \Sigma V^{*T} \quad (4.2)$$

where,

$$\Sigma = \begin{bmatrix} \Sigma_1 & 0 \\ 0 & 0 \end{bmatrix}$$

is an  $m \times n$  matrix and  $\Sigma_1$  is defined as,

$$\Sigma_1 = \begin{bmatrix} \sigma_1 & 0 & \cdot & 0 \\ 0 & \sigma_2 & \cdot & 0 \\ \cdot & \cdot & \cdot & \cdot \\ 0 & 0 & 0 & \sigma_r \end{bmatrix} \quad (4.3)$$

The singular values  $\sigma_1, \sigma_2 \dots \sigma_r$  are placed in descending order with  $r = \min\{m, n\}$ . U and V are unitary matrices; V are the right singular vectors and U are the left singular vectors[54, 55]. The maximum singular value of G ( $\sigma_1$ ) shows the largest gain for any input direction, while the smallest singular value ( $\sigma_r$ ) is a useful controllability measure showing the smallest gain for any input direction. It is desired that the minimum singular values be as large as possible when selecting between different input output variables[47].

For the linearized system model (4.1), the SVD of the matrix  $G = [A - \lambda I \ B]$ ; where  $B = [b_1 \ b_2 \ b_3 \ b_4 \ b_5]$  is to be carried out for each  $b_i$ . Here, the 12 Eigen values of the A matrix for a nominal loading of 65% are given in Table 4.2 & 4.3. The parameters of the variable speed wind turbine PMSG system are included in *Appendix-A*. The first pair of complex conjugate eigen values is contributed by the generator circuits, while second & third pair is from the drive-train model and fourth one from the DC link while the fifth pair arising from the grid side converter circuit and the last two pairs are from the STATCOM controller. The minimum singular value  $\sigma_{\min}$  of the matrix  $[\lambda_i I - A \ b_i]$  indicates the



capability of the  $i^{th}$  input to the lightly damped mode  $\lambda_i$ . The higher  $\sigma_{\min}$  the higher is the controllability of this mode for the input considered.

Figure 4.2 and 4.3 shows the plot of minimum singular value  $\sigma_{\min}$  for the 5 control variables  $[m_1 \ m_2 \ \alpha_2 \ m_{st} \ \psi_{st}]$  against a number of values of generator loading points. The firing angle of the STATCOM ( $\psi_{st}$ ) has the highest minimum singular value when STATCOM is connected at generator side-converter as shown in Figure 4.2, whereas from Figure 4.3 it can be observed that the minimum singular values of the modulation index of the generator-side converter ( $m_1$ ), however are significantly large compared to the other ones for each loading condition, suggesting this to be the most effective converter damping control when STATCOM is connected at grid side-converter.

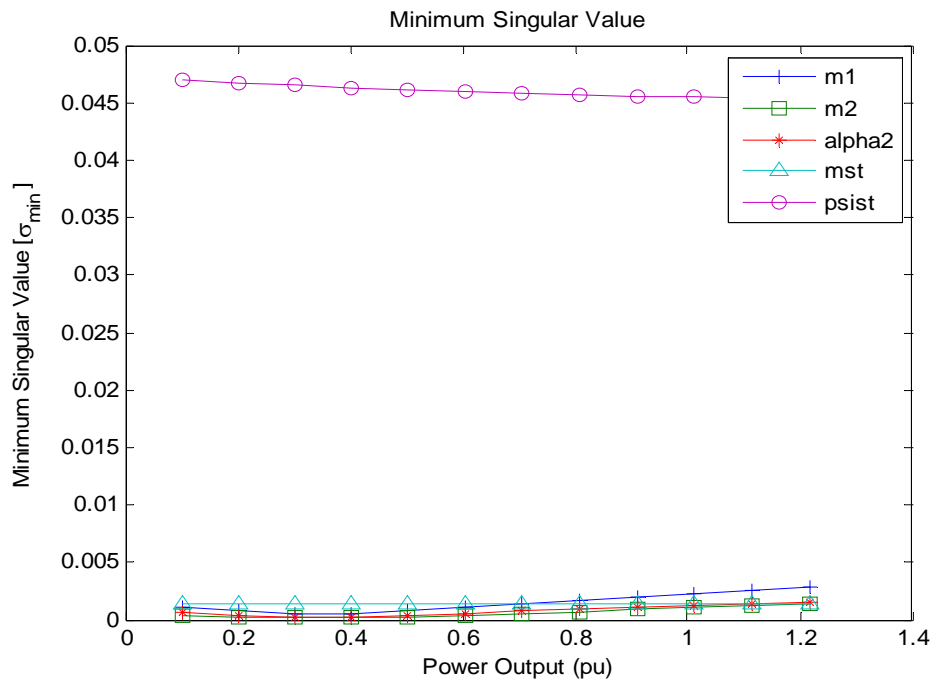


Figure 4.2 Minimum singular values for various controls as a function of generator output, when STATCOM is connected at generator side-converter

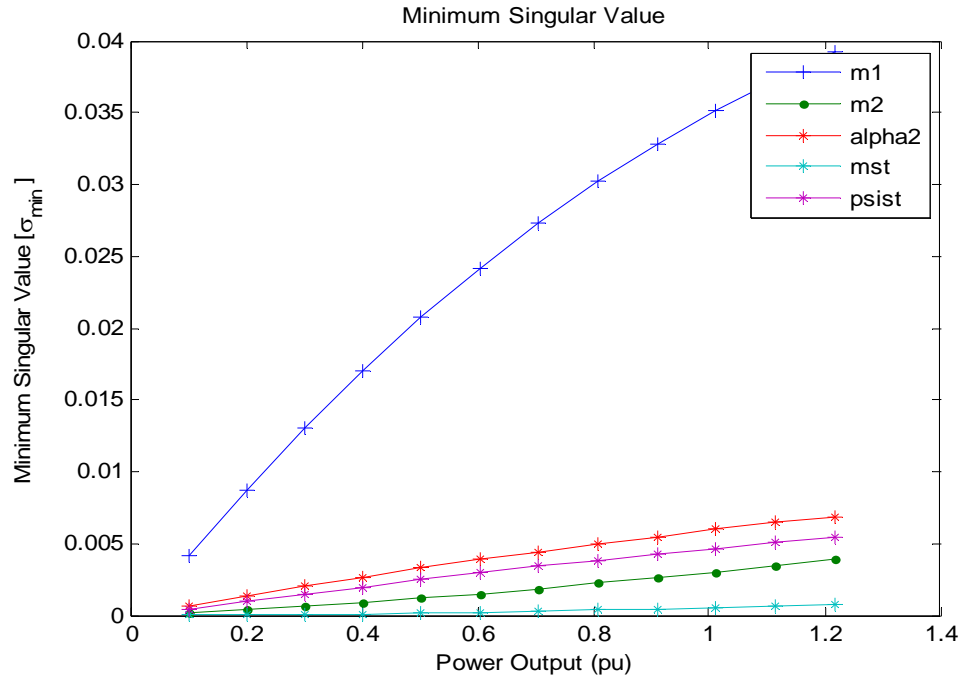


Figure 4.3 Minimum singular values for various controls as a function of generator output, when STATCOM is connected at grid side-converter

From the study of the minimum singular value, the following were observed.

- When STATCOM is connected at generator side-converter, then  $\psi_{st}$  has the largest damping content for different power loadings.
- The order of the other signals in terms of damping contribution is  $m_{st}$ ,  $m_1$ ,  $\alpha_2$  and  $m_2$ .
- When STATCOM is connected at grid side-converter, then rectifier modulation index ( $m_1$ ) has the largest damping content for different power loadings.
- The order of the other signals in terms of damping contribution is  $\alpha_2$ ,  $\psi_{st}$ ,  $m_2$  and  $m_{st}$ .

## 4.2.2 Hankel Singular Value Decomposition

The results obtained in the previous section using the singular value decomposition analysis can be verified with another decomposition technique known as hankel singular value decomposition for identifying the controllability of the inputs. Hankel singular values provide a measure of energy for a state in the system[55, 56]. It is the basis for the balanced model reduction, in which high energy states are retained, while the low energy states are discarded. For the linearized system equation of (4.1) hankel singular value (HSV) of the system can be obtained from the controllability and observability gramians.

The linear controllability gramian for pair (A, B) is defined as,

$$W_c = \int_0^{\infty} e^{At} B B^T e^{A^T t} dt \quad (4.4)$$

If the system is stable & controllable then the controllability gramian will have full rank.

The linear observability gramian for pair (A, C) is defined as,

$$W_o = \int_0^{\infty} e^{At} C C^T e^{A^T t} dt \quad (4.5)$$

For stable and observable systems the observability gramian will have full rank n. The linear gramians  $W_c$  and  $W_o$  are the unique positive definite solutions of the lyapunov equations,

$$\begin{aligned} A W_c + W_c A^T &= - B B^T \\ A^T W_o + W_o A &= - C^T C \end{aligned} \quad (4.6)$$

The Hankel singular value  $\sigma_i$  is an observability-controllability index, defined as,

$$\sigma_i = \sqrt{\lambda_i(W_c W_o)} \quad i=1,2,\dots,n \quad (4.7)$$

this reflects the joint controllability and observability of the states of a system where  $\lambda_i(WcWo)$  is the  $i$ -th eigen value of  $WcWo$ . Hankel singular values measure the contribution of each state to evaluate the input/output behavior of the linear system. Choosing different input and output signals, the HSV can be calculated for each combination of input and output; the candidate with the largest HSV shows better controllability and observability properties. Actually, the larger the hankel singular value, the higher the energy contained by that state.

Figure 4.4 shows the variation of the HSV indices for the 5 control variables against the states of the system corresponding to the 12 Eigen values. The states are arranged as defined in section 3.6 for all the inputs. As in the case of SVD, the HSV for modulation index of STATCOM ( $m_{st}$ ) is largest when STATCOM is connected at generator side-converter.

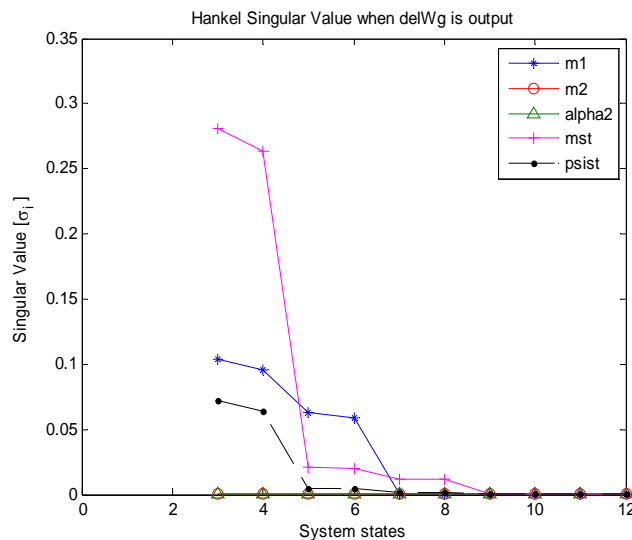


Figure 4.4 Hankel singular value indices for the 5 converter controls with  $\Delta\omega_g$  as output when STATCOM is connected at generator side-converter

Figure 4.5 shows the variation of the HSV indices for the 5 control variables against the states of the system corresponding to the 12 Eigen values. As in the case of SVD, the HSV for modulation index of rectifier ( $m_1$ ) is largest when STATCOM is connected at grid side-converter.

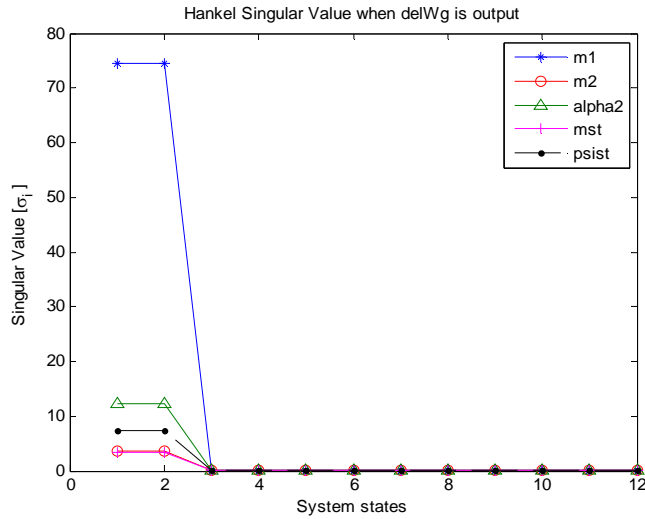


Figure 4.5 Hankel singular value indices for the 5 converter controls with  $\Delta\omega_g$  as output when STATCOM is connected at grid side-converter

### 4.2.3 Residue Method:

Using the residue principles of the linearized system, feedback control signals which have the higher potential for providing damping can be identified and controller structures designed. Consider that the controller is located at the feedback path in the plant configuration as shown in Fig. 4.6.  $K$  is the overall gain of the feedback circuit. The plant transfer function of the SISO system (4.1), assuming  $D=0$  is,

$$G_p(s) = C(sI - A)^{-1}B \quad (4.8)$$

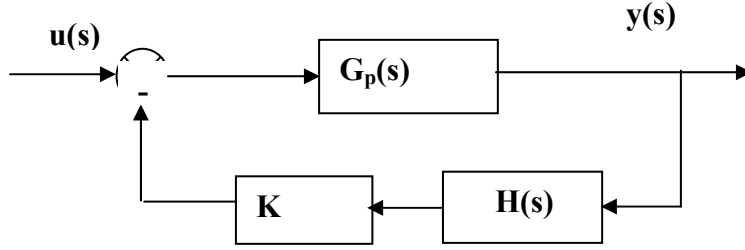


Figure 4.6 Location of controller in the plant

The transfer function  $G_p(s)$  can be expanded in partial fraction in terms of B and C matrices, right eigenvectors  $V_i$ , and the left eigenvectors  $U_i$  as;

$$G(s) = \sum_{i=1}^n \frac{CV_iU_iB}{(s - \lambda_i)} = \sum_{i=1}^n \frac{R_i}{(s - \lambda_i)} \quad (4.9)$$

The residue  $R_i$  of a particular mode  $i$  gives a measure of that mode's sensitivity to the feedback between the output  $y$  and input  $u$ . The residue associated with an eigen value  $\lambda_i$  and feedback transfer function  $KH(s)$  are related by [57],

$$\frac{\partial \lambda_i}{\partial K} = R_i \frac{\partial [KH(\lambda_i)]}{\partial K} = R_i H(\lambda_i) \quad (4.10)$$

For small changes of gain  $K$ , the above can be written as,

$$\Delta \lambda_i = R_i [KH(\lambda_i)] \quad (4.11)$$

This indicates that the controller is most effective in damping mode  $i$  if an input is chosen so that  $R_i$  is maximum. Therefore, the signal with highest observability is chosen as input to the controller. The change in eigen value must be directed to the left half complex  $\lambda$ -plane. Figure 4.7 shows the plot of the residues against the state numbers of the variable speed wind turbine PMSG system with STATCOM on generator side-converter when  $\Delta \omega_g$  is taken as output signal whereas figure 4.8 shows the plot of residues when STATCOM is connected at grid side-converter when  $\Delta \omega_g$  is taken as output signal.

Figure 4.7 gives us two information: a) the phase angle of STATCOM ( $\psi_{st}$ ), exhibiting the largest residue properties will influence the behavior of the mode of oscillation corresponding to eigen value # 3 and #4 ( $+0.33 \pm j53.74$ ) and b) the feedback input signal should be the one corresponding to the eigen value of state #4, which is the generator speed variation ( $\Delta\omega_g$ ) of the variable speed wind turbine PMSG system when STATCOM is connected at generator side-converter.

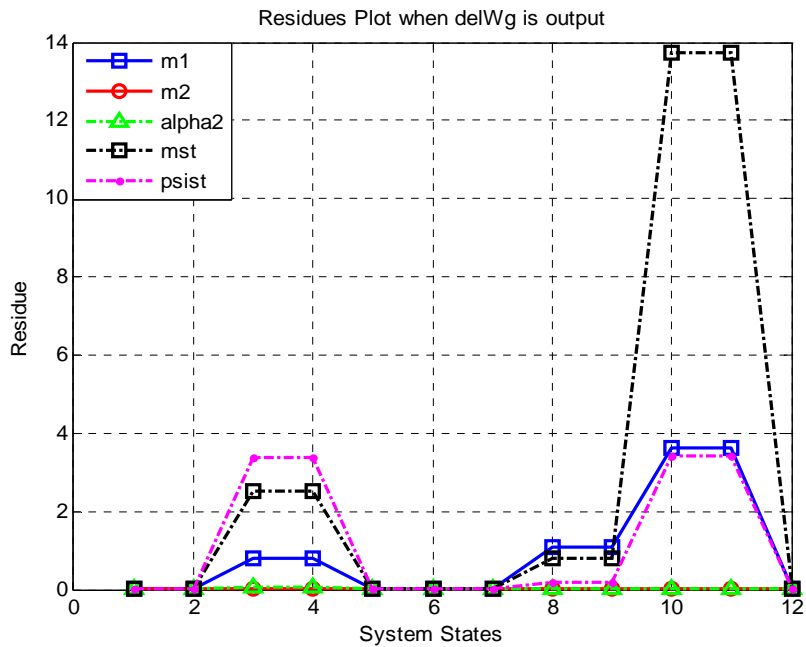


Figure 4.7 Residues when  $\Delta\omega_g$  is taken as plant output, with STATCOM on generator side-converter

Figure 4.8 gives us two information when STATCOM is connected at grid side-converter: a) the rectifier modulation index ( $m_1$ ), exhibiting the largest residue properties will influence the behavior of the mode of oscillation corresponding to eigen value # 8 and #9 ( $-5.3 \pm j315.0$ ), and b) the feedback input signal should be the one corresponding to the eigen value of state #8 & 9, which is the inverter current ( $\Delta i_i$ ) of the variable speed wind turbine PMSG system.

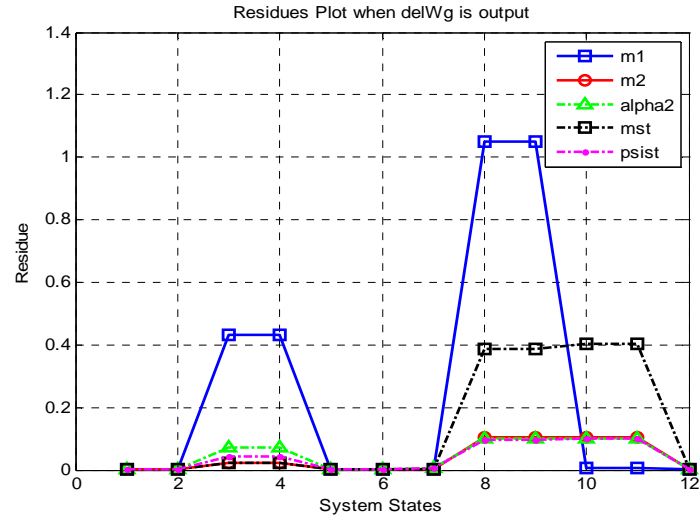


Figure 4.8 Residues when  $\Delta\omega_g$  is taken as plant output, with STATCOM on grid side-converter

Hence, from this section we conclude that;

- Phase angle of STATCOM ( $\psi_{st}$ ) is a preferred choice amongst the 5 inputs as indicated by SVD and Residue indices, when STATCOM is connected at generator side-converter with generator speed ( $\Delta\omega_g$ ) as the plant output.
- When selecting generator speed ( $\Delta\omega_g$ ) as the plant output then the same signal ( $\Delta\omega_g$ ) having the eigen value # 4 will be the best feedback controller input signal.
- Rectifier modulation index ( $m_1$ ) is a preferred choice amongst the 5 inputs as indicated by SVD, HSV and residue method, when STATCOM is connected at grid side-converter with generator speed ( $\Delta\omega_g$ ) as the plant output.
- When selecting generator speed ( $\Delta\omega_g$ ) as the plant output then d-q components of inverter currents (eigen values #8 and #9) will be the best feedback control signal.

### 4.3 Stabilizing Controller Design

As observed the amount of wind power loading and the location of STATCOM play important roles in system performance and stability. This demands that voltage source



converters shall be controlled in such a way that maximum possible power extraction from the wind below the rated wind speed is done continuously without affecting the system stability. A controller installed in the PMSG system can generally monitor the performance of the system in terms of real, reactive flow as well as system voltage. The controller should also be able to take emergency action to help the PMSG system operating near the stability threshold. In this chapter a control strategy is designed based on the information obtained about possible inputs which can be modulated by the appropriate control signals. Once the selection of controller input from the five control variables  $[m_1 \ m_2 \ \alpha_2 \ m_{st} \ \psi_{st}]$  in terms of providing the damping to the system is determined, the next step is to design the controllers which will appropriately modulate the control variables. The controller structures used in this thesis are PI as well as PID controls.

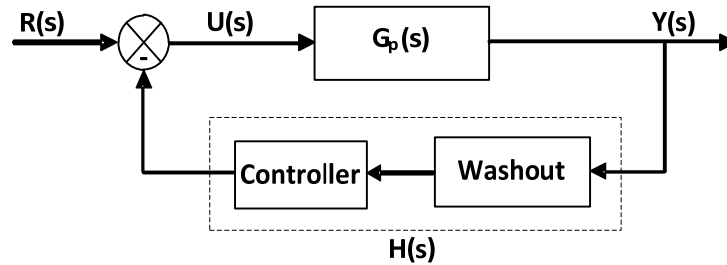


Figure 4.9 Feedback control system

From previous section, it was observed that for  $(\Delta\omega_g)$  as the plant output the input  $(\psi_{st})$  is more responsive to system damping needs and the residue analysis indicated that  $(\Delta\omega_g)$  is the best feedback controller input signal when STATCOM is connected at generator side-converter. Similarly when STATCOM is connected at grid side-converter the input  $(m_1)$  is more responsive to system damping needs and d-q components of inverter currents are

the best candidates for any possible control action. Accordingly, the input signal to the controller configuration as shown in Figure 4.13 is considered to be inverter current ( $\Delta i_i$ ), and input to the plant is considered to be ( $m_1$ ) when STATCOM is connected at grid side-converter. Therefore, for the input-output pair ( $m_1, \Delta \omega_g$ ), the plant transfer function is given by the equation (4.9) when STATCOM is connected at grid side-converter. Similarly when STATCOM is connected at the generator side-converter the input-output pair will be ( $\psi_{st}, \Delta \omega_g$ ).

PI/PID controllers are designed in this chapter to enhance performance of the variable speed wind turbine PMSG system. A PI/PID controller will normally be placed in the feedback path as shown in Figure 4.13. A washout is provided in cascade with the controller to deactivate it under steady state conditions. The controller transfer function for PI controller takes the form [58, 59],

$$H(s) = \frac{sT_w}{1+sT_w} \left( K_p + \frac{K_I}{s} \right) \quad (4.12)$$

and for PID controller, the controller transfer function will be[59],

$$H(s) = \frac{sT_w}{1+sT_w} \left( K_p + \frac{K_I}{s} + s K_D \right) \quad (4.13)$$

where  $K_p$ ,  $K_I$  and  $K_D$  are the proportional, integral and differential constants.  $T_w$  is the time constant of the washout block. Starting with the linearized system equations, the gains of the PI/PID controllers are obtained using frequency based optimization procedure [60].

### 4.3.1 Pole Placement technique

Pole placement or full state feedback is a method employed in the feedback control system theory to place the poles of closed loop plant in the desired location in the s-plane.

Placement of the poles for a specific damping ratio ( $\zeta_{\text{new}}$ ) is desirable because it allows controlling the characteristics of the response by changing the eigen values of the system.

This method is applicable only if the system is controllable. The steps involved are:

1. Determine the poles of the uncompensated plant given by the system equations

$$\begin{aligned}\dot{x} &= Ax + Bu \\ y &= Cx\end{aligned}\tag{4.14}$$

2. Calculate the damping ratio ( $\zeta_{\text{old}}$ ) for the dominant eigen values of the system.
3. Determine how much to the left of  $\lambda$ -plane, the eigen values have to be shifted in order to get the desired damping. Record these eigen values as  $\lambda_{1,2} = -\sigma \pm j\omega$ .
4. For the desired eigen values, the closed loop system including the feedback controller  $H(\lambda)$  should satisfy the requirement,

$$\det[I - (\lambda I)^{-1} B H(\lambda) C] = 0$$

this yield; 
$$H(\lambda) = (C(\lambda I - A)^{-1} B)^{-1}\tag{4.15}$$

5. Another expression for  $H(\lambda)$  comes from the feedback controller being selected such as PI/PID controller.
6. On equating the expressions of  $H(\lambda)$  from step 4 & 5, controller gains can be computed.

### 4.3.2 PID Controller Design using Pole Placement technique

The PID design through the pole placement method forces the closed loop eigen values to the desired location. The gain settings  $K_P$ ,  $K_I$  and  $K_D$  can be computed by assigning a pair of pre-specified eigen values  $\lambda = \lambda_1$  and  $\lambda = \lambda_2$  of the closed loop of Figure 4.14. This is usually referred to as the pole-assignment or pole-placement method. Hence, it is expected that the transient response provided by this controller will be better than the PI controller.

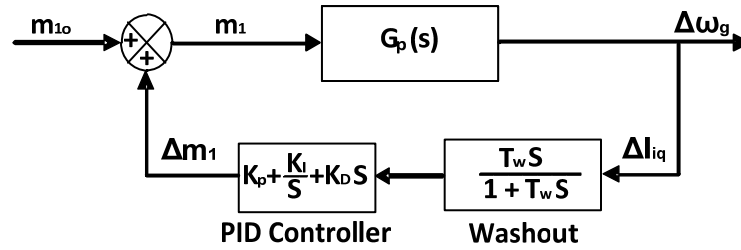


Figure 4.10 Feedback Control with PID Controller

From the equation (4.13), it can be shown that for any eigen value  $\lambda_i$ ,

$$H(\lambda_i) = \frac{\lambda_i T_w}{1 + \lambda_i T_w} (K_p + \frac{K_i}{\lambda_i} + \lambda_i K_D) \quad (4.16)$$

For dominant eigen values  $\lambda_1 = -\sigma_1 + j\omega_1$ ,  $\lambda_2 = -\sigma_2$  equation (4.15) can be written as

$$H(\lambda_1) = H_{R1} + j H_{I1} = (C (\lambda_1 I - A)^{-1} B)^{-1} \quad (4.17)$$

$$H(\lambda_2) = H_{R2} = (C (\lambda_2 I - A)^{-1} B)^{-1} \quad (4.18)$$

Before applying pole-placement technique, we shall find the damping ratio ( $\zeta_{old}$ ) of the dominant eigen value for the uncompensated system[58, 59].

$$\text{i.e., } \zeta_{old} = \frac{-\sigma_1}{\sqrt{(\sigma_1^2 + \omega_1^2)}} \quad \omega_{ln} = \frac{\sigma_1}{\zeta_{old}} \quad (4.19)$$

After knowing the damping ratio ( $\zeta_{old}$ ) for the dominant eigen value being selected based on the residue method, we shall utilize the pole-placement technique to provide the desired damping ratio ( $\zeta_{new}$ ) for improving the stability of the system. The new location of the dominant eigen value ( $\lambda_{1new}$ ) in terms of the desired damping ratio ( $\zeta_{new}$ ) will be;

$$\lambda_{1new} = -\sigma_{1n} + j \omega_{1n} = -\zeta_{new} \omega_{1n} + j \omega_{1n} \sqrt{1 - \zeta_{new}^2} \quad (4.20)$$

For the new eigen value ( $\lambda_{1new}$ ), equations (4.16) & (4.17) can be written as;

$$H(\lambda_{1new}) = \frac{\lambda_{1new} T_w}{1 + \lambda_{1new} T_w} (K_P + \frac{K_I}{\lambda_{1new}} + \lambda_{1new} K_D) \quad (4.21)$$

$$H(\lambda_{1new}) = H_{R1} + j H_{I1} = (C (\lambda_{1new} I - A)^{-1} B)^{-1} \quad (4.22)$$

By using equations (4.18), (4.20) - (4.22), we get;

$$K_P = \frac{H_{I1}}{T_w \omega_{1n}} + \frac{(H_{R1} \omega_{1n} + H_{I1} \sigma_{1n})}{\omega_{1n}} - 2\sigma_{1n} K_D \quad (4.23)$$

$$K_I = \frac{H_{R2}}{T_w} + \sigma_2 (H_{R2} - K_P - \sigma_2 K_D) \quad (4.24)$$

$$K_D = \frac{(H_{R2} - H_{R1}) \omega_{1n} (1 + \sigma_2 T_w) + H_{I1} (\sigma_{1n} - \sigma_2) (1 + \sigma_{1n} T_w)}{T_w \omega_{1n} ((\sigma_{1n} - \sigma_2)^2 + \omega_{1n}^2)} + \frac{H_{I1} \omega_{1n}}{(\sigma_{1n} - \sigma_2)^2 + \omega_{1n}^2} \quad (4.25)$$

Hence, equations (4.23) - (4.25) give the values of the proportional, integral and differential gains,  $K_P$ ,  $K_I$  and  $K_D$  when PID controller is taken in feedback as shown in figure 4.18. For designing a PI controller the same procedure mentioned above can be utilized except that instead of using two different dominant eigen values as in the case of PID only one dominant eigen value is sufficient to find the gains of the PI controller, i.e., by substituting  $\lambda_2 = 0$ ,  $H_{R2} = 0$  and  $K_D = 0$  in equations (4.23) - (4.25), we get the expression of  $K_P$  and  $K_I$  for PI controller given by equations (4.26) and (4.27).

$$K_p = \frac{H_{I1}}{T_w \omega_{1n}} + \frac{(H_{R1} \omega_{1n} + H_{I1} \sigma_{1n})}{\omega_{1n}} \quad (4.26)$$

$$K_i = \frac{H_{R1}}{T_w} + \sigma_1 (H_{R1} - K_p) - \omega_1 H_{I1} \quad (4.27)$$

Table 4.5 and 4.6 below shows the controller gains for PI/PID controller when  $\Delta\omega_g$  is taken as plant output for variable speed wind turbine PMSG system with / without STATCOM device.

Table 4.5 PI Controller gains when  $\Delta\omega_g$  is taken as plant output

System Configuration	Input Control	Feedback signal	Actual damping ( $\zeta_{old}$ )	Desired damping ( $\zeta_{new}$ )	$K_p$	$K_i$
Without STATCOM	$m_1$	$\Delta I_i$	0.0122	0.0145	-45.3347	-1984.7
	$m_1$	$\Delta\omega_g$	-2.168e-6	0.30	23.8550	858.2947
STATCOM at generator side-converter	$\psi_{st}$	$\Delta\omega_g$	-0.0061	0.30	4.8517	240.5115
STATCOM at grid side-converter	$m_1$	$\Delta I_i$	0.0124	0.0145	-45.2943	-1986.7
	$m_1$	$\Delta\omega_g$	1.097e-4	0.30	23.8410	857.9652

Table 4.6 PID Controller gains when  $\Delta\omega_g$  is taken as plant output

<b>System Configuration</b>	<b>Input Control</b>	<b>Feedback signal</b>	<b>Actual damping (<math>\zeta_{old}</math>)</b>	<b>Desired damping (<math>\zeta_{new}</math>)</b>	<b><math>K_P</math></b>	<b><math>K_I</math></b>	<b><math>K_D</math></b>
Without STATCOM	$m_1$	$\Delta I_i$	0.0122	0.0145	-45.3347	-1984.7	-1984.7
STATCOM at generator side-converter	$\psi_{st}$	$\Delta\omega_g$	-0.0061	0.30	2.2106	3.9380	-0.0819
STATCOM at grid side-converter	$m_1$	$\Delta I_i$	0.0124	0.0145	-45.1386	-58.6852	0.0150

## CHAPTER 5

### SIMULATION STUDIES

From small signal analysis of chapter 4, we observed that for low power outputs the STATCOM on the grid side-converter is showing better stability behavior as shown in figure 4.1. In this section non-linear time domain simulations were used to verify the ideality of STATCOM location for variable speed wind turbine PMSG system without any feedback control. Simulation results are shown for three cases;

- a) Without STATCOM
- b) STATCOM on generator side-converter and
- c) STATCOM on grid side-converter

Figures (5.1 – 5.3) are plotted for a nominal loading of 0.65 p.u. when subjected to a torque pulse of 15% for 0.1 sec duration. From figure 5.1 we observe, there is improvement in terminal voltage when STATCOM is connected at grid side-converter.

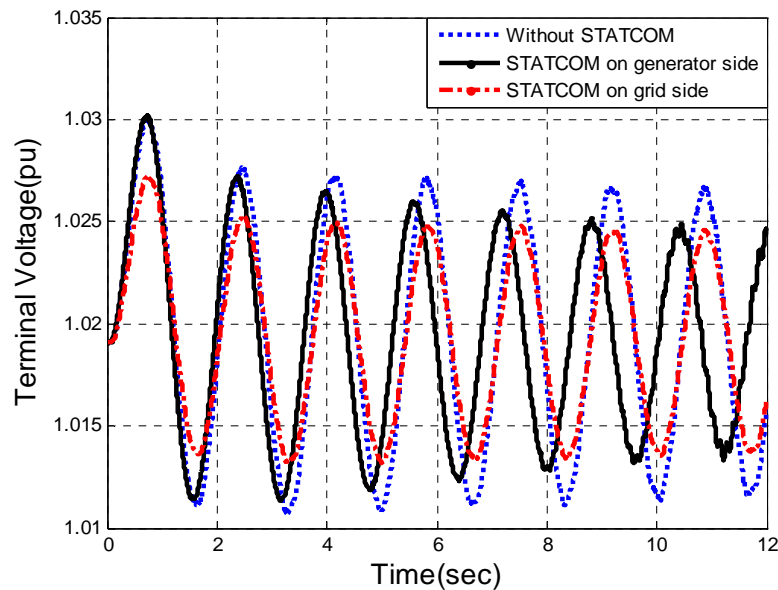


Figure 5.1 Terminal voltage of variable speed wind turbine PMSG with and without STATCOM.



From Figure 5.2 it can be seen that generator speed variations are almost same when variable speed wind turbine PMSG system is without STATCOM device or with STATCOM at grid side-converter whereas with STATCOM on generator side-converter, the generator speed variations are initially less compare to other two configurations but it is increasing with respect to time which is not desirable.

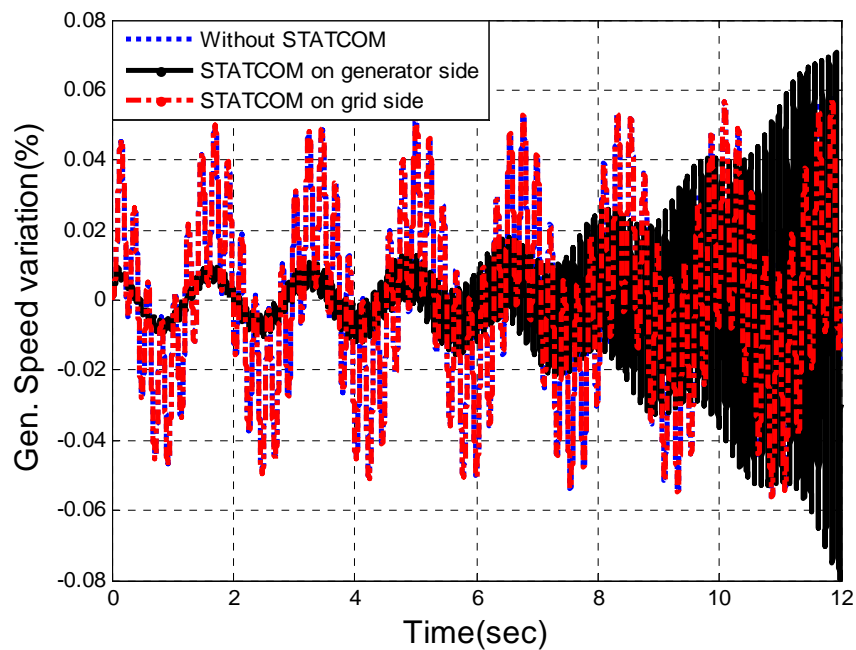


Figure 5.2 Generator speed variation for variable speed wind turbine PMSG with & without STATCOM

From Figure 5.3 it can be seen that power angle variations are almost same when variable speed wind turbine PMSG system is without STATCOM device or with STATCOM at grid side-converter whereas with STATCOM on generator side-converter, the power angle variations are initially less compare to other two configurations but it is increasing with respect to time which is not desirable.

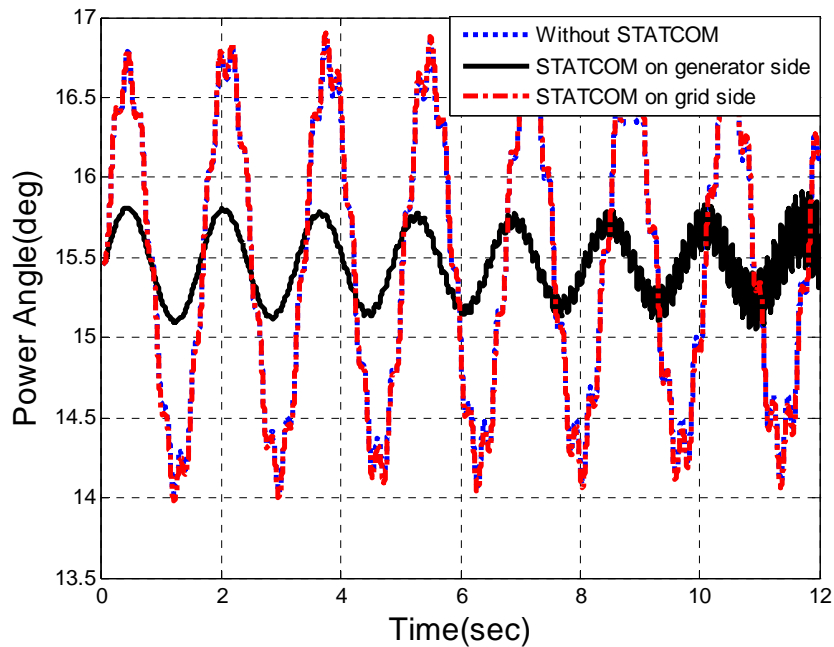


Figure 5.3 Power angle of the variable speed wind turbine PMSG with and without STATCOM.

Hence it can be concluded from figure 4.1 and figures (5.1-5.3) that, for the variable speed wind turbine PMSG system the ideal location for the STATCOM device is at the grid side-converter.

From control system theory we know that feedback control provides improvement in the system response. Therefore feedback control using PI controller will be provided to explore the behavior of variable speed wind turbine PMSG system for STATCOM connected at generator side-converter as well as grid side-converter independently. Non-linear time domain simulations were used to assess the effectiveness of the controller designed.

## **5.1 Simulation studies for a disturbance (15% torque pulse) on wind turbine**

The non-linear time domain simulations are done using PI/PID controller for a nominal loading of 0.65 p.u. with a 15% torque pulse for 0.1 sec duration. The washout time constant was selected to be 0.02 sec which is optimized in such a manner that it has minimum interference with the eigen value of interest under transient condition.

### **5.1.1 STATCOM connected at gen. side-converter using feedback control**

From decomposition techniques of chapter-4 it was concluded that  $\psi_{st}$  is the best control signal when  $\Delta\omega_g$  is taken as the plant output as shown in Figure 4.9. It was also shown that  $\Delta\omega_g$  is the best feedback controller input signal. The PI/PID controller design was carried out in the previous chapter using pole-placement technique, where the controller gains are adjusted to give desired closed loop system damping ratio ( $\zeta_{new} = 0.3$ ), with  $\Delta\omega_g$  as feedback signal having the input-output pair as  $(\psi_{st}, \Delta\omega_g)$ .

Figures (5.4 – 5.8) does not show any improvement in terminal voltage, STATCOM converter voltage and current, inverter output current and DC link converter voltage even with the best control signal ( $\psi_{st}$ ) being selected. It was observed that, with higher values of damping ratio also there was no change in the plots.

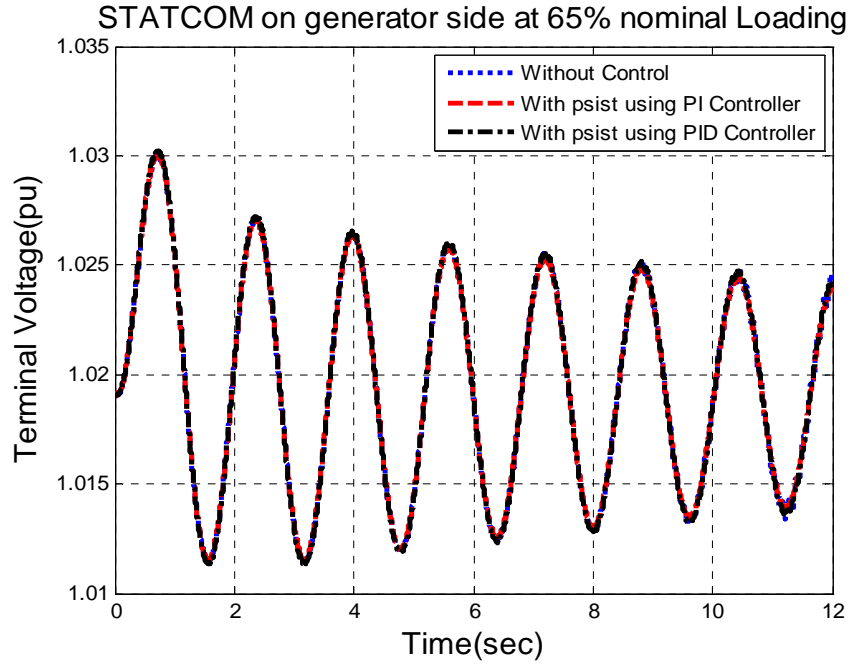


Figure 5.4 Terminal Voltage of variable speed wind turbine PMSG system with  $\psi_{st}$  control

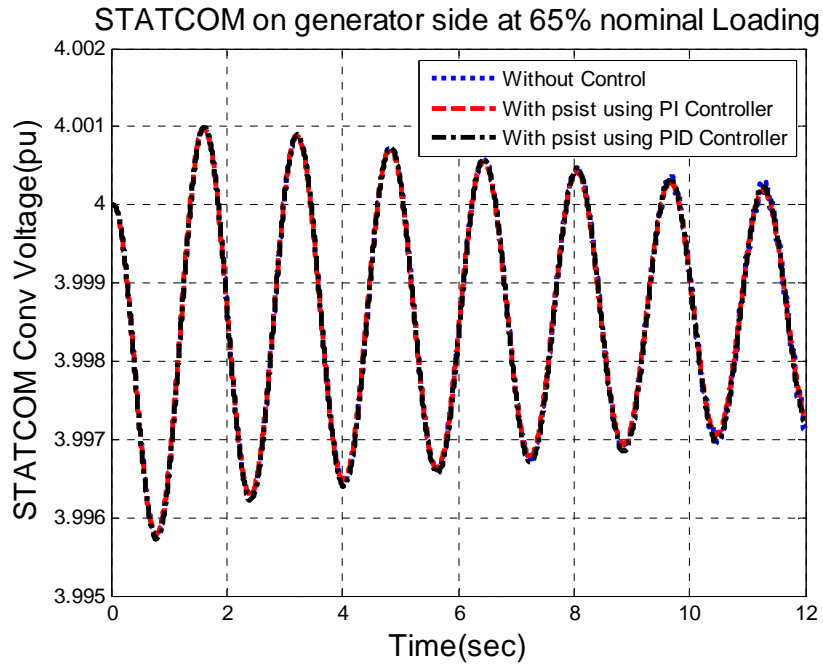


Figure 5.5 STATCOM converter voltage of variable speed wind turbine PMSG system with  $\psi_{st}$  control

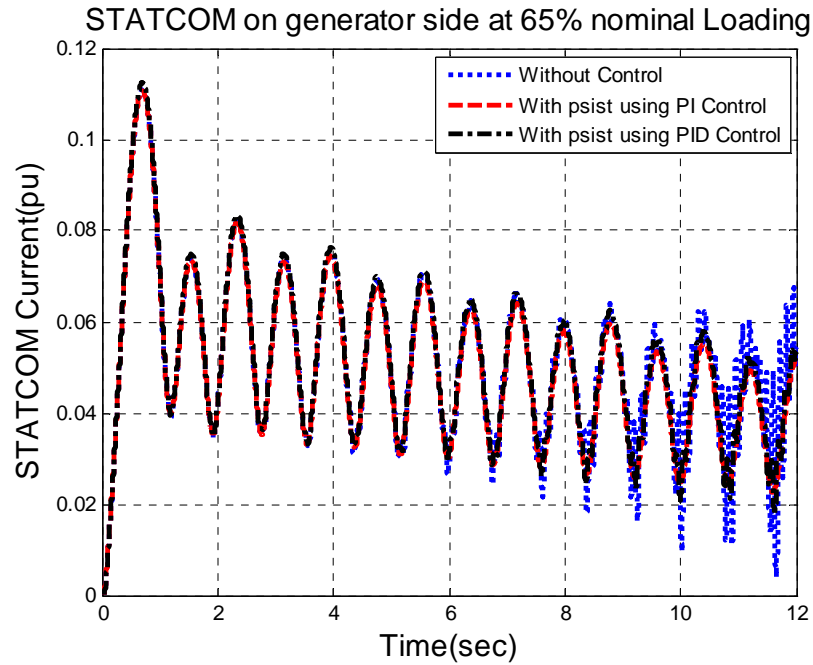


Figure 5.6 STATCOM current of variable speed wind turbine PMSG system with  $\psi_{st}$  control

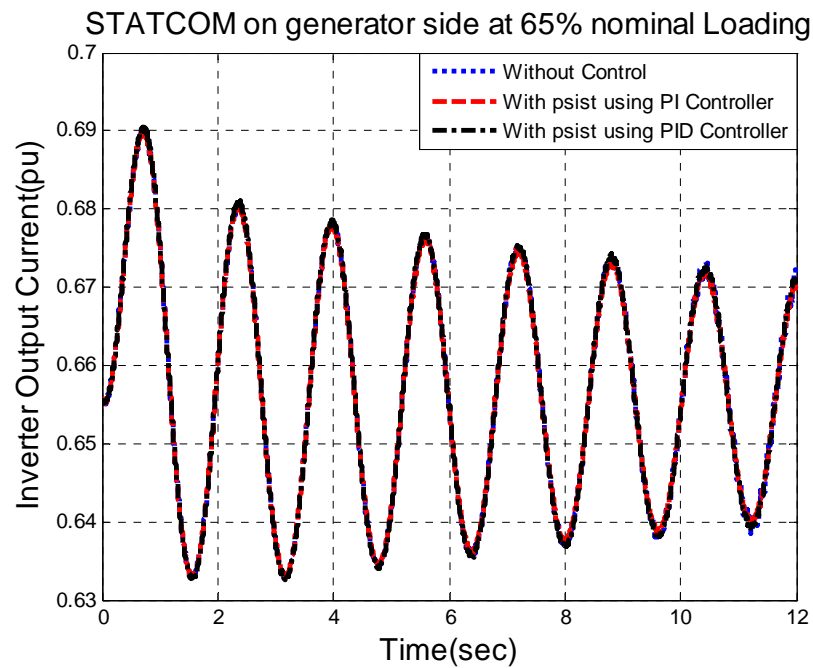


Figure 5.7 Inverter output current of variable speed wind turbine PMSG system with  $\psi_{st}$  control

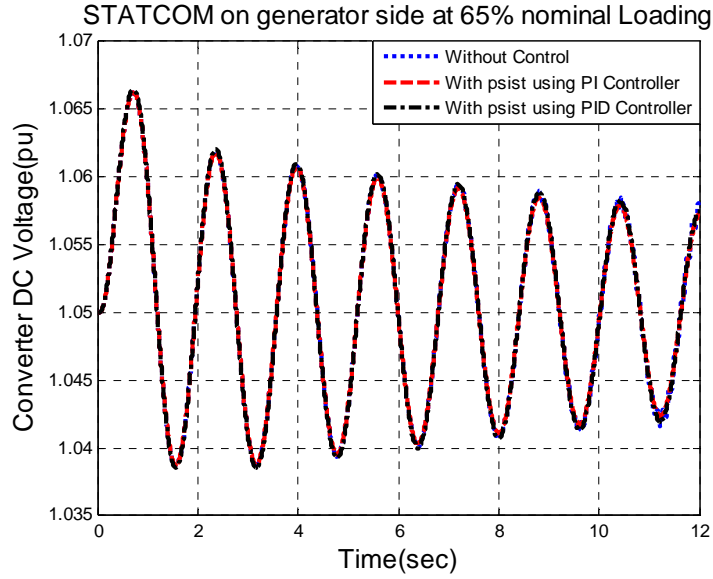


Figure 5.8 Converter dc voltage of variable speed wind turbine PMSG system with  $\psi_{st}$  control

As seen from figure 5.9 there is improvement in generator speed variations with  $\psi_{st}$  control. Therefore feedback control helps in achieving speed control of variable speed wind turbine PMSG system which in turn provides active power control for wind turbine.

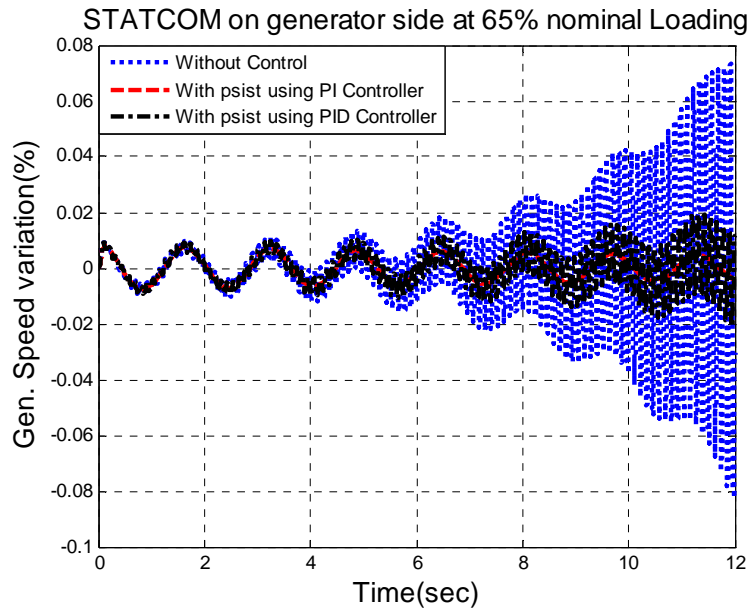


Figure 5.9 Generator speed variations of variable speed wind turbine PMSG system with  $\psi_{st}$  control

Figure 5.10 shows some improvement in power angle variations with  $\psi_{st}$  control as time elapses. For higher values of damping ratio also approx. same result is achieved.

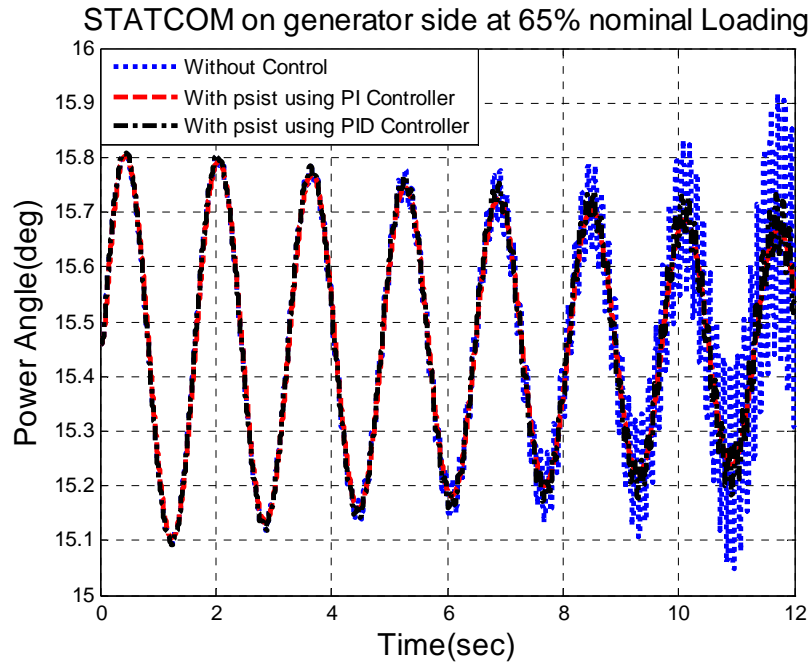


Figure 5.10 Power angle of variable speed wind turbine PMSG system with  $\psi_{st}$  control

Therefore from Figures (5.4 to 5.10) we observe that STATCOM connected to variable speed wind turbine PMSG system at generator side-converter does not play a major role in improvement of system output.

### 5.1.2 STATCOM connected at grid side-converter using feedback control

From decomposition techniques of chapter-4 it was concluded that  $m_1$  is the best control signal and  $\Delta i_i$  as the best feedback controller input signal when  $\Delta \omega_g$  is taken as the plant output as shown in Figure 4.11. The PI/PID controller design was carried out in the previous chapter using pole-placement technique, where the controller gains are adjusted

to give desired closed loop system damping ratio ( $\zeta_{new} = 0.0145$ ), with  $\Delta i_i$  as feedback signal having the input-output pair as  $(m_1, \Delta \omega_g)$ .

Figures (5.11 – 5.15) shows improvements in terminal voltage, STATCOM converter voltage and current, inverter output current and DC link converter voltage with  $m_1$  control having damping ratio of ( $\zeta_{new} = 0.0145$ ) for a variable speed wind turbine PMSG system with STATCOM on grid side-converter.

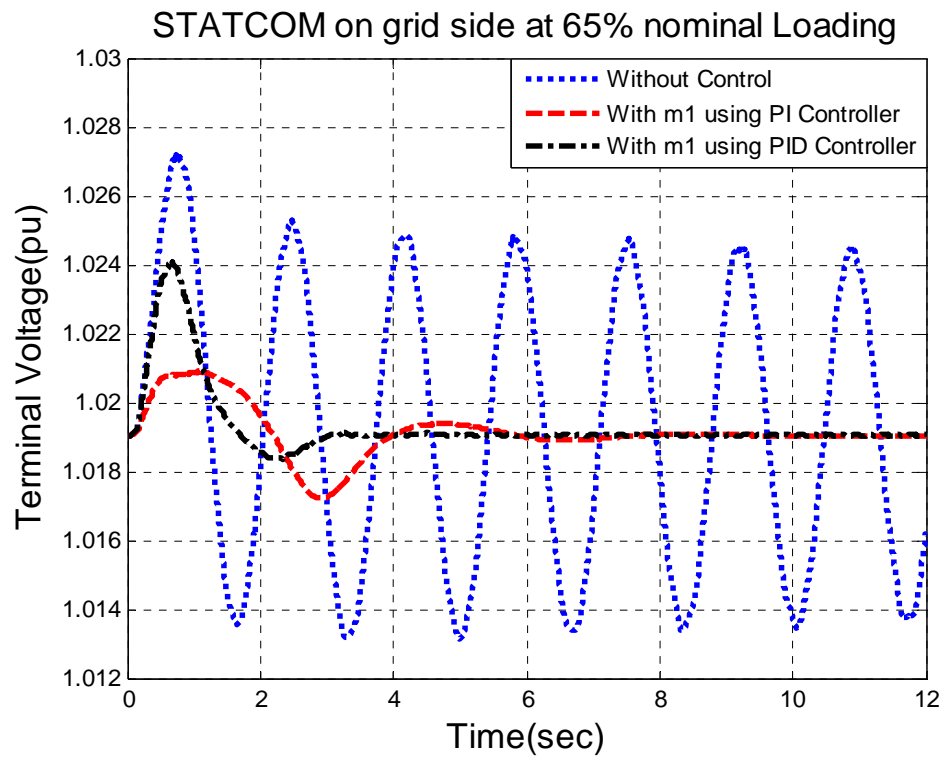


Figure 5.11 Terminal Voltage of variable speed wind turbine PMSG system with  $m_1$  control



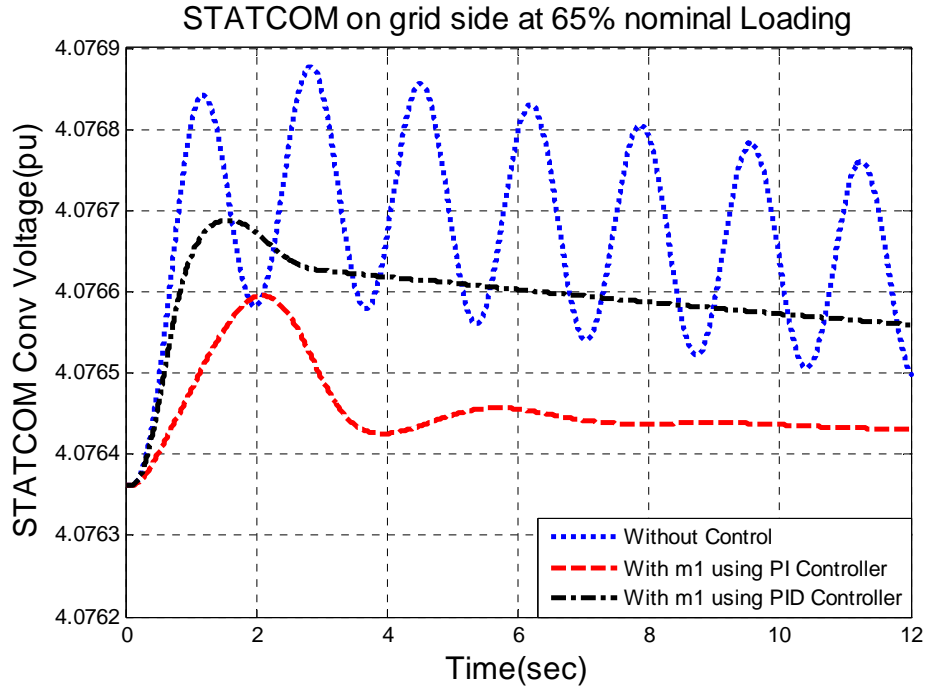


Figure 5.12 STATCOM converter voltage of variable speed wind turbine PMSG system with  $m_1$  control

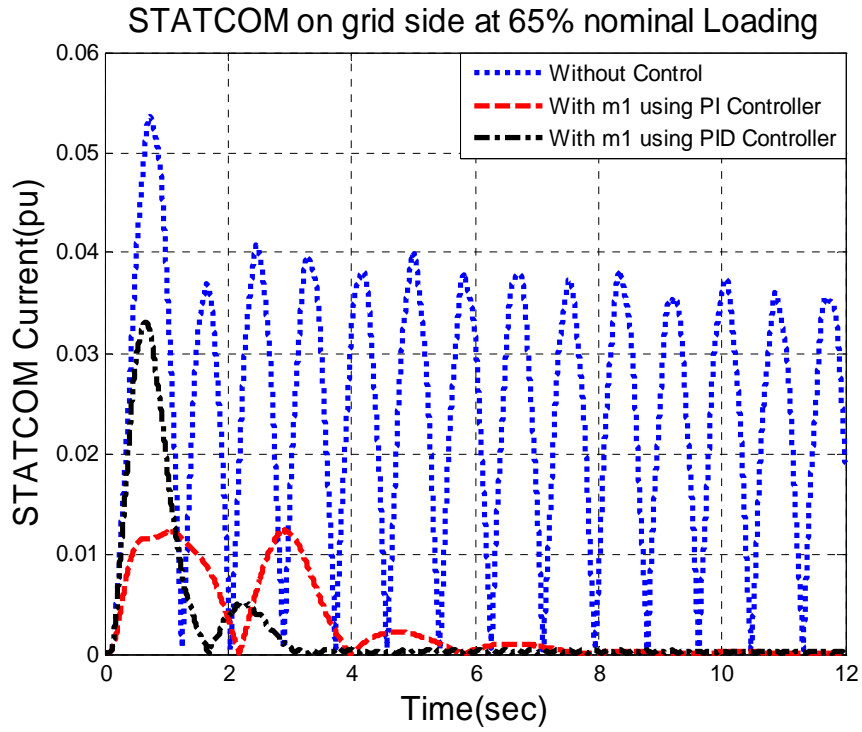


Figure 5.13 STATCOM current of variable speed wind turbine PMSG system with  $m_1$  control

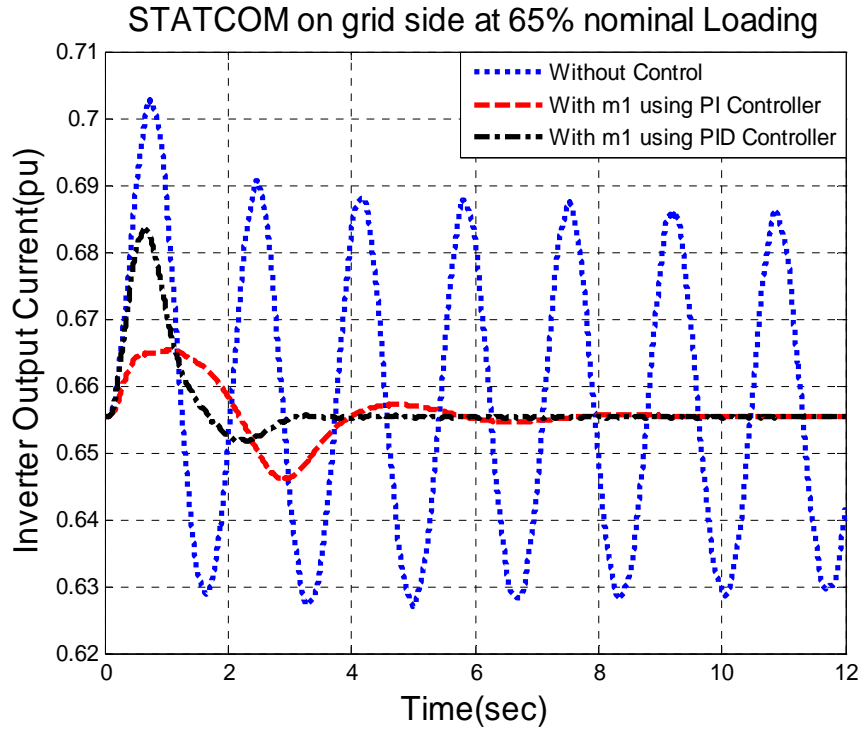


Figure 5.14 Inverter output current of variable speed wind turbine PMSG system with  $m_1$  control

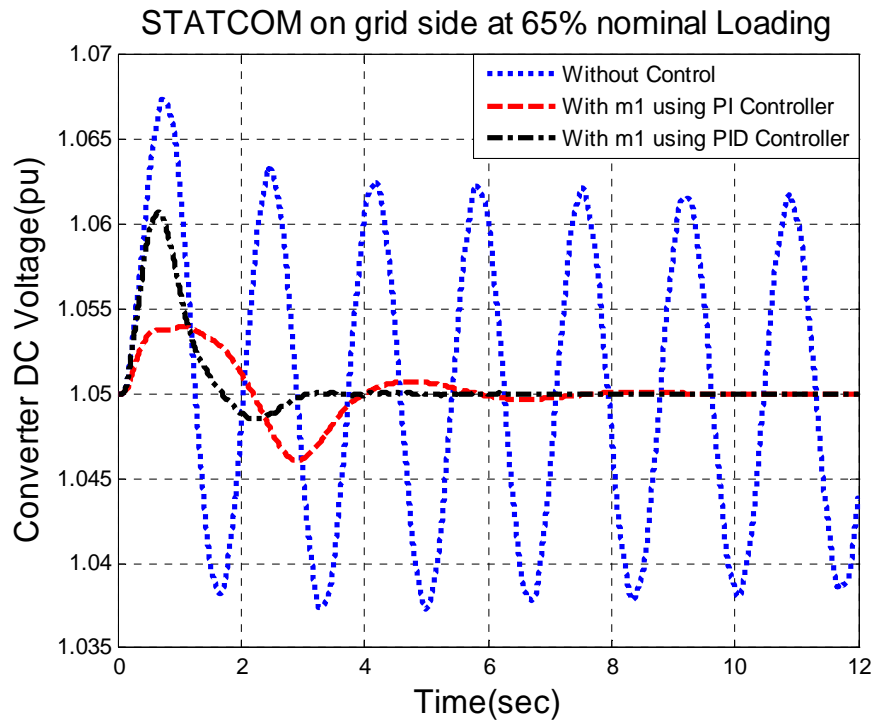


Figure 5.15 Converter dc voltage of variable speed wind turbine PMSG system with  $m_1$  control

From figure 5.16 it can be seen that there is a small overshoot in starting but as time elapses generator speed variations are reduced. Hence  $m_1$  control helps in achieving speed control of variable speed wind turbine PMSG system which in turn provides active power control for wind turbine.

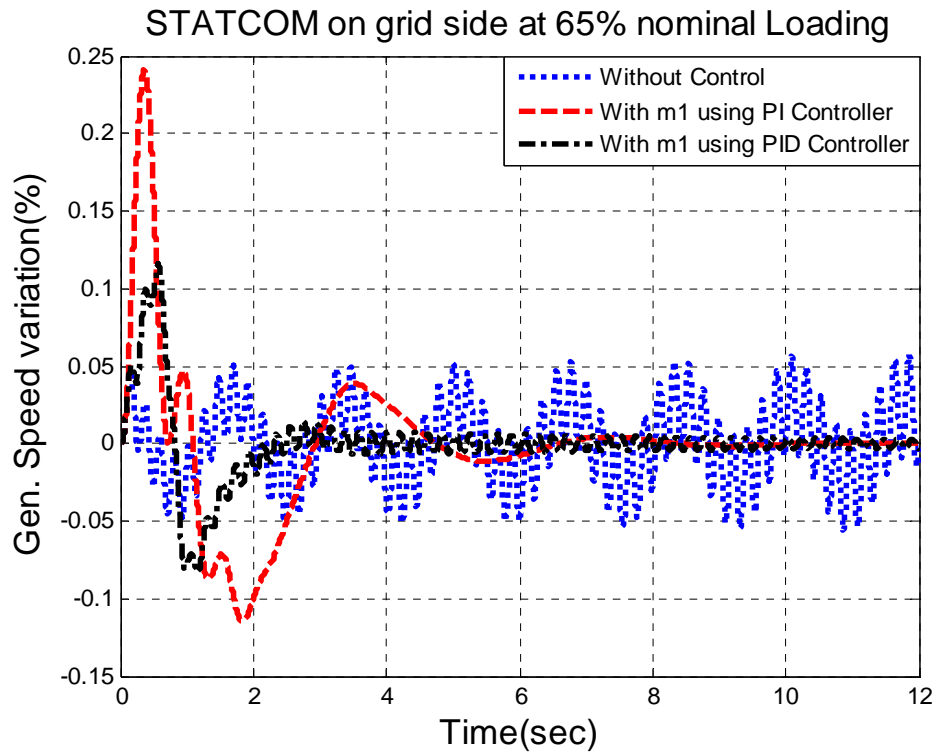


Figure 5.16 Generator speed variations of variable speed wind turbine PMSG system with  $m_1$  control

From figure 5.17 it can be seen that there is overshoot in starting but as time elapses power angle variations are reduced.

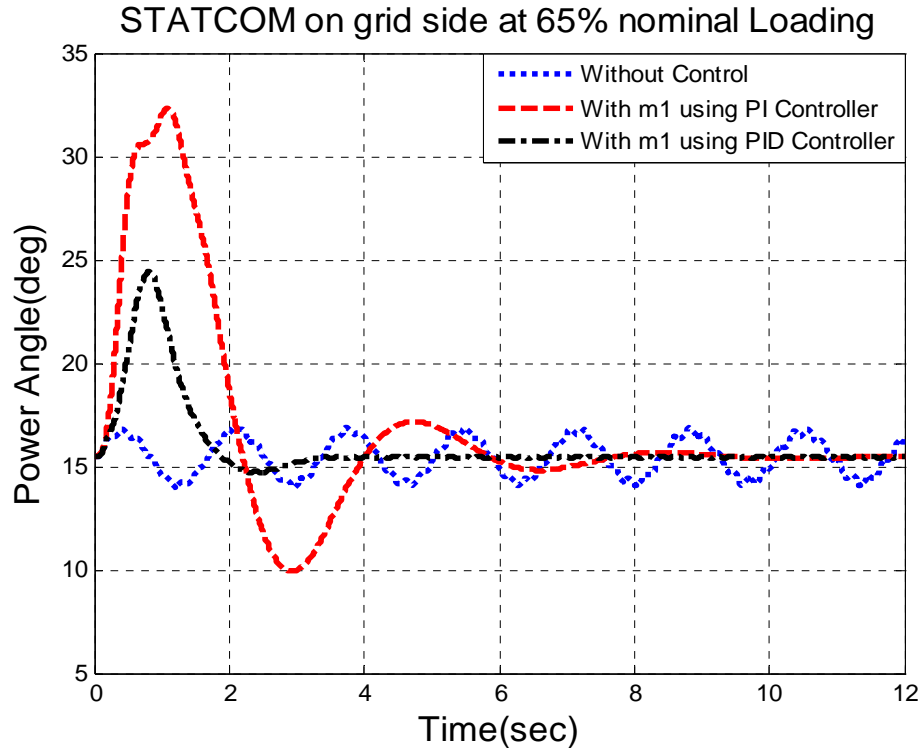


Figure 5.17 Power angle of variable speed wind turbine PMSG system with  $m_1$  control

Therefore from figures (5.11 to 5.17) we observe that STATCOM connected to variable speed wind turbine PMSG system at grid side-converter provides best damping only with  $m_1$  as input signal. This was also confirmed from small signal analysis and decomposition methods in chapter 4.

## 5.2 Robustness of variable speed WT-PMSG system using feedback control

From earlier sections, we come to the following conclusion:

- a) When STATCOM is connected at generator side-converter, system stability will not improve with any input signal.
- b) When STATCOM is connected at grid side-converter, it will provide good damping only with  $m_1$  as input signal.

To show the ideal location of STATCOM, let us verify the robustness of variable speed wind turbine PMSG system with STATCOM at different operating conditions.

### **5.2.1 For 45% loading with / without STATCOM**

The non-linear time domain simulations are done using PI controller for 0.45 p.u. loading with a 15% torque pulse for 0.1 sec duration. The washout time constant was selected to be 0.02 sec which is optimized in such a manner that it has minimum interference with the eigen value of interest under transient condition.

For STATCOM connected at generator side  $\psi_{st}$  is taken as input signal to give desired closed loop system damping ratio ( $\zeta_{new} = 0.3$ ) with  $\Delta\omega_g$  as feedback signal having the input-output pair as  $(\psi_{st}, \Delta\omega_g)$ . Similarly, for STATCOM connected at grid side  $m_1$  is taken as input signal to give desired closed loop system damping ratio ( $\zeta_{new} = 0.0145$ ) with  $\Delta i_i$  as feedback signal having the input-output pair as  $(m_1, \Delta\omega_g)$ .

Figures (5.18 – 5.22) shows improvements in terminal voltage, STATCOM converter voltage and current, inverter output current and DC link converter voltage with  $m_1$  control having damping ratio of ( $\zeta_{new} = 0.0145$ ) for a variable speed wind turbine PMSG system with STATCOM on grid side-converter.

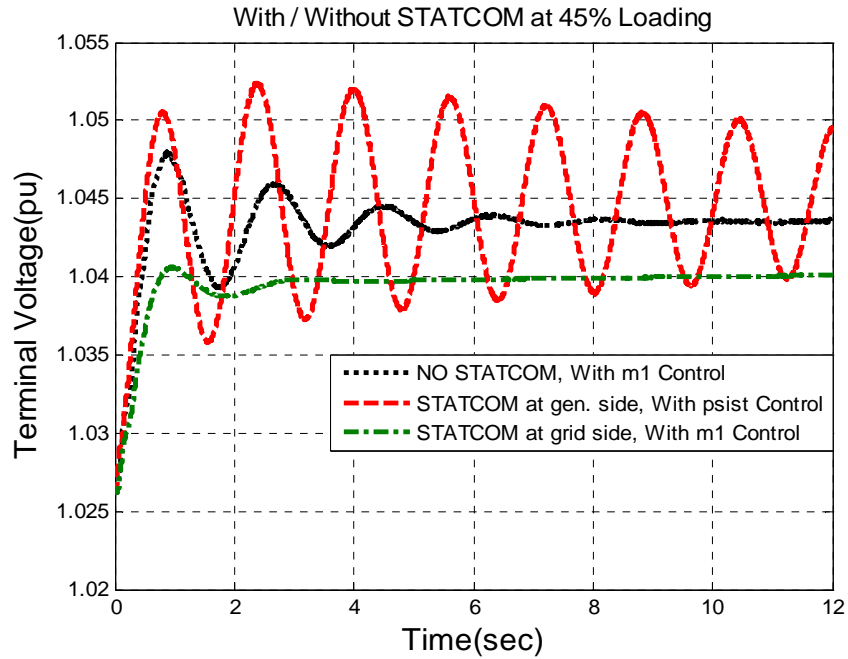


Figure 5.18 Terminal voltage of variable speed wind turbine PMSG system at 45% loading

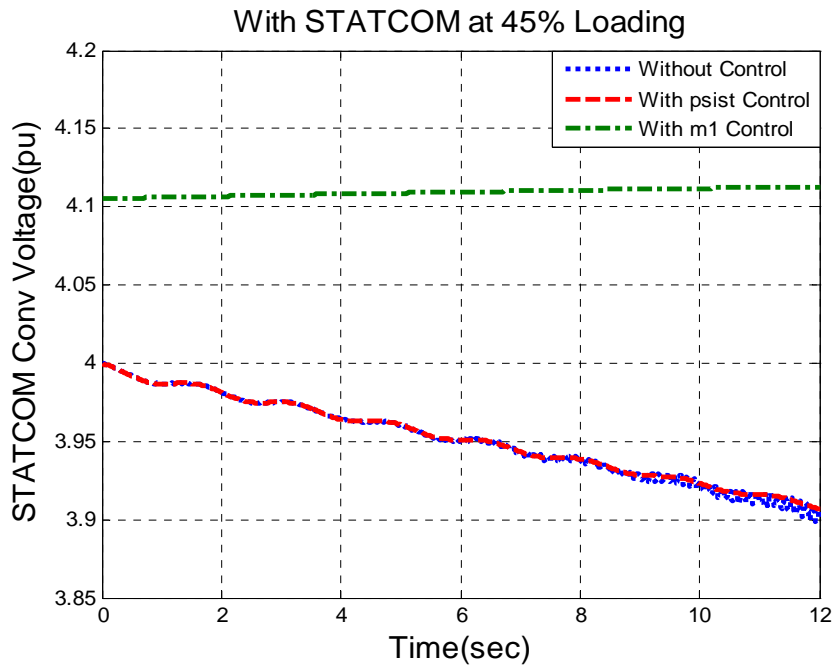


Figure 5.19 STATCOM converter voltage of variable speed wind turbine PMSG system at 45% loading

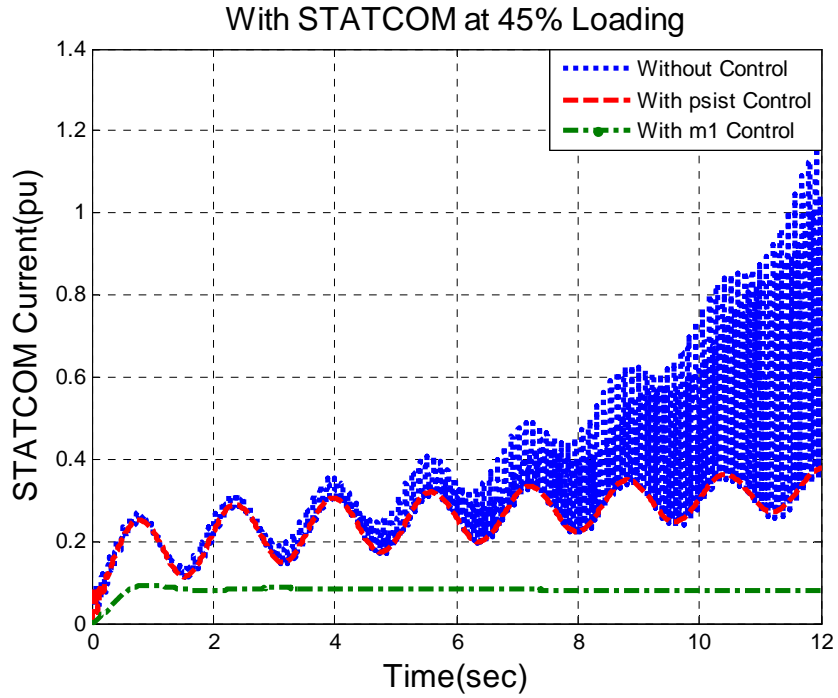


Figure 5.20 STATCOM current of variable speed wind turbine PMSG system at 45% loading

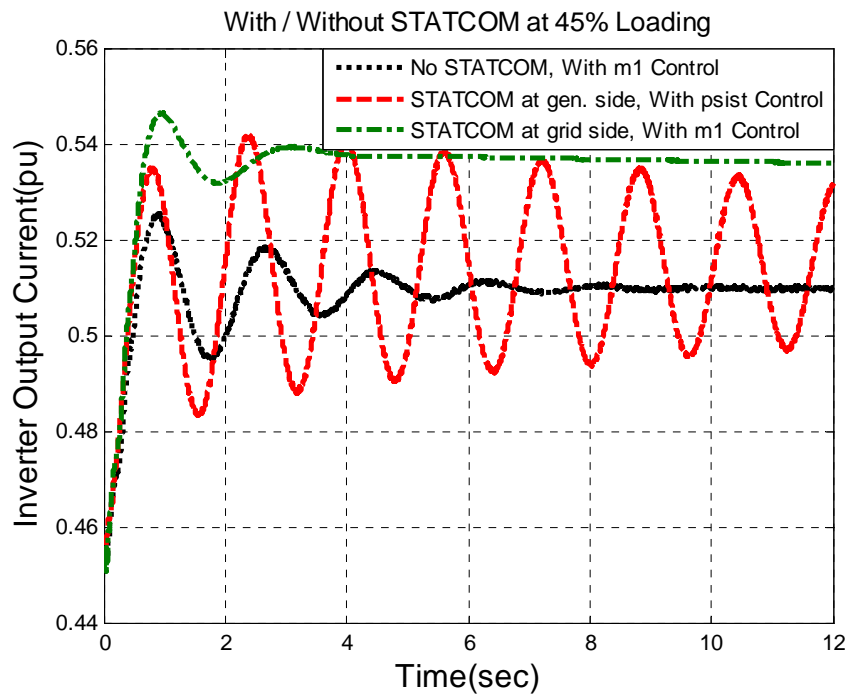


Figure 5.21 Inverter output current of variable speed wind turbine PMSG system at 45% loading

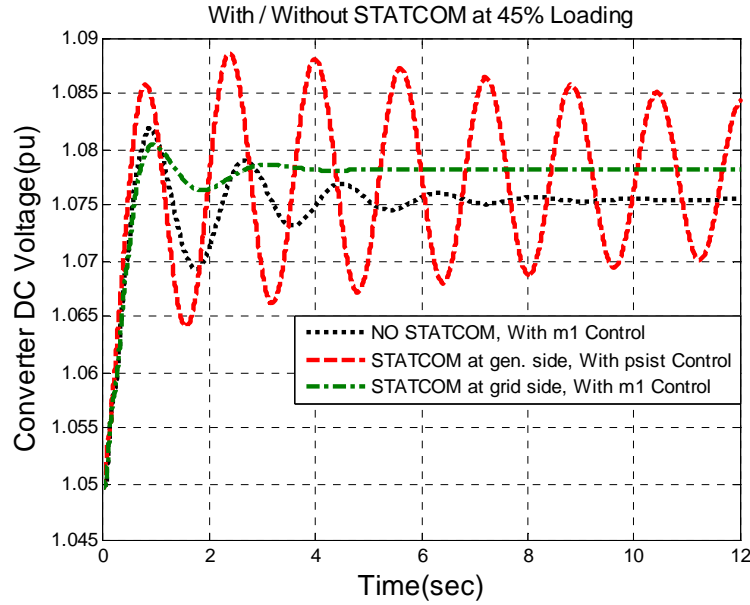


Figure 5.22 DC link voltage of variable speed wind turbine PMSG system at 45% loading

From figure 5.23 it can be seen that, there is more overshoot for STATCOM connected on grid side converter with  $m_1$  control but as time elapses generator speed variations are reduced. The settling time is less with small oscillations in starting when compared to STATCOM connected at generator side converter with  $\Psi_{st}$  control.

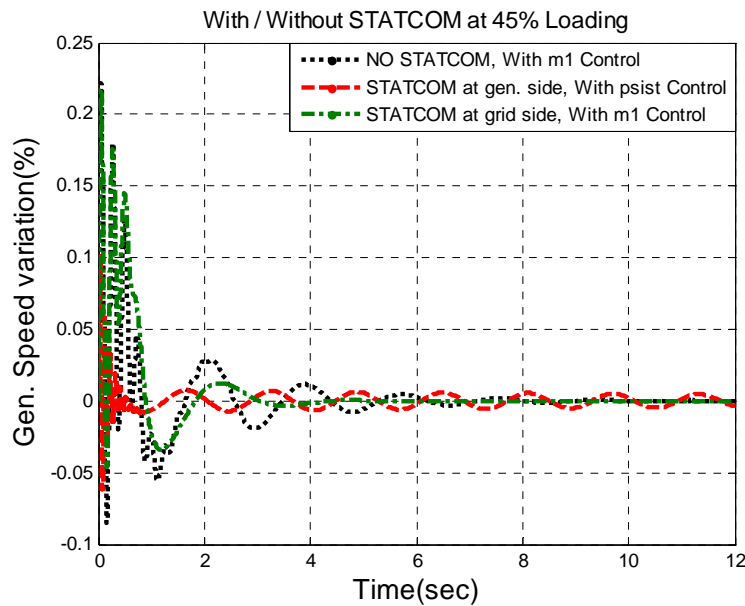


Figure 5.23 Generator speed variation of variable speed wind turbine PMSG system at 45% loading



From figure 5.24 it can be seen that, there is more overshoot for STATCOM connected on grid side converter with  $m_1$  control when compared to STATCOM connected at generator side converter with  $\Psi_{st}$  control. The settling time is less with no oscillations when STATCOM is connected at grid side converter.

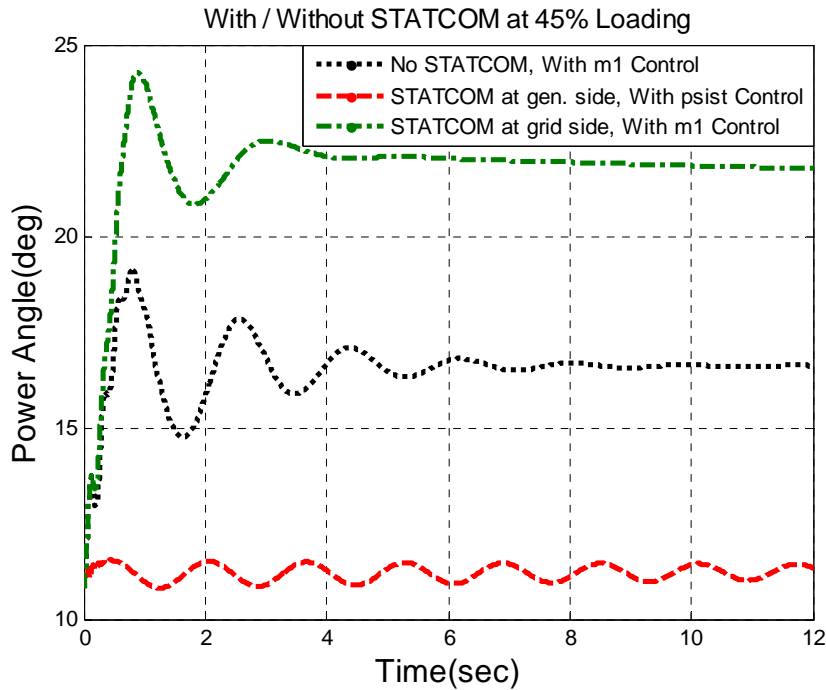


Figure 5.24 Power angle variation of variable speed wind turbine PMSG system at 45% loading

Hence from figures (5.18 to 5.24) we observe that, STATCOM connected at grid side converter is more robust at 45% loading when subjected to 15% torque pulse for 0.1sec duration using PI controller.

### 5.2.2 For 85% loading with / without STATCOM

The non-linear time domain simulations are done using PI controller for a nominal loading of 0.85 p.u. with a 15% torque pulse for 0.1 sec duration. The washout time

constant was selected to be 0.02 sec which is optimized in such a manner that it has minimum interference with the eigen value of interest under transient condition.

For STATCOM connected at generator side  $\psi_{st}$  is taken as input signal to give desired closed loop system damping ratio ( $\zeta_{new} = 0.3$ ) with  $\Delta\omega_g$  as feedback signal having the input-output pair as  $(\psi_{st}, \Delta\omega_g)$ . Similarly, for STATCOM connected at grid side  $m_1$  is taken as input signal to give desired closed loop system damping ratio ( $\zeta_{new} = 0.0145$ ) with  $\Delta i_i$  as feedback signal having the input-output pair as  $(m_1, \Delta\omega_g)$ .

Figures (5.25 – 5.29) shows improvements in terminal voltage, STATCOM converter voltage and current, inverter output current and DC link converter voltage with  $m_1$  control having damping ratio of ( $\zeta_{new} = 0.0145$ ) for a variable speed wind turbine PMSG system with STATCOM on grid side-converter.

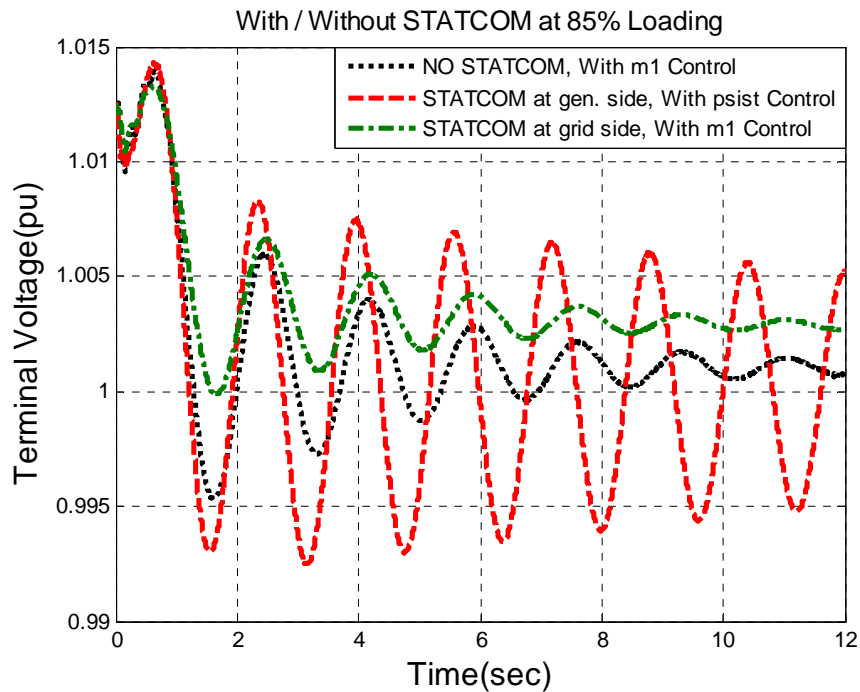


Figure 5.25 Terminal voltage of variable speed wind turbine PMSG system at 85% loading

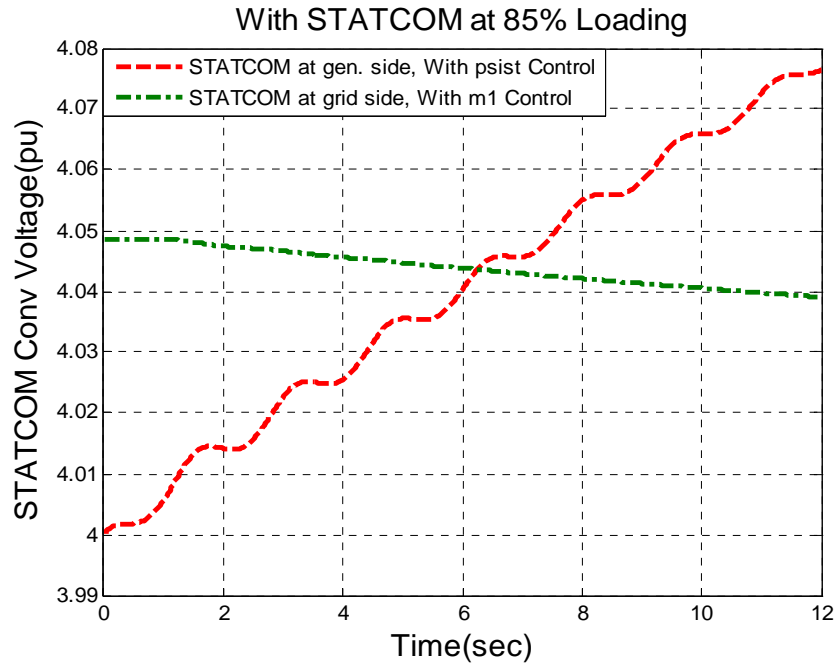


Figure 5.26 STATCOM converter voltage of variable speed wind turbine PMSG system at 85% loading

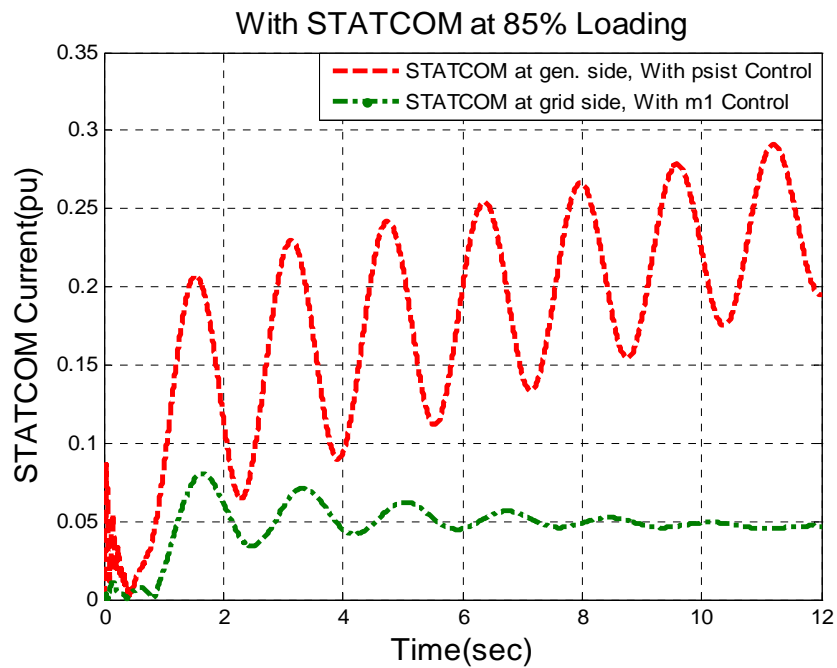


Figure 5.27 STATCOM current of variable speed wind turbine PMSG system at 85% loading

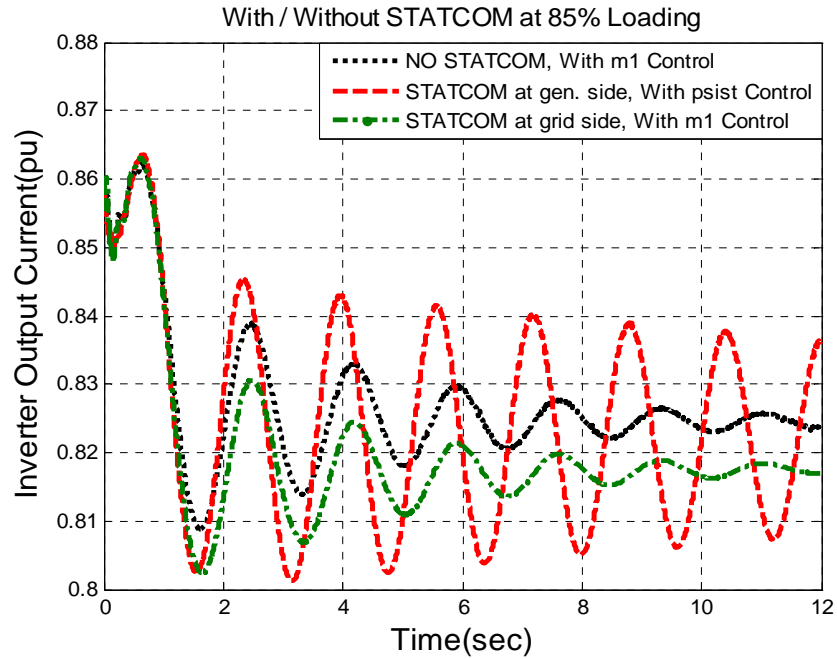


Figure 5.28 Inverter output current of variable speed wind turbine PMSG system at 85% loading

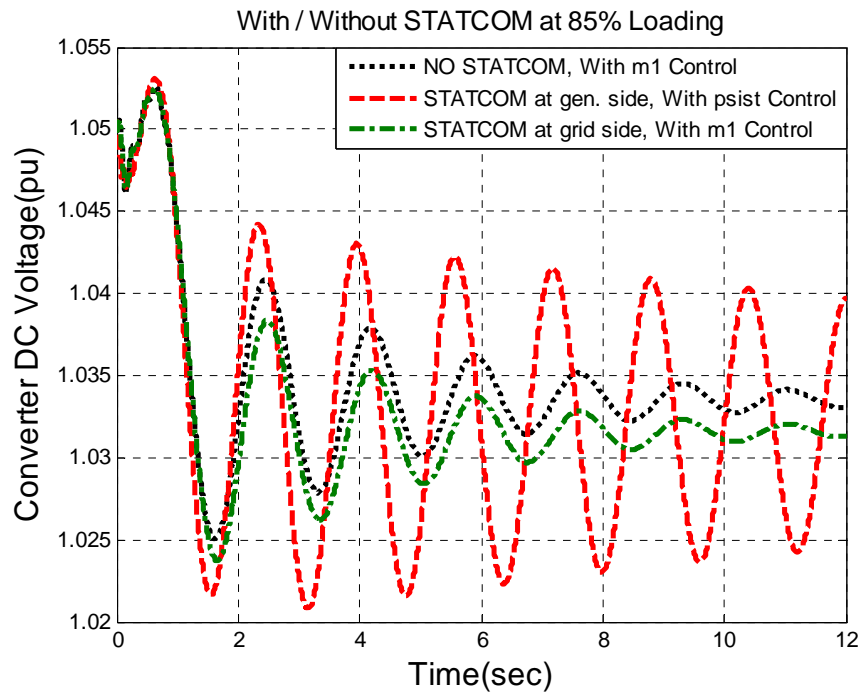


Figure 5.29 DC link voltage of variable speed wind turbine PMSG system at 85% loading

From figure 5.30 it can be seen that, there is more overshoot for STATCOM connected on grid side converter with  $m_1$  control but as time elapses generator speed variations are reduced. The settling time is less with small oscillations in starting when compared to STATCOM connected at generator side converter with  $\Psi_{st}$  control.

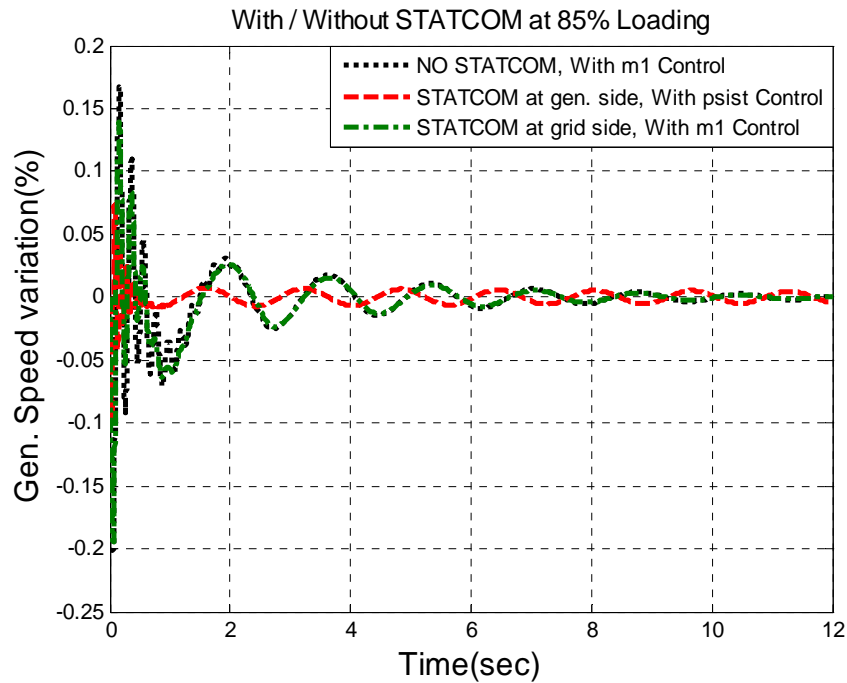


Figure 5.30 Generator speed variation of variable speed wind turbine PMSG system at 85% loading

From figure 5.31 it can be seen that, there is more overshoot for STATCOM connected on grid side converter with  $m_1$  control when compared to STATCOM connected at generator side converter with  $\Psi_{st}$  control. The settling time is more with oscillations when STATCOM is connected at grid side converter.

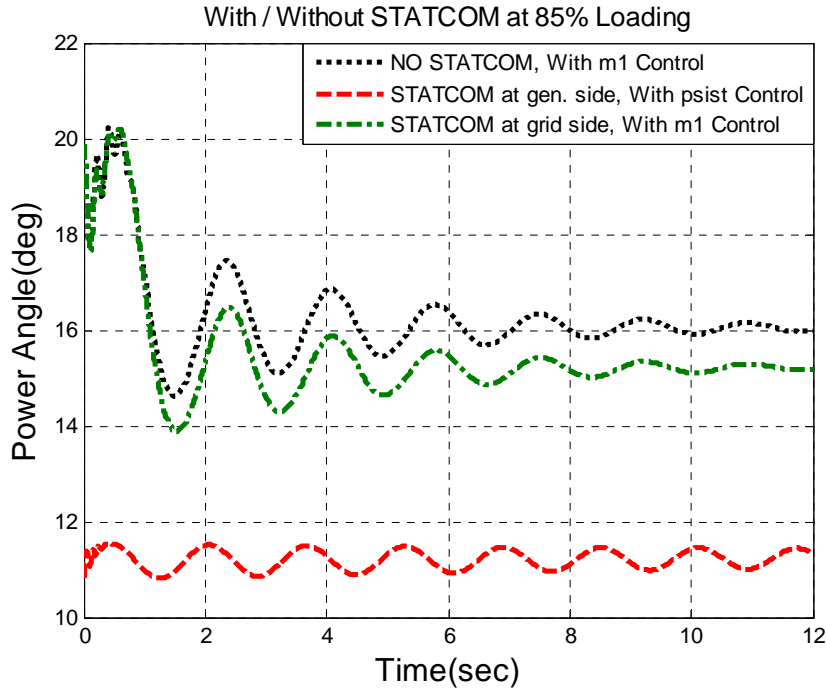


Figure 5.31 Power angle variation of variable speed wind turbine PMSG system at 85% loading

Hence from figures (5.25 to 5.31) we observe that, STATCOM connected at grid side converter is more robust at 85% loading when subjected to 15% torque pulse for 0.1 sec duration using PI controller.

### 5.2.3 For change in STATCOM parameters

The non-linear time domain simulations are done using PI controller for a nominal loading of 0.65 p.u. with a 15% torque pulse for 0.1 sec duration. The STATCOM parameters are changed from ( $R_{st} = 0.01$ ,  $L_{st} = 0.15$ ) in p.u. to new values as ( $R_{st} = 0.05$ ,  $L_{st} = 0.75$ ) in p.u. The capacitor value was kept same at 1 p.u i.e., ( $C_{dc} = 1$ ). The washout time constant was selected to be 0.02 sec which is optimized in such a manner that it has minimum interference with the eigen value of interest under transient condition.

For STATCOM connected at generator side  $\psi_{st}$  is taken as input signal to give desired closed loop system damping ratio ( $\zeta_{new} = 0.3$ ) with  $\Delta\omega_g$  as feedback signal having the input-output pair as  $(\psi_{st}, \Delta\omega_g)$ . Similarly, for STATCOM connected at grid side  $m_1$  is taken as input signal to give desired closed loop system damping ratio ( $\zeta_{new} = 0.0145$ ) with  $\Delta i_i$  as feedback signal having the input-output pair as  $(m_1, \Delta\omega_g)$ .

Figures (5.32 – 5.36) shows improvements in terminal voltage, STATCOM converter voltage and current, inverter output current and DC link converter voltage with  $m_1$  control having damping ratio of ( $\zeta_{new} = 0.0145$ ) for a variable speed wind turbine PMSG system with STATCOM on grid side-converter.

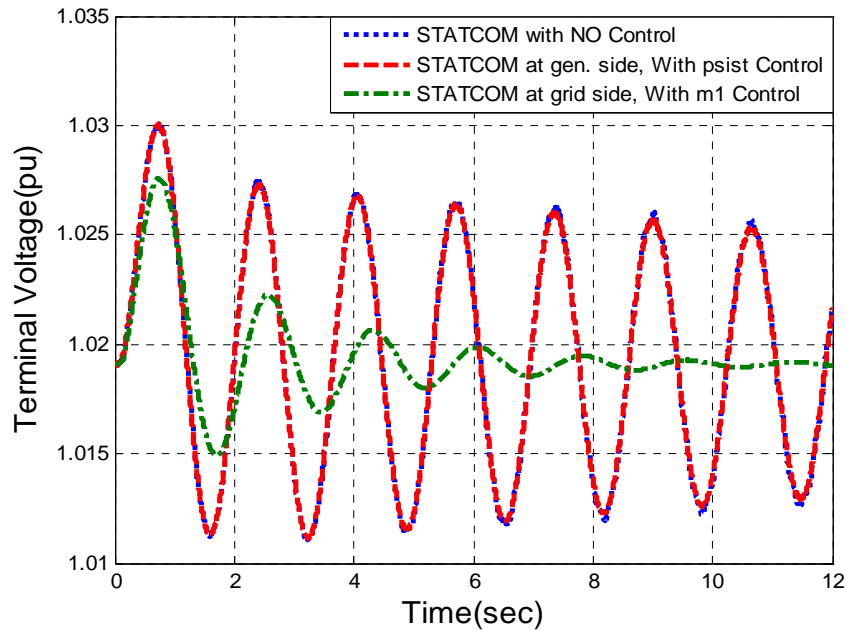


Figure 5.32 Terminal voltage of variable speed wind turbine PMSG at different  $R_{st}$  &  $L_{st}$

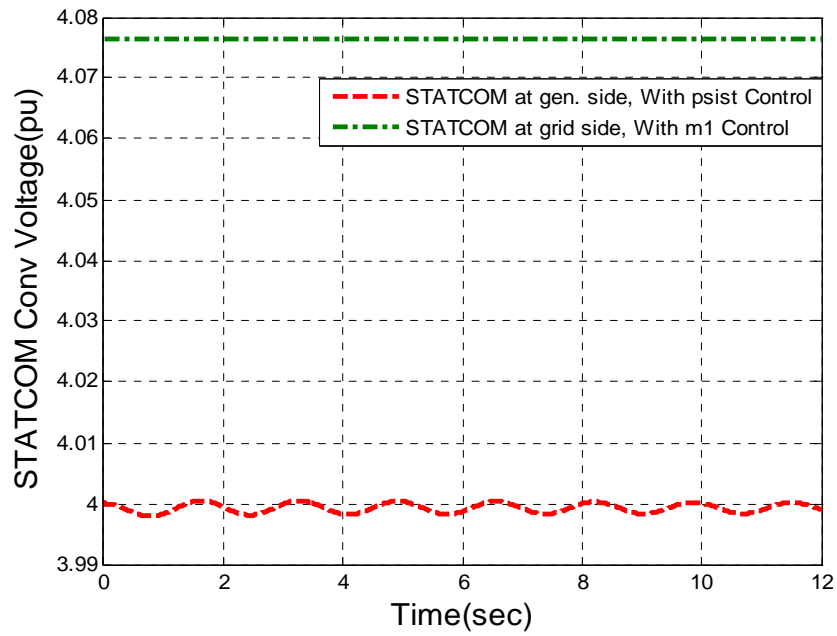


Figure 5.33 STATCOM conv. voltage of variable speed wind turbine PMSG at different  $R_{st}$  &  $L_{st}$

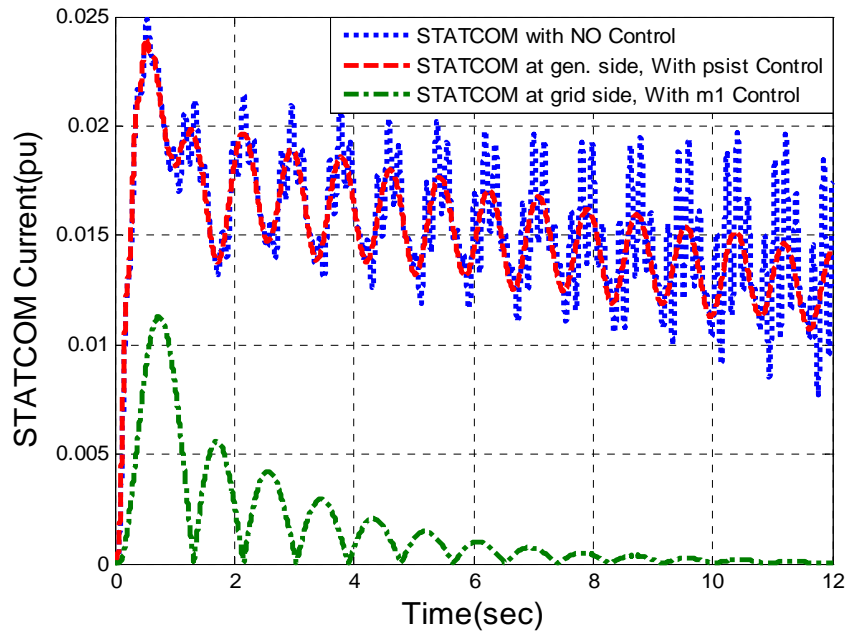


Figure 5.34 STATCOM current of variable speed wind turbine PMSG at different  $R_{st}$  &  $L_{st}$



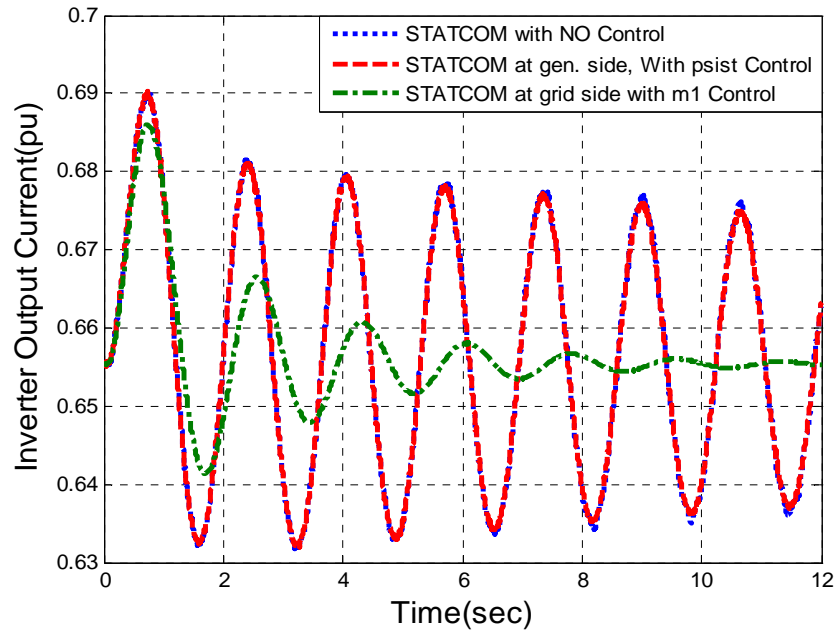


Figure 5.35 Inverter output current of variable speed wind turbine PMSG at different  $R_{st}$  &  $L_{st}$

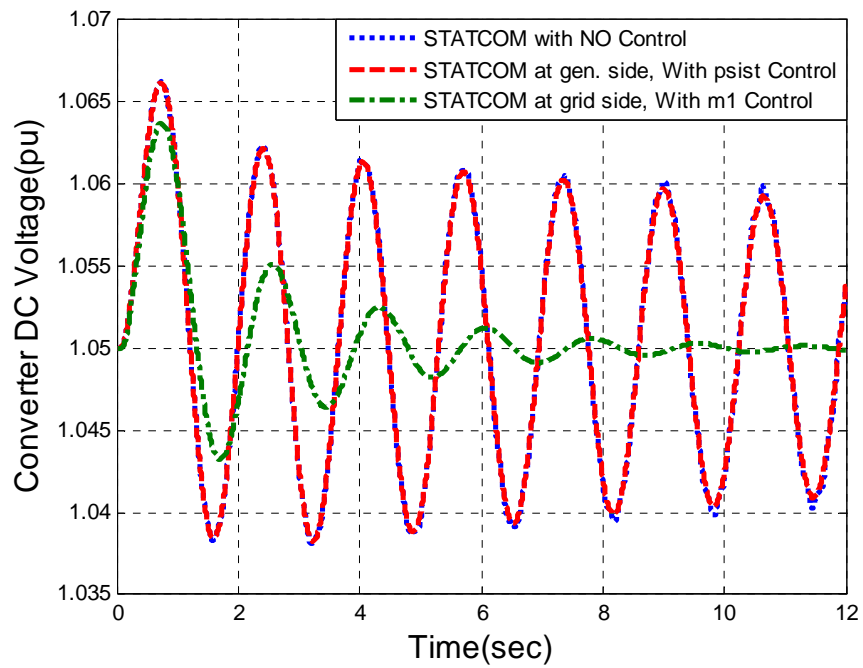


Figure 5.36 DC link voltage of variable speed wind turbine PMSG at different  $R_{st}$  &  $L_{st}$

From figure 5.37 it can be seen that, there is more overshoot for STATCOM connected on grid side converter with  $m_1$  control but as time elapses generator speed variations are reduced. The settling time is less with small oscillations in starting when compared to STATCOM connected at generator side converter with  $\Psi_{st}$  control.

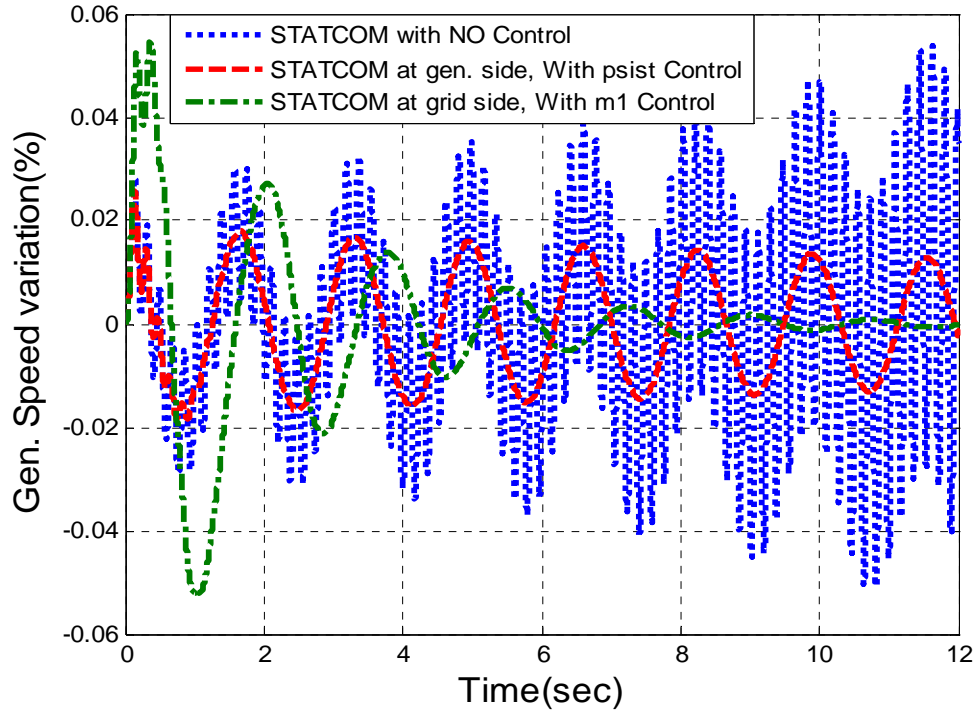


Figure 5.37 Generator speed variation of variable speed wind turbine PMSG at different  $R_{st}$  &  $L_{st}$

From figure 5.38 it can be seen that, there is more overshoot for STATCOM connected on grid side converter with  $m_1$  control when compared to STATCOM connected at generator side converter with  $\Psi_{st}$  control. The settling time is more with oscillations when STATCOM is connected at grid side converter.

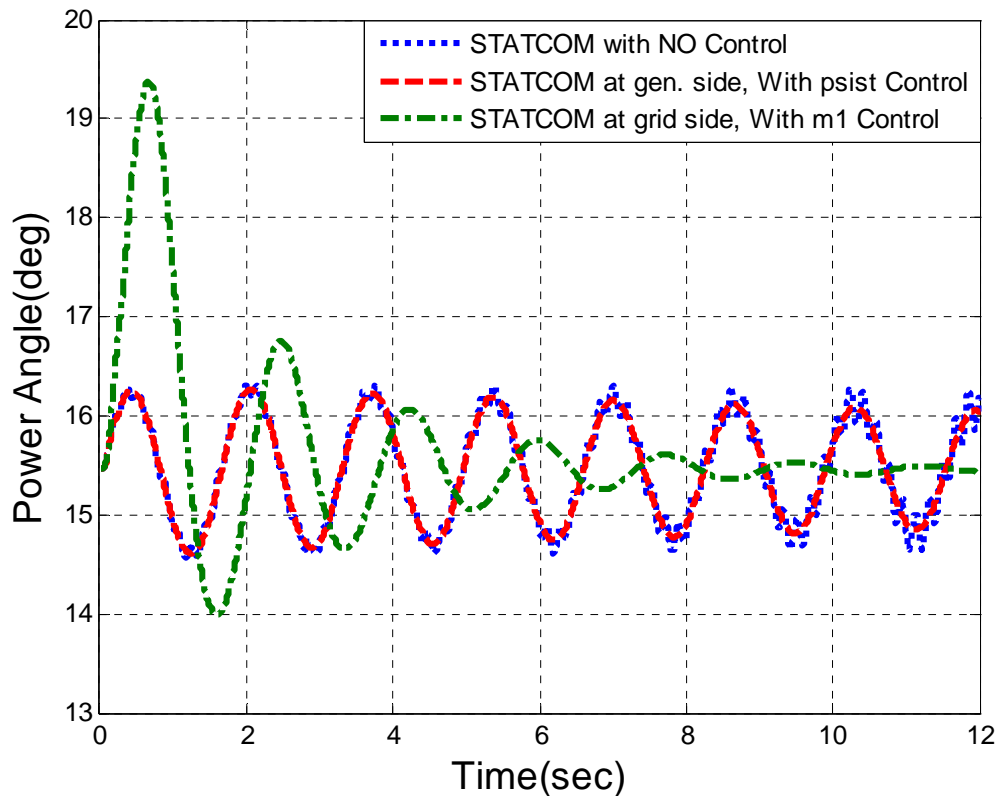


Figure 5.38 Power angle variation of variable speed wind turbine PMSG at different  $R_{st}$  &  $L_{st}$

Hence from figures (5.32 to 5.38) we observe that, STATCOM connected at grid side converter is more robust even with change in STATCOM parameters when subjected to 15% torque pulse for 0.1sec duration using PI controller.

Hence, it can be concluded that ideal location of STATCOM for variable speed wind turbine PMSG system is at the grid side converter. The system will be robust when a disturbance is on the wind turbine. Let us check when disturbance is on the load side or grid side of variable speed wind turbine PMSG system with STATCOM.

### 5.3 Simulation studies with disturbance (symmetrical 3 $\Phi$ fault) on grid bus

Let us check the behavior of variable speed wind turbine PMSG system with STATCOM connected at generator side-converter as well as grid side-converter independently, when a symmetrical 3 $\phi$  fault is applied on the grid bus,  $V_b$ . As concluded in chapter 4,  $\psi_{st}$  is the best control signal when STATCOM is connected at generator side-converter whereas  $m_1$  is the best control signal when STATCOM is connected at grid side-converter. Therefore non-linear time domain simulations are done using PI controller for a nominal loading of 0.65 p.u. when subjected to a symmetrical 3 $\phi$  fault on the grid bus for 0.1 sec duration. It was observed that system output is improved for both the configurations only when  $\Delta\omega_g$  is taken as the plant output as well as feedback signal for the PI controller.

The PI controller design was carried out in the previous chapter using pole-placement technique where the PI gains are adjusted to give desired closed loop system damping ratio ( $\zeta_{new} = 0.3$ ) when  $\Delta\omega_g$  is taken as plant output as well as feedback signal. The washout time constant was selected to be 0.02 sec.

From figure (5.39 – 5.43), we observe that there is almost no variation in grid power, terminal voltage and inverter output current with/without STATCOM device except during the fault period of 0.1 sec. It was also observed that figure 5.40 & 5.43 of generator power and DC link converter voltage takes more time, (around 1sec) to reach the steady state value.

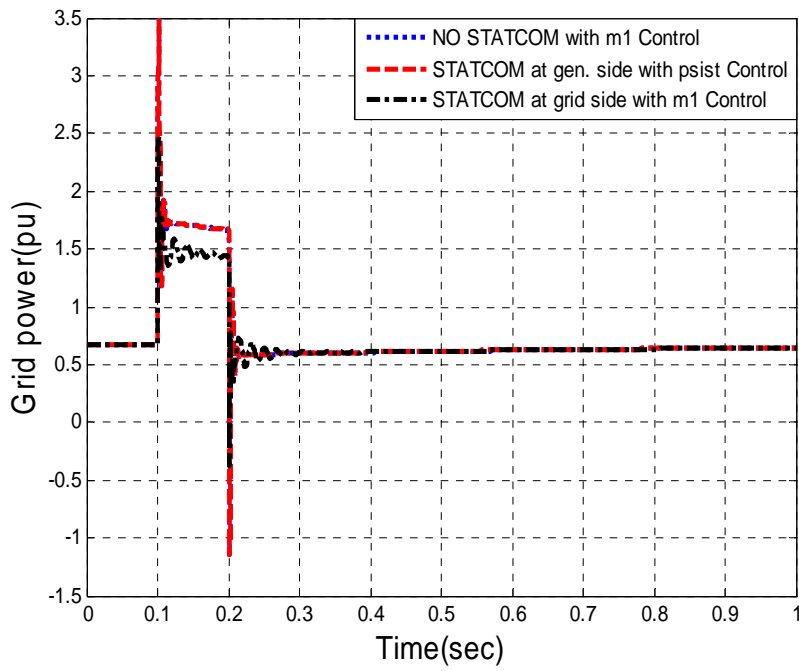


Figure 5.39 Grid power of variable speed wind turbine PMSG with and without STATCOM for a 3-phase fault on grid bus

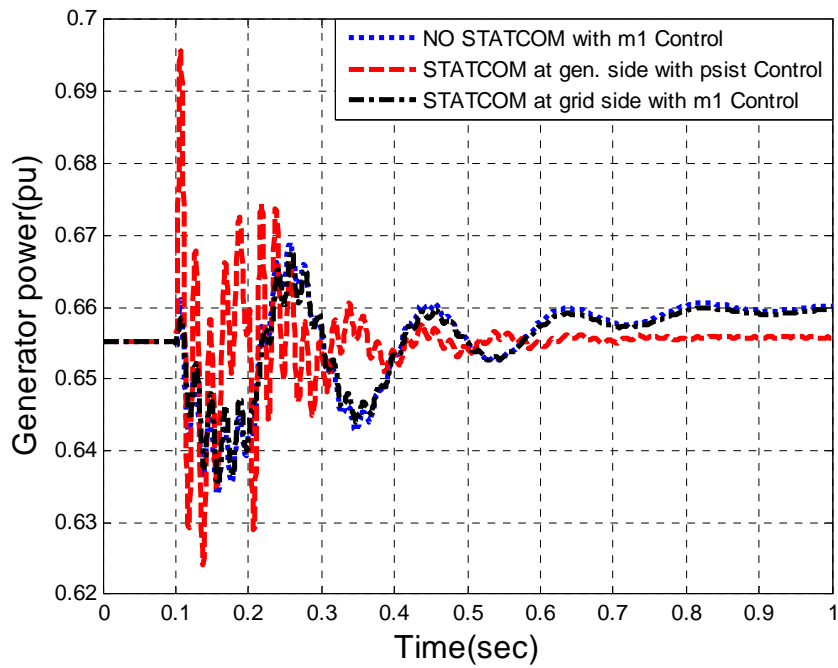


Figure 5.40 Generator power of variable speed wind turbine PMSG with and without STATCOM for a 3-phase fault on grid bus

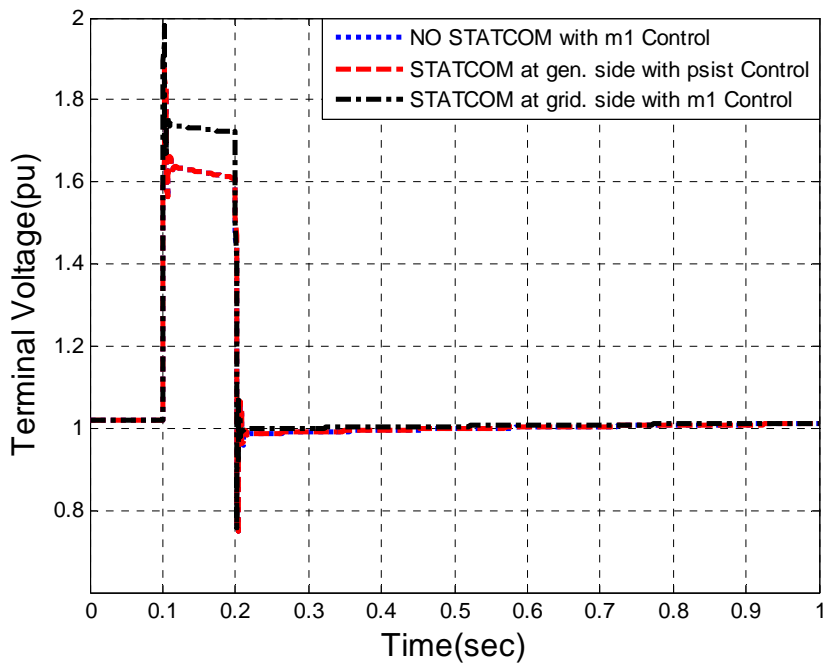


Figure 5.41 Terminal voltage of variable speed wind turbine PMSG with and without STATCOM for a 3-phase fault on grid bus

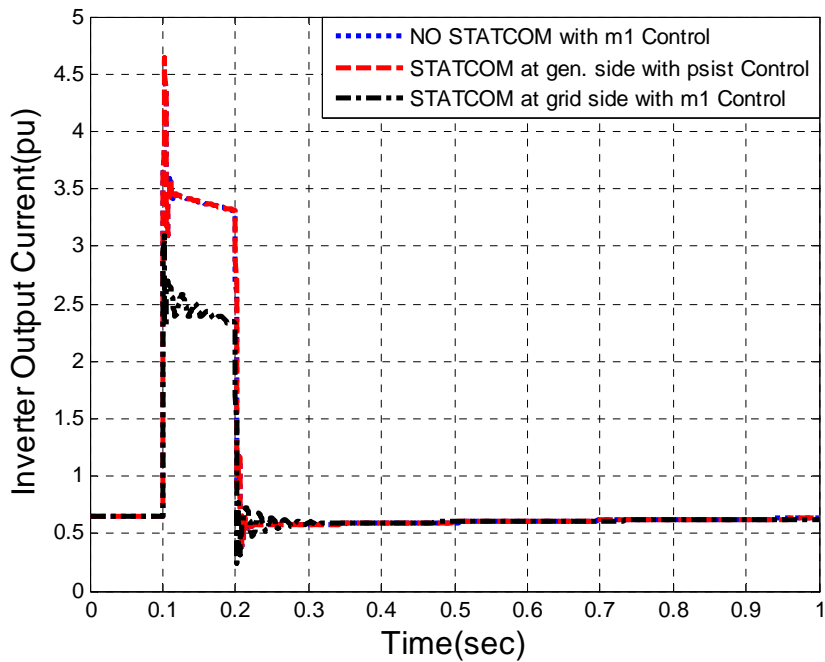


Figure 5.42 Inverter output current of variable speed wind turbine PMSG with and without STATCOM for a 3-phase fault on grid bus

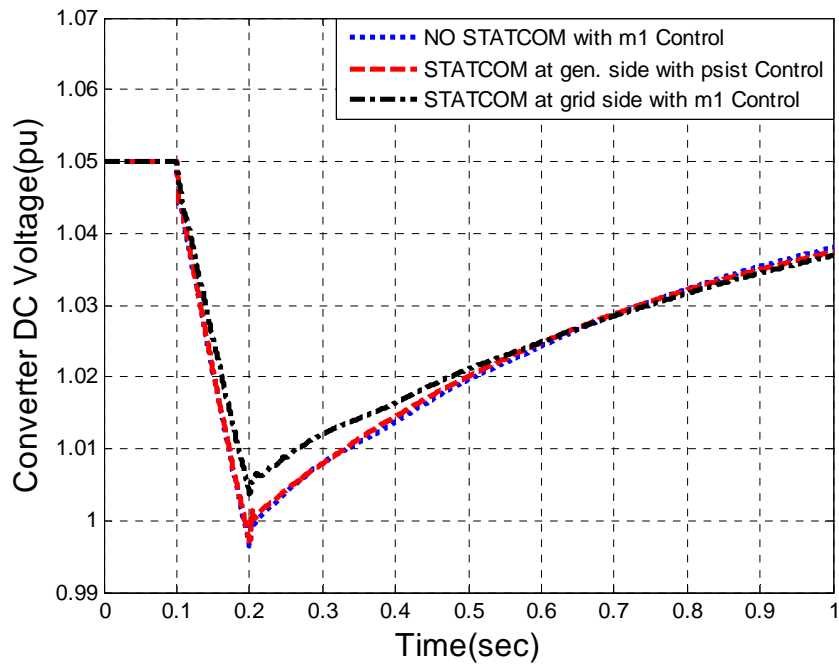


Figure 5.43 DC link voltage of variable speed wind turbine PMSG with and without STATCOM for a 3-phase fault on grid bus

From figures 5.44 & 5.45 it can be seen that generator speed variations and power angle variations are much improved when connected with STATCOM device. It was also observed that with STATCOM on generator side-converter, the generator speed and power angle variations are the lowest and steady state value is reached quickly when compared to STATCOM on grid side-converter during a 3 $\phi$  fault on the grid bus.

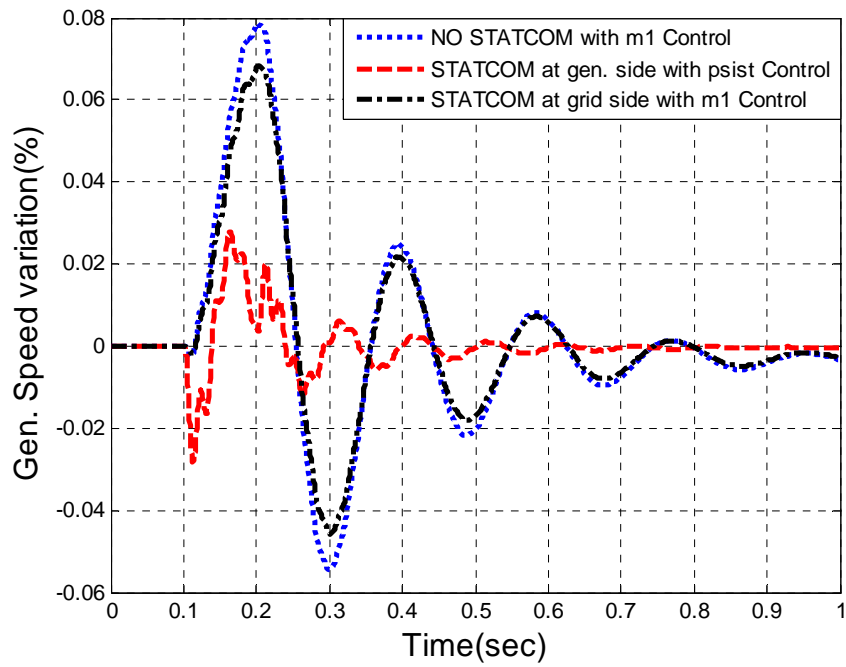


Figure 5.44 Generator speed variations of the variable speed wind turbine PMSG with and without STATCOM for a 3-phase fault on grid bus

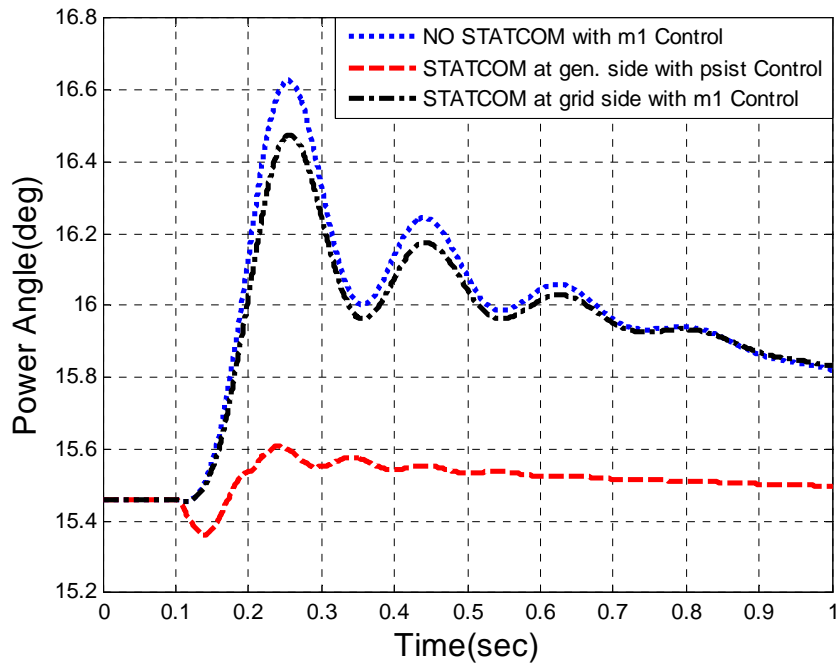


Figure 5.45 Power angle of the variable speed wind turbine PMSG with and without STATCOM for a 3-phase fault on grid bus



Hence it can be concluded from figures (5.39 - 5.45) that, STATCOM device helps in improving the system output when a 3 $\phi$  fault is applied on the grid bus.

#### **5.4 Simulation studies with disturbance (symmetrical 3 $\Phi$ fault) on load bus**

Let us check the behavior of variable speed wind turbine PMSG system with STATCOM connected at generator side-converter as well as grid side-converter independently, when a symmetrical 3 $\phi$  fault is applied on the load bus,  $V_t$ . As concluded in chapter 4,  $\psi_{st}$  is the best control signal when STATCOM is connected at generator side-converter whereas  $m_1$  is the best control signal when STATCOM is connected at grid side-converter. Therefore non-linear time domain simulations are done using PI controller for a nominal loading of 0.65 p.u. when subjected to a symmetrical 3 $\phi$  fault at the load bus for 0.1 sec duration. It was observed that system output is improved for both the configurations only when  $\Delta\omega_g$  is taken as the plant output as well as feedback signal for the PI controller.

The PI controller design was carried out in the previous chapter using pole-placement technique where the PI gains are adjusted to give desired closed loop system damping ratio ( $\zeta_{new} = 0.3$ ) when  $\Delta\omega_g$  is taken as plant output as well as feedback signal. The washout time constant was selected to be 0.02 sec.

From figure (5.46 – 5.50), we observe that there is almost no variation in grid power, terminal voltage and inverter output current with/without STATCOM device except during the fault period of 0.1 sec there is large overshoot. It was also observed that figure

5.47 & 5.50 of generator power and DC link converter voltage takes more time, (around 1sec) with less overshoot to reach the steady state value.

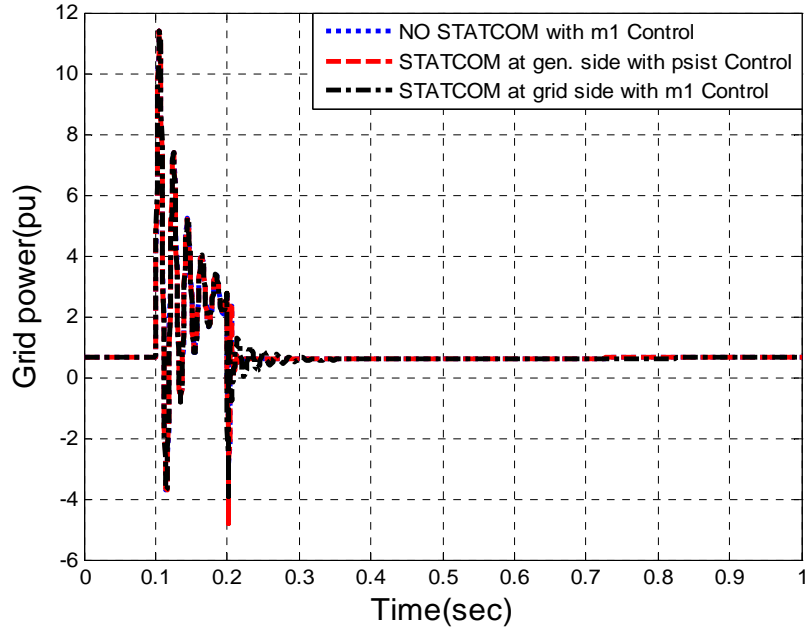


Figure 5.46 Grid power of variable speed wind turbine PMSG with and without STATCOM for a 3-phase fault on load bus

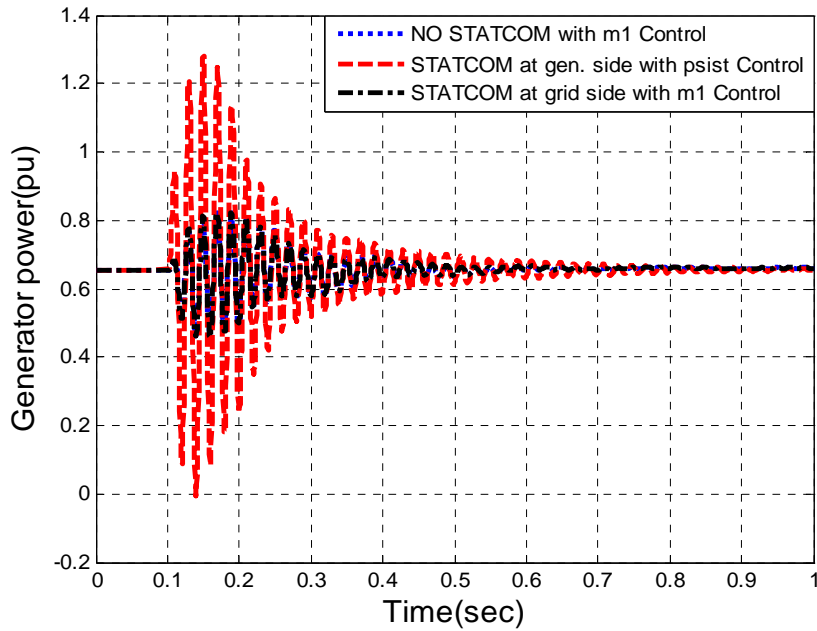


Figure 5.47 Generator power of variable speed wind turbine PMSG with and without STATCOM for a 3-phase fault on load bus

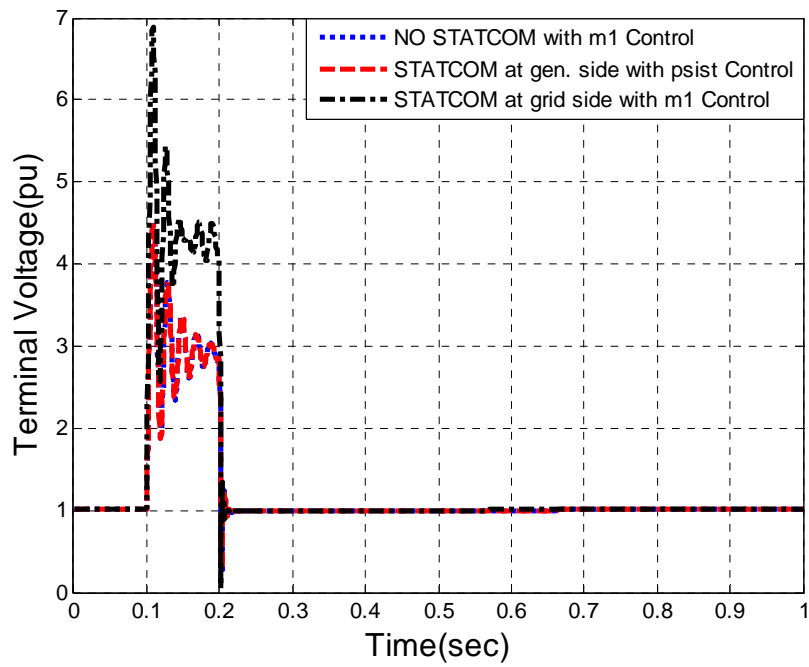


Figure 5.48 Terminal voltage of variable speed wind turbine PMSG with and without STATCOM for a 3-phase fault on load bus

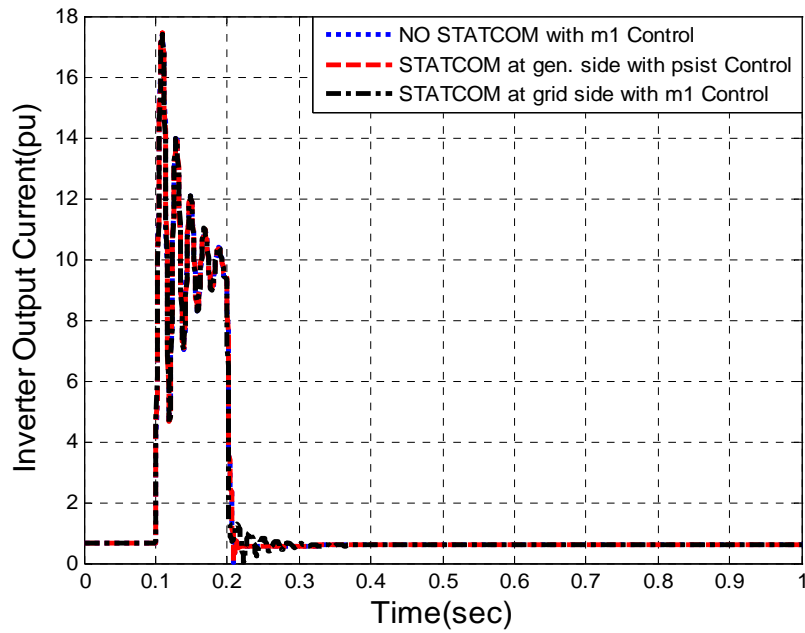


Figure 5.49 Inverter output current of variable speed wind turbine PMSG with and without STATCOM for a 3-phase fault on load bus

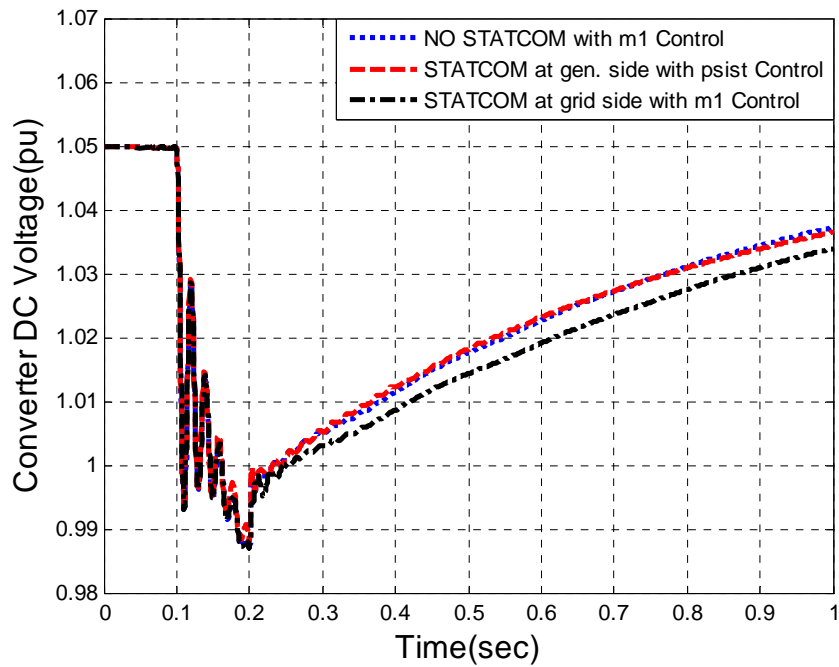


Figure 5.50 DC link voltage of variable speed wind turbine PMSG with and without STATCOM for a 3-phase fault on load bus

From figures 5.51 & 5.52 it can be seen that generator speed variations and power angle variations are much improved when connected with STATCOM device. It was also observed that with STATCOM on generator side-converter, the generator speed and power angle variations are the lowest and steady state value is reached quickly when compared to STATCOM on grid side-converter during a 3 $\phi$  fault on the load bus.

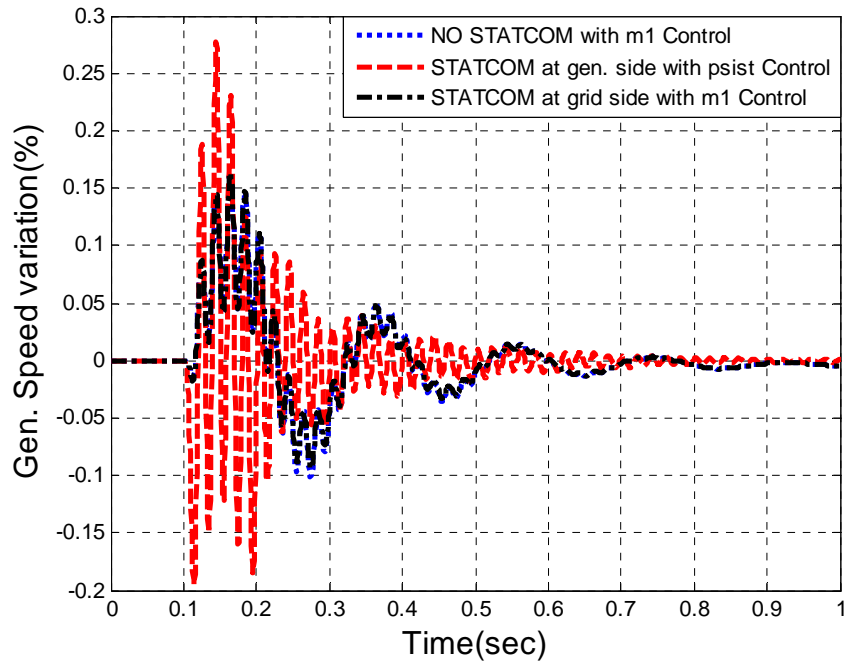


Figure 5.51 Generator speed variations of the variable speed wind turbine PMSG with and without STATCOM for a 3-phase fault on load bus

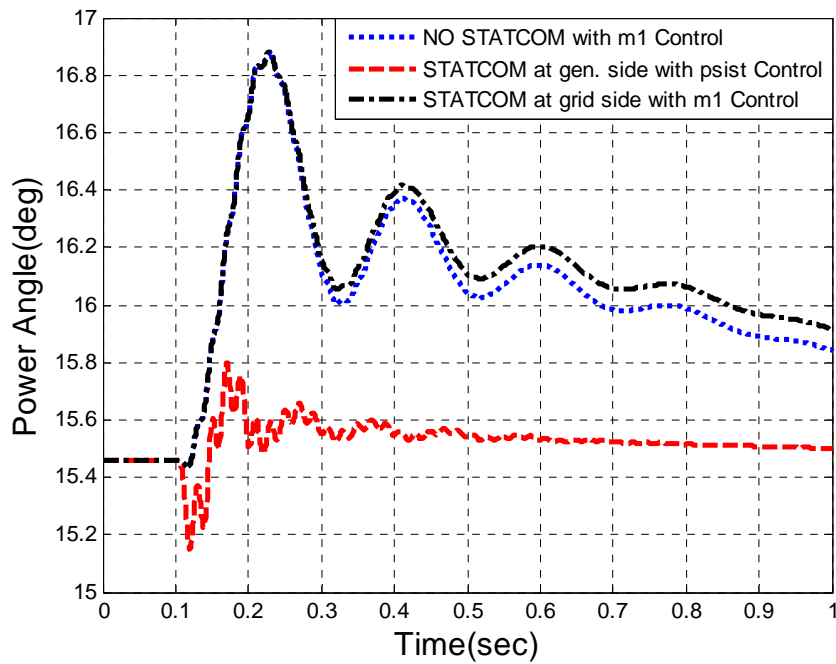


Figure 5.52 Power angle of the variable speed wind turbine PMSG with and without STATCOM for a 3-phase fault on load bus

Hence it can be concluded from figures (5.46 - 5.52) that, STATCOM device helps in improving the system output when a 3 $\phi$  fault is applied on the load bus.

From sections 5.3 & 5.4 it is found that 3 $\phi$  fault occurred near the variable speed wind turbine PMSG system is more severe than 3 $\phi$  fault occurred far from it. It is seen that when 3 $\phi$  fault is at the load bus,  $V_t$  more overshoot in system response is found when compare to 3 $\phi$  fault at grid bus,  $V_b$ .

## CHAPTER 6

### CONCLUSION AND FUTURE WORK

#### 6.1 Conclusion

The dynamic modeling of the variable speed wind turbine PMSG system along with STATCOM has been developed in this work. Nonlinear and linear models of the individual components of the variable speed PMSG system and STATCOM controller are obtained. The behavior of STATCOM controller interaction has been analyzed by placing it at generator side-converter and then on the grid side-converter independently.

From small signal analysis it has been observed that for the STATCOM participation at generator side-converter, the stability of the variable speed wind turbine PMSG system worsens as the amount of generator power increases. For power loading of 0.65 p.u. there exists critical value of electro-mechanical modes above which variable speed wind turbine PMSG performance degrades. Non-linear simulations were carried out in chapter 5 to verify the results obtained through small-signal analysis.

Decomposition techniques were utilized to identify the best control signal for controller design to damp the power system oscillations. It was found from decomposition techniques that phase angle of the STATCOM ( $\psi_{st}$ ) is the best control signal when STATCOM is connected at generator side-converter and modulation index of the generator side-converter, ( $m_1$ ) was identified to have the higher controllability to damp the oscillatory modes of the system when STATCOM is connected at grid side-converter

for variable speed wind turbine PMSG system. Frequency based approach is utilized to design the PI/PID controllers where the controller gains are tuned through an optimal pole placement technique. Comparisons were done between PI and PID controllers for a given control signal to show the effectiveness of the controller designed. Finally non-linear time domain simulations were performed when a symmetrical 3 $\phi$  fault is applied on the grid bus with STATCOM connected at generator side-converter as well as grid side-converter independently. Results are compared for both the cases when no STATCOM device is considered.

## **6.2 Future Work**

The following are the recommendations for further research in this work:

- In this thesis, variable speed wind turbine PMSG system is operated without pitch angle control. It will be interesting to study the behavior with pitch angle control.
- Throughout the thesis, single machine infinite bus system was adopted for the variable speed wind turbine PMSG system which operates in connection with the grid. It will be interesting to study the behavior of the PMSG in multi-machine power system environment.
- The effectiveness of the controllers other than PI/PID should be explored.
- Optimization techniques other than pole placement can be used to optimize controller parameters of the controller.
- Effect of different kinds of loads and also the impact of unsymmetrical faults on the variable speed wind turbine PMSG system can be studied.



## APPENDIX A

System parameters and operating values

### **Wind Plant:**

Nominal Power = 2MW

Rotor diameter = 75 m

Rotating Speed = 6.0 – 19.5 rpm

Nominal Wind Speed = 11.95 m/sec

### **PMSG:**

Rated Power = 2MW;            Stator rated line voltage = 690V;

Rated frequency = 50Hz.      Number of Pole Pairs = 154

$R_a = 0.01 \text{ p.u.}$     $X_d = 0.8 \text{ p.u.}$     $X_q = 0.5 \text{ p.u.}$     $D_g = 0.6 \text{ p.u.}$

$H_g = 0.5 \text{ p.u.}$     $H_t = 3 \text{ p.u.}$     $K_s = 0.3 \text{ p.u.}$     $D_t = 0.6 \text{ p.u.}$

$R_i = 0.01 \text{ p.u.}$     $X_i = 0.1 \text{ p.u.}$     $C = 1 \text{ p.u.}$

### **STATCOM:**

$R_{st} = 0.01 \text{ p.u.}$     $L_{st} = 0.15 \text{ p.u.}$     $C_{dc} = 1 \text{ p.u.}$

### **Load & Transmission Line:**

Load Admittance ( $Y_{11}$ ) =  $0.2 - j0.4 \text{ p.u.}$

Transmission Line Impedance ( $Z_{line}$ ) =  $R + jX = 0.16 + j0.2 \text{ p.u.}$

## APPENDIX B

### The LOAD and LINE Model

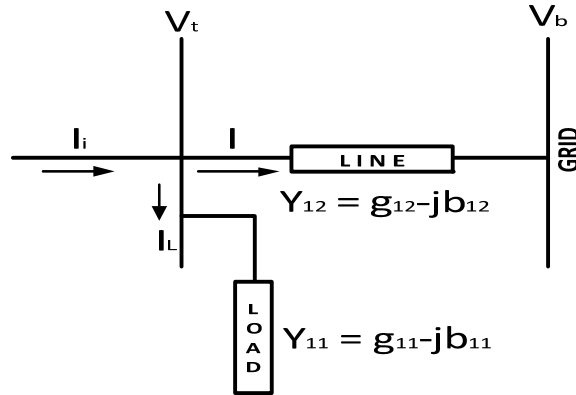


**Figure B .1**The transmission line-load network

Retaining the notation for generator operation, the current in the transmission line shown in Fig.B.1 is written as,

$$I_i = I_L + I = V_t \cdot Y_{11} + (V_t - V_b) \cdot Y_{12} \quad (\text{B.1})$$

Here,

$Y_{11} = g_{11} - j b_{11}$  is the local load admittance and  $Y_{12} = g_{12} - j b_{12}$  is the Tr. line admittance,

$V_t = V_{td} + jV_{tq}$  is the load terminal voltage, and  $V_b = V_{bd} + j0$  is the grid voltage referenced

along the d-axis. Substituting the above expressions in equation ( B.1 ), we get;

$$i_{id} + j i_{iq} = (V_{td} + jV_{tq}) \cdot (g_{11} - jb_{11}) + (V_{td} - V_{bd} + jV_{tq}) \cdot (g_{12} - jb_{12}) \quad (\text{B.2})$$

Equating real and imaginary parts, we get;

$$\begin{aligned}
i_{id} &= (V_{td}g_{11} + V_{tq}b_{11}) + ((V_{td} - V_{bd})g_{12} + V_{tq}b_{12}) \\
i_{iq} &= (V_{tq}g_{11} - V_{td}b_{11}) + (V_{tq}g_{12} - (V_{td} - V_{bd})b_{12})
\end{aligned} \tag{B.3}$$

Simplifying the above equation and replacing  $V_{bd}$  by  $V_b$ , we get;

$$\begin{aligned}
i_{id} &= V_{td}(g_{11} + g_{12}) + V_{tq}(b_{11} + b_{12}) - V_b g_{12} \\
i_{iq} &= -V_{td}(b_{11} + b_{12}) + V_{tq}(g_{11} + g_{12}) + V_b b_{12}
\end{aligned} \tag{B.4}$$

Writing the above equation in matrix form we get;

$$\begin{bmatrix} i_{id} \\ i_{iq} \end{bmatrix} = \begin{bmatrix} (g_{11} + g_{12}) & (b_{11} + b_{12}) \\ -(b_{11} + b_{12}) & (g_{11} + g_{12}) \end{bmatrix} \begin{bmatrix} V_{td} \\ V_{tq} \end{bmatrix} + \begin{bmatrix} -g_{12} \\ +b_{12} \end{bmatrix} [V_b] \tag{B.5}$$

Modifying the above equation to get expression for  $V_{td}$ ,  $V_{tq}$ , we get;

$$\begin{bmatrix} i_{id} + V_b \cdot g_{12} \\ i_{iq} - V_b \cdot b_{12} \end{bmatrix} = \begin{bmatrix} (g_{11} + g_{12}) & (b_{11} + b_{12}) \\ -(b_{11} + b_{12}) & (g_{11} + g_{12}) \end{bmatrix} \begin{bmatrix} V_{td} \\ V_{tq} \end{bmatrix} \tag{B.6}$$

On taking inverse,

$$\begin{bmatrix} (g_{11} + g_{12}) & (b_{11} + b_{12}) \\ -(b_{11} + b_{12}) & (g_{11} + g_{12}) \end{bmatrix}^{-1} \begin{bmatrix} i_{id} + V_b \cdot g_{12} \\ i_{iq} - V_b \cdot b_{12} \end{bmatrix} = \begin{bmatrix} V_{td} \\ V_{tq} \end{bmatrix}$$

For simplicity, let us take;

$$\begin{bmatrix} (g_{11} + g_{12}) & (b_{11} + b_{12}) \\ -(b_{11} + b_{12}) & (g_{11} + g_{12}) \end{bmatrix}^{-1} = \begin{bmatrix} k_1 & k_2 \\ k_3 & k_4 \end{bmatrix} \tag{B.7}$$

Therefore, the equations for  $V_{td}$ ,  $V_{tq}$  in terms of  $i_{id}$ ,  $i_{iq}$  in matrix form will be;

$$\begin{bmatrix} V_{td} \\ V_{tq} \end{bmatrix} = \begin{bmatrix} k_1 & k_2 \\ k_3 & k_4 \end{bmatrix} \begin{bmatrix} i_{id} + V_b \cdot g_{12} \\ i_{iq} - V_b \cdot b_{12} \end{bmatrix} = \begin{bmatrix} k_1(i_{id} + V_b \cdot g_{12}) + k_2(i_{iq} - V_b \cdot b_{12}) \\ k_3(i_{id} + V_b \cdot g_{12}) + k_4(i_{iq} - V_b \cdot b_{12}) \end{bmatrix}$$

On further simplifying we get the final expression as;

$$\begin{aligned} V_{td} &= k_1 i_{id} + k_2 i_{iq} + V_b (k_1 \cdot g_{12} - k_2 \cdot b_{12}) \\ V_{tq} &= k_3 i_{id} + k_4 i_{iq} + V_b (k_3 \cdot g_{12} - k_4 \cdot b_{12}) \end{aligned} \tag{B.8}$$

## APPENDIX C

In this section the small signal model of various components of the variable Speed PMSG system without STATCOM Controller is obtained by linearizing the non-linear equations developed in sections (3.1-3.3). The small signal model of the WECS includes the linearized state space model of wind-turbine & wind system, PMSG model, drive train model and static converters model. The state equations from section (3.1-3.3) are as follows;

$$p(i_{gd}) = \frac{\omega_o}{X_d} [-R_a i_{gd} + X_q i_{gq} \omega_g - m_1 V_c \sin \delta]$$

$$p(i_{gq}) = \frac{\omega_o}{X_q} [-X_d i_{gd} \omega_g - R_a i_{gq} + \psi_o \omega_g - m_1 V_c \cos \delta]$$

$$p(\delta) = \omega_o (\omega_g - 1)$$

$$p(\omega_g) = \frac{1}{2H_g} (K_s \theta_s - P_{ag} - D_g (\omega_g - 1))$$

$$p(\theta_s) = \omega_o (\omega_t - \omega_g)$$

$$p(\omega_t) = \frac{1}{2H_t} (P_m - K_s \theta_s - D_t (\omega_t - 1))$$

$$p(V_c) = \frac{1}{C} [m_1 i_{gd} \sin \delta + m_1 i_{gq} \cos \delta - m_2 i_{id} \cos \alpha_2 + m_2 i_{iq} \sin \alpha_2]$$

$$p(i_{id}) = \frac{\omega_o}{X_i} [-(R_i + k_1) i_{id} + (\omega_e X_i - k_2) i_{iq} - m_2 V_c \cos \alpha_2 - V_b (k_3 g_{12} - k_4 b_{12})]$$

$$p(i_{iq}) = \frac{\omega_o}{X_i} [-(\omega_e X_i + k_3) i_{id} - (R_i + k_4) i_{iq} + m_2 V_c \sin \alpha_2 - V_b (k_3 g_{12} - k_4 b_{12})]$$

$$[1] \quad p(i_{gd}) = \frac{\omega_o}{X_d} [-R_a i_{gd} + X_q i_{gq} \omega_g - m_1 V_c \sin \delta]$$

$$p(\Delta i_{gd}) = \frac{\omega_o}{X_d} [-R_a \Delta i_{gd} + X_q \omega_{go} \Delta i_{gq} + X_q i_{gqo} \Delta \omega_g - m_{1o} V_{co} \cos \delta_o \Delta \delta - m_{1o} \sin \delta_o \Delta V_c - V_{co} \sin \delta_o \Delta m_1]$$

where,

$$\Delta V_{gd} = m_{1o} V_{co} \cos \delta_o \Delta \delta + m_{1o} \sin \delta_o \Delta V_c + V_{co} \sin \delta_o \Delta m_1$$

$$[2] \quad p(i_{gq}) = \frac{\omega_o}{X_q} [-X_d i_{gd} \omega_g - R_a i_{gq} + \psi_o \omega_g - m_1 V_c \cos \delta]$$

$$p(\Delta i_{gq}) = \frac{\omega_o}{X_q} [-R_a \Delta i_{gq} - X_d \omega_{go} \Delta i_{gd} - X_d i_{gdo} \Delta \omega_g + \psi_o \Delta \omega_g + m_{1o} V_{co} \sin \delta_o \Delta \delta - m_{1o} \cos \delta_o \Delta V_c - V_{co} \cos \delta_o \Delta m_1]$$

where,

$$\Delta V_{gq} = -m_{1o} V_{co} \sin \delta_o \Delta \delta + m_{1o} \cos \delta_o \Delta V_c + V_{co} \cos \delta_o \Delta m_1$$

$$[3] \quad p(\Delta \delta) = \omega_o (\Delta \omega_g - 0)$$

$$p(\Delta \delta) = \omega_o \Delta \omega_g$$

$$[4] \quad p(\Delta\omega_g) = \frac{1}{2H_g} [K_s \Delta\theta_s - \Delta P_{ag} - D_g (\Delta\omega_g - 0)]$$

$$p(\Delta\omega_g) = \frac{1}{2H_g} \{ K_s \Delta\theta_s - [(2R_a i_{gdo} + m_{1o} V_{co} \sin\delta_o) \Delta i_{gd} + (2R_a i_{gqo} + m_{1o} V_{co} \cos\delta_o) \Delta i_{gq}] + m_{1o} V_{co} (\cos\delta_o i_{gdo} - \sin\delta_o i_{gqo}) \Delta\delta + m_{1o} (\sin\delta_o i_{gdo} + \cos\delta_o i_{gqo}) \Delta V_c + V_{co} (\sin\delta_o i_{gdo} + \cos\delta_o i_{gqo}) \Delta m_1 - D_g \Delta\omega_g \}$$

where,

$$\Delta P_{ag} = [(2R_a i_{gdo} + m_{1o} V_{co} \sin\delta_o) \Delta i_{gd} + (2R_a i_{gqo} + m_{1o} V_{co} \cos\delta_o) \Delta i_{gq}] + m_{1o} V_{co} (\cos\delta_o i_{gdo} - \sin\delta_o i_{gqo}) \Delta\delta + m_{1o} (\sin\delta_o i_{gdo} + \cos\delta_o i_{gqo}) \Delta V_c + V_{co} (\sin\delta_o i_{gdo} + \cos\delta_o i_{gqo}) \Delta m_1]$$

$$[5] \quad p(\Delta\theta_s) = \omega_o (\Delta\omega_t - \Delta\omega_g)$$

$$[6] \quad p(\Delta\omega_t) = \frac{1}{2H_t} [\Delta P_m - K_s \Delta\theta_s - D_t (\Delta\omega_t - 0)]$$

$$\Delta P_m = [6c_1 n_{to}^5 + 5c_2 n_{to}^4 + \dots + c_6] \Delta n_t$$

$$\text{Here, } \Delta n_t = -\frac{30}{\pi} \Delta\omega_t \text{ and,}$$

$$p(\Delta\omega_t) = \frac{-K_s}{2H_t} \Delta\theta_s + \frac{-1}{2H_t} ([6c_1 n_{to}^5 + 5c_2 n_{to}^4 + \dots + c_6] \frac{30}{\pi} + D_t) \Delta\omega_t$$

$$[7] \quad p(V_c) = \frac{1}{C} [m_1 i_{gd} \sin \delta + m_1 i_{gq} \cos \delta - m_2 i_{id} \cos \alpha_2 + m_2 i_{iq} \sin \alpha_2]$$

$$\begin{aligned} p(\Delta V_c) = \frac{1}{C} [ & m_{1o} \sin \delta_o \Delta i_{gd} + \sin \delta_o i_{gdo} \Delta m_1 + m_{1o} \cos \delta_o i_{gdo} \Delta \delta \\ & + m_{1o} \cos \delta_o \Delta i_{gq} + \cos \delta_o i_{gqo} \Delta m_1 - m_{1o} \sin \delta_o i_{gqo} \Delta \delta \\ & - m_{2o} \cos \alpha_{2o} \Delta i_{id} - \cos \alpha_{2o} i_{ido} \Delta m_2 + m_{2o} \sin \alpha_{2o} i_{ido} \Delta \alpha_2 \\ & + m_{2o} \sin \alpha_{2o} \Delta i_{iq} + \sin \alpha_{2o} i_{iqo} \Delta m_2 + m_{2o} \cos \alpha_{2o} i_{iqo} \Delta \alpha_2] \end{aligned}$$

$$[8] \quad p(i_{id}) = \frac{\omega_o}{X_i} [-(R_i + k_1) i_{id} + (\omega_e X_i - k_2) i_{iq} - m_2 V_c \cos \alpha_2 - V_b (k_1 g_{12} - k_2 b_{12})]$$

$$\begin{aligned} p(\Delta i_{id}) = \frac{\omega_o}{X_i} [ & -(R_i + k_1) \Delta i_{id} + (\omega_{eo} X_i - k_2) \Delta i_{iq} + X_i i_{iqo} \Delta \omega_e \\ & - m_{2o} \cos \alpha_{2o} \Delta V_c - V_{co} \cos \alpha_{2o} \Delta m_2 + m_{2o} V_{co} \sin \alpha_{2o} \Delta \alpha_2 - 0] \end{aligned}$$

$$[9] \quad p(i_{iq}) = \frac{\omega_o}{X_i} [-(\omega_e X_i + k_3) i_{id} - (R_i + k_4) i_{iq} + m_2 V_c \sin \alpha_2 - V_b (k_3 g_{12} - k_4 b_{12})]$$

$$\begin{aligned} p(\Delta i_{iq}) = \frac{\omega_o}{X_i} [ & -(\omega_{eo} X_i + k_3) \Delta i_{id} - X_i i_{ido} \Delta \omega_e - (R_i + k_4) \Delta i_{iq} \\ & + m_{2o} \sin \alpha_{2o} \Delta V_c + V_{co} \sin \alpha_{2o} \Delta m_2 + m_{2o} V_{co} \cos \alpha_{2o} \Delta \alpha_2 - 0] \end{aligned}$$



## APPENDIX D

In this section the small signal model of Variable Speed PMSG system with STATCOM Controller at Generator Side-Converter (Rectifier) system is obtained by linearizing the non-linear equations developed in the section 3.5 as given below;

$$p(i_{gd}) = \frac{\omega_o}{X_d} \left[ -R_a i_{gd} + X_q i_{gq} \omega_g - m_1 V_c \sin \delta \right]$$

$$p(i_{gq}) = \frac{\omega_o}{X_q} \left[ -X_d i_{gd} \omega_g - R_a i_{gq} + \psi_o \omega_g - m_1 V_c \cos \delta \right]$$

$$p(\delta) = \omega_o (\omega_g - 1)$$

$$p(\omega_g) = \frac{1}{2H_g} (K_s \theta_s - P_{ag} - D_g (\omega_g - 1))$$

$$p(\theta_s) = \omega_o (\omega_t - \omega_g)$$

$$p(\omega_t) = \frac{1}{2H_t} (P_m - K_s \theta_s - D_t (\omega_t - 1))$$

$$p(V_c) = \frac{1}{C} [m_1 (i_{gd} + i_{std}) \sin \delta + m_1 (i_{gq} + i_{stq}) \cos \delta - m_2 i_{id} \cos \alpha_2 + m_2 i_{iq} \sin \alpha_2]$$

$$p(i_{id}) = \frac{\omega_o}{X_i} \left[ -(R_i + k_1) i_{id} + (\omega_e X_i - k_2) i_{iq} - m_2 V_c \cos \alpha_2 - V_b (k_1 g_{12} - k_2 b_{12}) \right]$$

$$p(i_{iq}) = \frac{\omega_o}{X_i} \left[ -(\omega_e X_i + k_3) i_{id} - (R_i + k_4) i_{iq} + m_2 V_c \sin \alpha_2 - V_b (k_3 g_{12} - k_4 b_{12}) \right]$$

$$p(i_{std}) = \frac{\omega_o}{L_{st}} \left[ -R_{st} i_{std} + \omega_g L_{st} i_{stq} + m_{st} V_{dc} \cos(\psi_{st}) - m_1 V_c \sin \delta \right]$$

$$p(i_{stq}) = \frac{\omega_o}{L_{st}} \left[ -\omega_g L_{st} i_{std} - R_{st} i_{stq} + m_{st} V_{dc} \sin(\psi_{st}) - m_1 V_c \cos \delta \right]$$

$$p(V_{dc}) = -\frac{m_{st}}{C_{dc}} \left[ \cos(\psi_{st}) \cdot i_{std} + \sin(\psi_{st}) \cdot i_{stq} \right]$$

Since, linearization is done in Appendix C for 9 state equations. Therefore, only STATCOM controller state equations / state equations affected due to STATCOM controller will be linearized and the rest will be ignored to avoid repetition.

$$[7] \quad p(V_c) = \frac{1}{C} [m_1(i_{gd} + i_{std})\sin\delta + m_1(i_{gq} + i_{stq})\cos\delta - m_2i_{id}\cos\alpha_2 + m_2i_{iq}\sin\alpha_2]$$

$$\begin{aligned} p(\Delta V_c) = \frac{1}{C} [ & m_{1o}\sin\delta_o \Delta i_{gd} + \sin\delta_o i_{gdo} \Delta m_1 + m_{1o}\cos\delta_o i_{gdo} \Delta\delta \\ & + m_{1o}\cos\delta_o \Delta i_{gq} + \cos\delta_o i_{gqo} \Delta m_1 - m_{1o}\sin\delta_o i_{gqo} \Delta\delta \\ & - m_{2o}\cos\alpha_{2o} \Delta i_{id} - \cos\alpha_{2o} i_{ido} \Delta m_2 + m_{2o}\sin\alpha_{2o} i_{ido} \Delta\alpha_2 \\ & + m_{2o}\sin\alpha_{2o} \Delta i_{iq} + \sin\alpha_{2o} i_{iqo} \Delta m_2 + m_{2o}\cos\alpha_{2o} i_{iqo} \Delta\alpha_2 \\ & + m_{1o}\sin\delta_o \Delta i_{std} + m_{1o}\cos\delta_o \Delta i_{stq}] \end{aligned}$$

$$[10] \quad p(i_{std}) = \frac{\omega_o}{L_{st}} [-R_{st}i_{std} + \omega_g L_{st}i_{stq} + m_{st}V_{dc}\cos(\psi_{st}) - m_1V_c\sin\delta]$$

$$\begin{aligned} p(\Delta i_{std}) = \frac{\omega_o}{L_{st}} [ & -R_{st} \Delta i_{std} + \omega_{go} L_{st} \Delta i_{stq} + m_{sto}\cos(\psi_{sto}) \Delta V_{dc} + V_{dco}\cos(\psi_{sto}) \Delta m_{st} \\ & - m_{sto}V_{dco}\sin(\psi_{sto}) \Delta\psi_{st} - m_{1o}V_{co}\cos\delta_o \Delta\delta - m_{1o}\sin\delta_o \Delta V_c - V_{co}\sin\delta_o \Delta m_1] \end{aligned}$$

$$\begin{aligned} p(\Delta i_{std}) = \frac{\omega_o}{L_{st}} [ & -m_{1o}V_{co}\cos\delta_o \Delta\delta - m_{1o}\sin\delta_o \Delta V_c - R_{st} \Delta i_{std} + \omega_{go} L_{st} \Delta i_{stq} \\ & + m_{sto}\cos(\psi_{sto}) \Delta V_{dc} - V_{co}\sin\delta_o \Delta m_1 + V_{dco}\cos(\psi_{sto}) \Delta m_{st} - m_{sto}V_{dco}\sin(\psi_{sto}) \Delta\psi_{st}] \end{aligned}$$

$$[11] \quad p(i_{stq}) = \frac{\omega_o}{L_{st}} \left[ -\omega_g L_{st} i_{std} - R_{st} i_{stq} + m_{st} V_{dc} \sin(\psi_{st}) - m_1 V_c \cos\delta \right]$$

$$p(\Delta i_{stq}) = \frac{\omega_o}{L_{st}} \left[ -\omega_{go} L_{st} \Delta i_{std} - R_{st} \Delta i_{stq} + m_{sto} \sin(\psi_{sto}) \Delta V_{dc} + V_{dco} \sin(\psi_{sto}) \Delta m_{st} \right. \\ \left. + m_{sto} V_{dco} \cos(\psi_{sto}) \Delta \psi_{st} + m_{lo} V_{co} \sin\delta_o \Delta \delta - m_{lo} \cos\delta_o \Delta V_c - V_{co} \cos\delta_o \Delta m_1 \right]$$

$$p(\Delta i_{stq}) = \frac{\omega_o}{L_{st}} \left[ m_{lo} V_{co} \sin\delta_o \Delta \delta - m_{lo} \cos\delta_o \Delta V_c - \omega_{go} L_{st} \Delta i_{std} - R_{st} \Delta i_{stq} \right. \\ \left. + m_{sto} \sin(\psi_{sto}) \Delta V_{dc} - V_{co} \cos\delta_o \Delta m_1 + V_{dco} \sin(\psi_{sto}) \Delta m_{st} + m_{sto} V_{dco} \cos(\psi_{sto}) \Delta \psi_{st} \right]$$

$$[12] \quad p(V_{dc}) = -\frac{m_{st}}{C_{dc}} \left[ \cos(\psi_{st}) \cdot i_{std} + \sin(\psi_{st}) \cdot i_{stq} \right]$$

$$p(\Delta V_{dc}) = -\frac{1}{C_{dc}} \left[ m_{sto} \cos(\psi_{sto}) \Delta i_{std} + \cos(\psi_{sto}) i_{stdo} \Delta m_{st} + m_{sto} \cos(\psi_{sto}) i_{stqo} \Delta \psi_{st} \right. \\ \left. + m_{sto} \sin(\psi_{sto}) \Delta i_{stq} + \sin(\psi_{sto}) i_{stqo} \Delta m_{st} - m_{sto} \sin(\psi_{sto}) i_{stdo} \Delta \psi_{st} \right]$$

$$p(\Delta V_{dc}) = -\frac{1}{C_{dc}} \left[ m_{sto} \cos(\psi_{sto}) \Delta i_{std} + m_{sto} \sin(\psi_{sto}) \Delta i_{stq} \right]$$

(Since,  $i_{stdo}$  &  $i_{stqo}$  are having zero initial value).

The matrix representation of Linearized 12<sup>th</sup> order model of variable Speed PMSG system with STATCOM Controller on Rectifier side is as shown below;

$$\begin{bmatrix} p(\Delta i_{gd}) \\ p(\Delta i_{gq}) \\ p(\Delta \delta) \\ p(\Delta \omega_g) \\ p(\Delta \theta_s) \\ p(\Delta \omega_t) \\ p(\Delta V_c) \\ p(\Delta i_{id}) \\ p(\Delta i_{iq}) \\ p(\Delta i_{std}) \\ p(\Delta i_{stq}) \\ p(\Delta V_{dc}) \end{bmatrix} = \begin{bmatrix} A_{11} & A_{12} & A_{13} & A_{14} & A_{15} & A_{16} & A_{17} & A_{18} & A_{19} & A_{1,10} & A_{1,11} & A_{1,12} \\ A_{21} & A_{22} & A_{23} & A_{24} & A_{25} & A_{26} & A_{27} & A_{28} & A_{29} & A_{2,10} & A_{2,11} & A_{2,12} \\ A_{31} & A_{32} & A_{33} & A_{34} & A_{35} & A_{36} & A_{37} & A_{38} & A_{39} & A_{3,10} & A_{3,11} & A_{3,12} \\ A_{41} & A_{42} & A_{43} & A_{44} & A_{45} & A_{46} & A_{47} & A_{48} & A_{49} & A_{4,10} & A_{4,11} & A_{4,12} \\ A_{51} & A_{52} & A_{53} & A_{54} & A_{55} & A_{56} & A_{57} & A_{58} & A_{59} & A_{5,10} & A_{5,11} & A_{5,12} \\ A_{61} & A_{62} & A_{63} & A_{64} & A_{65} & A_{66} & A_{67} & A_{68} & A_{69} & A_{6,10} & A_{6,11} & A_{6,12} \\ A_{71} & A_{72} & A_{73} & A_{74} & A_{75} & A_{76} & A_{77} & A_{78} & A_{79} & A_{7,10} & A_{7,11} & A_{7,12} \\ A_{81} & A_{82} & A_{83} & A_{84} & A_{85} & A_{86} & A_{87} & A_{88} & A_{89} & A_{8,10} & A_{8,11} & A_{8,12} \\ A_{91} & A_{92} & A_{93} & A_{94} & A_{95} & A_{96} & A_{97} & A_{98} & A_{99} & A_{9,10} & A_{9,11} & A_{9,12} \\ A_{10,1} & A_{10,2} & A_{10,3} & A_{10,4} & A_{10,5} & A_{10,6} & A_{10,7} & A_{10,8} & A_{10,9} & A_{10,10} & A_{10,11} & A_{10,12} \\ A_{11,1} & A_{11,2} & A_{11,3} & A_{11,4} & A_{11,5} & A_{11,6} & A_{11,7} & A_{11,8} & A_{11,9} & A_{11,10} & A_{11,11} & A_{11,12} \\ A_{12,1} & A_{12,2} & A_{12,3} & A_{12,4} & A_{12,5} & A_{12,6} & A_{12,7} & A_{12,8} & A_{12,9} & A_{12,10} & A_{12,11} & A_{12,12} \end{bmatrix} \begin{bmatrix} \Delta i_{gd} \\ \Delta i_{gq} \\ \Delta \delta \\ \Delta \omega_g \\ \Delta \theta_s \\ \Delta \omega_t \\ \Delta V_c \\ \Delta i_{id} \\ \Delta i_{iq} \\ \Delta i_{std} \\ \Delta i_{stq} \\ \Delta V_{dc} \end{bmatrix}$$

$$+ \begin{bmatrix} B_{11} & B_{12} & B_{13} & B_{14} & B_{15} \\ B_{21} & B_{22} & B_{23} & B_{24} & B_{25} \\ B_{31} & B_{32} & B_{33} & B_{34} & B_{35} \\ B_{41} & B_{42} & B_{43} & B_{44} & B_{45} \\ B_{51} & B_{52} & B_{53} & B_{54} & B_{55} \\ B_{61} & B_{62} & B_{63} & B_{64} & B_{65} \\ B_{71} & B_{72} & B_{73} & B_{74} & B_{75} \\ B_{81} & B_{82} & B_{83} & B_{84} & B_{85} \\ B_{91} & B_{92} & B_{93} & B_{94} & B_{95} \\ B_{10,1} & B_{10,2} & B_{10,3} & B_{10,4} & B_{10,5} \\ B_{11,1} & B_{11,2} & B_{11,3} & B_{11,4} & B_{11,5} \\ B_{12,1} & B_{12,12} & B_{12,3} & B_{12,4} & B_{12,5} \end{bmatrix} \begin{bmatrix} \Delta m_1 \\ \Delta m_2 \\ \Delta \alpha_2 \\ \Delta m_{st} \\ \Delta \psi_{st} \end{bmatrix}$$

Where A, B are known as state matrix and input matrix of order [12 x 12], [12 x 5].

The matrix elements of [ A ] are as given below;

$$A_{11} = -\frac{\omega_o R_a}{X_d} \quad A_{12} = \frac{\omega_o X_q}{X_d} \quad A_{13} = -\frac{\omega_o m_{10} V_{co} \cos \delta_o}{X_d} \quad A_{14} = \frac{\omega_o X_q i_{gqo}}{X_d}$$

$$A_{15} = A_{16} = 0 \quad A_{17} = -\frac{\omega_o m_{10} \sin \delta_o}{X_d} \quad A_{18} = A_{19} = A_{1,10} = A_{1,11} = A_{1,12} = 0$$

$$A_{21} = -\frac{\omega_o X_d}{X_q} \quad A_{22} = -\frac{\omega_o R_a}{X_q} \quad A_{23} = \frac{\omega_o m_{10} V_{co} \sin \delta_o}{X_q} \quad A_{24} = \frac{\omega_o (\psi_o - X_d i_{gdo})}{X_q}$$

$$A_{25} = A_{26} = 0 \quad A_{27} = -\frac{\omega_o m_{10} \cos \delta_o}{X_q} \quad A_{28} = A_{29} = A_{2,10} = A_{2,11} = A_{2,12} = 0$$

$$A_{31} = A_{32} = A_{33} = 0 \quad A_{34} = \omega_o \quad A_{35} = A_{36} = A_{37} = A_{38} = A_{39} = A_{3,10} = A_{3,11} = A_{3,12} = 0$$

$$A_{41} = \frac{-(2R_a i_{gdo} + V_{gdo})}{2H_g} \quad A_{42} = \frac{-(2R_a i_{gqo} + V_{gqo})}{2H_g}$$

$$A_{43} = \frac{(V_{gdo} i_{gqo} - V_{gqo} i_{gdo})}{2H_g} \quad A_{44} = \frac{-D_g}{2H_g} \quad A_{45} = \frac{K_s}{2H_g} \quad A_{46} = 0$$

$$A_{47} = \frac{-(V_{gdo} i_{gdo} + V_{gqo} i_{gqo})}{V_{co} 2H_g} \quad A_{48} = A_{49} = A_{4,10} = A_{4,11} = A_{4,12} = 0$$

$$A_{51} = A_{52} = A_{53} = 0 \quad A_{54} = -\omega_o \quad A_{56} = \omega_o \quad A_{55} = A_{57} = A_{58} = A_{59} = A_{5,10} = A_{5,11} = A_{5,12} = 0$$

$$A_{61} = A_{62} = A_{63} = A_{64} = 0 \quad A_{65} = -\frac{K_s}{2H_t} \quad A_{67} = A_{68} = A_{69} = A_{6,10} = A_{6,11} = A_{6,12} = 0$$

$$A_{66} = -\frac{(6C_1 \omega_{to}^5 + 5C_2 \omega_{to}^4 + 4C_3 \omega_{to}^3 + 3C_4 \omega_{to}^2 + 2C_5 \omega_{to}^1 + C_6) + D_t}{2H_t}$$

$$A_{71} = \frac{m_{10} \sin \delta_o}{C} \quad A_{72} = \frac{m_{10} \cos \delta_o}{C} \quad A_{73} = \frac{m_{10} (\cos \delta_o i_{gdo} - \sin \delta_o i_{gqo})}{C}$$

$$A_{74} = A_{75} = A_{76} = A_{77} = 0 \quad A_{78} = -\frac{m_{20} \cos\alpha_{20}}{C} \quad A_{79} = \frac{m_{20} \sin\alpha_{20}}{C}$$

$$A_{7,10} = \frac{m_{10} \sin\delta_0}{C} \quad A_{7,11} = \frac{m_{10} \cos\delta_0}{C} \quad A_{7,12} = 0$$

$$A_{81} = A_{82} = A_{83} = A_{84} = A_{85} = A_{86} = A_{8,10} = A_{8,11} = A_{8,12} = 0$$

$$A_{87} = -\frac{\omega_o m_{20} \cos\alpha_{20}}{X_i} \quad A_{88} = -\frac{\omega_o (R_i + K_1)}{X_i} \quad A_{89} = \frac{\omega_o (X_i - K_2)}{X_i}$$

$$A_{91} = A_{92} = A_{93} = A_{94} = A_{95} = A_{96} = A_{9,10} = A_{9,11} = A_{9,12} = 0$$

$$A_{97} = -\frac{\omega_o m_{20} \sin\alpha_{20}}{X_i} \quad A_{98} = -\frac{\omega_o (X_i + K_3)}{X_i} \quad A_{99} = \frac{\omega_o (R_i + K_4)}{X_i}$$

$$A_{10,1} = A_{10,2} = A_{10,4} = A_{10,5} = A_{10,6} = A_{10,8} = A_{10,9} = 0$$

$$A_{10,3} = \frac{-\omega_o V_{gqo}}{L_{st}} \quad A_{10,7} = \frac{-\omega_o m_{10} \sin\delta_o}{L_{st}}$$

$$A_{10,10} = \frac{-\omega_o R_{st}}{L_{st}} \quad A_{10,12} = \omega_o \quad A_{10,12} = \frac{\omega_o m_{sto} \cos\psi_{sto}}{L_{st}}$$

$$A_{11,1} = A_{11,2} = A_{11,4} = A_{11,5} = A_{11,6} = A_{11,8} = A_{11,9} = 0$$

$$A_{11,3} = \frac{\omega_o V_{gdo}}{L_{st}} \quad A_{11,7} = \frac{-\omega_o m_{10} \cos\delta_o}{L_{st}}$$

$$A_{11,10} = -\omega_o \quad A_{11,11} = \frac{-\omega_o R_{st}}{L_{st}} \quad A_{11,12} = \frac{\omega_o m_{sto} \sin\psi_{sto}}{L_{st}}$$

$$A_{12,1} = A_{12,2} = A_{12,4} = A_{12,5} = A_{12,6} = A_{12,8} = A_{12,9} = 0$$

$$A_{12,10} = \frac{-m_{sto} \cos \psi_{sto}}{C_{dc}} \quad A_{12,11} = \frac{-m_{sto} \sin \psi_{sto}}{C_{dc}} \quad A_{12,12} = 0$$

The matrix elements of [ B ] are as given below;

$$B_{11} = -\frac{\omega_o V_{co} \sin \delta_o}{X_d} \quad B_{12} = B_{13} = B_{14} = B_{15} = 0$$

$$B_{21} = -\frac{\omega_o V_{co} \cos \delta_o}{X_q} \quad B_{22} = B_{23} = B_{24} = B_{25} = 0$$

$$B_{31} = B_{32} = B_{33} = B_{34} = B_{35} = 0$$

$$B_{41} = -\frac{V_{co} (\sin \delta_o i_{gdo} + \cos \delta_o i_{gqo})}{2H_g} \quad B_{42} = B_{43} = B_{44} = B_{45} = 0$$

$$B_{51} = B_{52} = B_{53} = B_{54} = B_{55} = 0 \quad B_{61} = B_{62} = B_{63} = B_{64} = B_{65} = 0$$

$$B_{71} = \frac{(\sin \delta_o i_{gdo} + \cos \delta_o i_{gqo})}{C} \quad B_{72} = \frac{(\sin \alpha_{2o} i_{iqo} - \cos \alpha_{2o} i_{ido})}{C}$$

$$B_{73} = \frac{m_{2o} (\sin \alpha_{2o} i_{ido} + \cos \alpha_{2o} i_{iqo})}{C} \quad B_{74} = B_{75} = 0$$

$$B_{81} = 0 \quad B_{82} = -\frac{\omega_o V_{co} \cos \alpha_{2o}}{X_i} \quad B_{83} = \frac{\omega_o m_{2o} V_{co} \sin \alpha_{2o}}{X_i} \quad B_{84} = B_{85} = 0$$

$$B_{91} = 0 \quad B_{92} = \frac{\omega_o V_{co} \sin \alpha_{2o}}{X_i} \quad B_{93} = \frac{\omega_o m_{2o} V_{co} \cos \alpha_{2o}}{X_i} \quad B_{94} = B_{95} = 0$$

$$B_{10,1} = -\frac{\omega_o V_{co} \sin \delta_o}{L_{st}} \quad B_{10,2} = B_{10,3} = 0$$

$$B_{10,4} = \frac{\omega_o V_{dco} \cos \psi_{sto}}{L_{st}} \quad B_{10,5} = \frac{-\omega_o V_{stqo}}{L_{st}}$$

$$B_{11,1} = -\frac{\omega_o V_{co} \cos \delta_o}{L_{st}} \quad B_{11,2} = B_{11,3} = 0$$

$$B_{11,4} = \frac{\omega_o V_{dco} \sin \psi_{sto}}{L_{st}} \quad B_{11,5} = \frac{\omega_o V_{stdo}}{L_{st}}$$

$$B_{12,1} = B_{12,2} = B_{12,3} = B_{12,4} = B_{12,5} = 0$$

## APPENDIX E

In this section the small signal model of Variable Speed PMSG system with STATCOM Controller at Grid Side-Converter (Inverter) system is obtained by linearizing the non-linear equations developed in the section 3.5. The state equations for the 12<sup>th</sup> order model are as shown below;

$$p(i_{gd}) = \frac{\omega_o}{X_d} [-R_a i_{gd} + X_q i_{gq} \omega_g - m_1 V_c \sin \delta]$$

$$p(i_{gq}) = \frac{\omega_o}{X_q} [-X_d i_{gd} \omega_g - R_a i_{gq} + \psi_o \omega_g - m_1 V_c \cos \delta]$$

$$p(\delta) = \omega_o (\omega_g - 1)$$

$$p(\omega_g) = \frac{1}{2H_g} (K_s \theta_s - P_{ag} - D_g (\omega_g - 1))$$

$$p(\theta_s) = \omega_o (\omega_t - \omega_g)$$

$$p(\omega_t) = \frac{1}{2H_t} (P_m - K_s \theta_s - D_t (\omega_t - 1))$$

$$p(V_c) = \frac{1}{C} [m_1 i_{gd} \sin \delta + m_1 i_{gq} \cos \delta - m_2 i_{id} \cos \alpha_2 + m_2 i_{iq} \sin \alpha_2]$$

$$p(i_{id}) = \frac{\omega_o}{X_i} [-(R_i + k_1) i_{id} + (\omega_e X_i - k_2) i_{iq} - m_2 V_c \cos \alpha_2 - k_1 i_{std} - k_2 i_{stq} - V_b (k_1 g_{12} - k_2 b_{12})]$$

$$p(i_{iq}) = \frac{\omega_o}{X_i} [-(\omega_e X_i + k_3) i_{id} - (R_i + k_4) i_{iq} + m_2 V_c \sin \alpha_2 - k_3 i_{std} - k_4 i_{stq} - V_b (k_3 g_{12} - k_4 b_{12})]$$

$$p(V_{dc}) = -\frac{m_{st}}{C_{dc}} [\cos(\psi_{st}) \cdot i_{std} + \sin(\psi_{st}) \cdot i_{stq}]$$

Since, linearization is done in Appendix C for 9 state equations. Therefore, only STATCOM controller state equations / state equations affected due to STATCOM controller will be linearized and the rest will be ignored to avoid repetition.



$$[8] \quad p(i_{id}) = \frac{\omega_o}{X_i} \left[ - (R_i + k_1) i_{id} + (\omega_e X_i - k_2) i_{iq} - m_2 V_c \cos \alpha_2 - k_1 i_{std} - k_2 i_{stq} - V_b (k_1 g_{12} - k_2 b_{12}) \right]$$

$$p(\Delta i_{id}) = \frac{\omega_o}{X_i} \left[ - (R_i + k_1) \Delta i_{id} + (\omega_{eo} X_i - k_2) \Delta i_{iq} - m_{2o} \cos \alpha_{2o} \Delta V_c \right. \\ \left. - V_{co} \cos \alpha_{2o} \Delta m_2 + m_{2o} V_{co} \sin \alpha_{2o} \Delta \alpha_2 - k_1 \Delta i_{std} - k_2 \Delta i_{stq} \right]$$

$$p(\Delta i_{id}) = \frac{\omega_o}{X_i} \left[ - (R_i + k_1) \Delta i_{id} + (\omega_{eo} X_i - k_2) \Delta i_{iq} - m_{2o} \cos \alpha_{2o} \Delta V_c \right. \\ \left. - k_1 \Delta i_{std} - k_2 \Delta i_{stq} - V_{co} \cos \alpha_{2o} \Delta m_2 + m_{2o} V_{co} \sin \alpha_{2o} \Delta \alpha_2 \right]$$

$$[9] \quad p(i_{iq}) = \frac{\omega_o}{X_i} \left[ - (\omega_e X_i + k_3) i_{id} - (R_i + k_4) i_{iq} + m_2 V_c \sin \alpha_2 - k_3 i_{std} - k_4 i_{stq} - V_b (k_3 g_{12} - k_4 b_{12}) \right]$$

$$p(\Delta i_{iq}) = \frac{\omega_o}{X_i} \left[ - (\omega_{eo} X_i + k_3) \Delta i_{id} - (R_i + k_4) \Delta i_{iq} - m_{2o} \sin \alpha_{2o} \Delta V_c \right. \\ \left. + V_{co} \sin \alpha_{2o} \Delta m_2 + m_{2o} V_{co} \cos \alpha_{2o} \Delta \alpha_2 - k_3 \Delta i_{std} - k_4 \Delta i_{stq} \right]$$

$$p(\Delta i_{iq}) = \frac{\omega_o}{X_i} \left[ - (\omega_{eo} X_i + k_3) \Delta i_{id} - (R_i + k_4) \Delta i_{iq} - m_{2o} \sin \alpha_{2o} \Delta V_c \right. \\ \left. - k_3 \Delta i_{std} - k_4 \Delta i_{stq} + V_{co} \sin \alpha_{2o} \Delta m_2 + m_{2o} V_{co} \cos \alpha_{2o} \Delta \alpha_2 \right]$$

$$[10] \quad p(i_{std}) = \frac{\omega_o}{L_{st}} \left[ -k_1 i_{id} - k_2 i_{iq} - R_{st} i_{std} + \omega_e L_{st} i_{stq} + m_{st} V_{dc} \cos(\psi_{st}) - V_b (k_1 g_{12} - k_2 b_{12}) \right]$$

$$p(\Delta i_{std}) = \frac{\omega_o}{L_{st}} \left[ -k_1 \Delta i_{id} - k_2 \Delta i_{iq} - R_{st} \Delta i_{std} + \omega_{eo} L_{st} \Delta i_{stq} + m_{sto} \cos(\psi_{sto}) \Delta V_{dc} \right. \\ \left. + V_{dco} \cos(\psi_{sto}) \Delta m_{st} - m_{sto} V_{dco} \sin(\psi_{sto}) \Delta \psi_{st} \right]$$

$$[11] \quad p(i_{stq}) = \frac{\omega_o}{L_{st}} \left[ -k_3 i_{id} - k_4 i_{iq} - \omega_e L_{st} i_{std} - R_{st} i_{stq} + m_{st} V_{dc} \sin(\psi_{st}) - V_b (k_3 g_{12} - k_4 b_{12}) \right]$$

$$p(\Delta i_{stq}) = \frac{\omega_o}{L_{st}} \left[ -k_3 \Delta i_{id} - k_4 \Delta i_{iq} - \omega_{eo} L_{st} \Delta i_{std} - R_{st} \Delta i_{stq} + m_{sto} \sin(\psi_{sto}) \Delta V_{dc} \right. \\ \left. + V_{dco} \sin(\psi_{sto}) \Delta m_{st} + m_{sto} V_{dco} \cos(\psi_{sto}) \Delta \psi_{st} \right]$$

$$[12] \quad p(V_{dc}) = -\frac{m_{st}}{C_{dc}} \left[ \cos(\psi_{st}) \cdot i_{std} + \sin(\psi_{st}) \cdot i_{stq} \right]$$

$$p(\Delta V_{dc}) = -\frac{1}{C_{dc}} \left[ m_{sto} \cos(\psi_{sto}) \Delta i_{std} + \cos(\psi_{sto}) i_{stdo} \Delta m_{st} + m_{sto} \cos(\psi_{sto}) i_{stqo} \Delta \psi_{st} \right. \\ \left. + m_{sto} \sin(\psi_{sto}) \Delta i_{stq} + \sin(\psi_{sto}) i_{stqo} \Delta m_{st} - m_{sto} \sin(\psi_{sto}) i_{stdo} \Delta \psi_{st} \right]$$

$$p(\Delta V_{dc}) = -\frac{1}{C_{dc}} \left[ m_{sto} \cos(\psi_{sto}) \Delta i_{std} + m_{sto} \sin(\psi_{sto}) \Delta i_{stq} \right]$$

(Since  $i_{stdo}$ ,  $i_{stqo}$  are having zero initial value).

The matrix representation of Linearized 12<sup>th</sup> order model of variable Speed PMSG system with STATCOM Controller on Inverter side is as shown below;

$$\begin{bmatrix} p(\Delta i_{gd}) \\ p(\Delta i_{gq}) \\ p(\Delta \delta) \\ p(\Delta \omega_g) \\ p(\Delta \theta_s) \\ p(\Delta \omega_t) \\ p(\Delta V_c) \\ p(\Delta i_{id}) \\ p(\Delta i_{iq}) \\ p(\Delta i_{std}) \\ p(\Delta i_{stq}) \\ p(\Delta V_{dc}) \end{bmatrix} = \begin{bmatrix} A_{11} & A_{12} & A_{13} & A_{14} & A_{15} & A_{16} & A_{17} & A_{18} & A_{19} & A_{1,10} & A_{1,11} & A_{1,12} \\ A_{21} & A_{22} & A_{23} & A_{24} & A_{25} & A_{26} & A_{27} & A_{28} & A_{29} & A_{2,10} & A_{2,11} & A_{2,12} \\ A_{31} & A_{32} & A_{33} & A_{34} & A_{35} & A_{36} & A_{37} & A_{38} & A_{39} & A_{3,10} & A_{3,11} & A_{3,12} \\ A_{41} & A_{42} & A_{43} & A_{44} & A_{45} & A_{46} & A_{47} & A_{48} & A_{49} & A_{4,10} & A_{4,11} & A_{4,12} \\ A_{51} & A_{52} & A_{53} & A_{54} & A_{55} & A_{56} & A_{57} & A_{58} & A_{59} & A_{5,10} & A_{5,11} & A_{5,12} \\ A_{61} & A_{62} & A_{63} & A_{64} & A_{65} & A_{66} & A_{67} & A_{68} & A_{69} & A_{6,10} & A_{6,11} & A_{6,12} \\ A_{71} & A_{72} & A_{73} & A_{74} & A_{75} & A_{76} & A_{77} & A_{78} & A_{79} & A_{7,10} & A_{7,11} & A_{7,12} \\ A_{81} & A_{82} & A_{83} & A_{84} & A_{85} & A_{86} & A_{87} & A_{88} & A_{89} & A_{8,10} & A_{8,11} & A_{8,12} \\ A_{91} & A_{92} & A_{93} & A_{94} & A_{95} & A_{96} & A_{97} & A_{98} & A_{99} & A_{9,10} & A_{9,11} & A_{9,12} \\ A_{10,1} & A_{10,2} & A_{10,3} & A_{10,4} & A_{10,5} & A_{10,6} & A_{10,7} & A_{10,8} & A_{10,9} & A_{10,10} & A_{10,11} & A_{10,12} \\ A_{11,1} & A_{11,2} & A_{11,3} & A_{11,4} & A_{11,5} & A_{11,6} & A_{11,7} & A_{11,8} & A_{11,9} & A_{11,10} & A_{11,11} & A_{11,12} \\ A_{12,1} & A_{12,2} & A_{12,3} & A_{12,4} & A_{12,5} & A_{12,6} & A_{12,7} & A_{12,8} & A_{12,9} & A_{12,10} & A_{12,11} & A_{12,12} \end{bmatrix} \begin{bmatrix} \Delta i_{gd} \\ \Delta i_{gq} \\ \Delta \delta \\ \Delta \omega_g \\ \Delta \theta_s \\ \Delta \omega_t \\ \Delta V_c \\ \Delta i_{id} \\ \Delta i_{iq} \\ \Delta i_{std} \\ \Delta i_{stq} \\ \Delta V_{dc} \end{bmatrix} + \begin{bmatrix} B_{11} & B_{12} & B_{13} & B_{14} & B_{15} \\ B_{21} & B_{22} & B_{23} & B_{24} & B_{25} \\ B_{31} & B_{32} & B_{33} & B_{34} & B_{35} \\ B_{41} & B_{42} & B_{43} & B_{44} & B_{45} \\ B_{51} & B_{52} & B_{53} & B_{54} & B_{55} \\ B_{61} & B_{62} & B_{63} & B_{64} & B_{65} \\ B_{71} & B_{72} & B_{73} & B_{74} & B_{75} \\ B_{81} & B_{82} & B_{83} & B_{84} & B_{85} \\ B_{91} & B_{92} & B_{93} & B_{94} & B_{95} \\ B_{10,1} & B_{10,2} & B_{10,3} & B_{10,4} & B_{10,5} \\ B_{11,1} & B_{11,2} & B_{11,3} & B_{11,4} & B_{11,5} \\ B_{12,1} & B_{12,2} & B_{12,3} & B_{12,4} & B_{12,5} \end{bmatrix} \begin{bmatrix} \Delta m_1 \\ \Delta m_2 \\ \Delta \alpha_2 \\ \Delta m_{st} \\ \Delta \Psi_{st} \end{bmatrix}$$

Where A, B are known as state matrix and input matrix of order [12 x 12], [12 x 5].

The matrix elements of [ A ] are as given below;

$$A_{11} = -\frac{\omega_o R_a}{X_d} \quad A_{12} = \frac{\omega_o X_q}{X_d} \quad A_{13} = -\frac{\omega_o m_{10} V_{co} \cos \delta_o}{X_d} \quad A_{14} = \frac{\omega_o X_q i_{gqo}}{X_d}$$

$$A_{15} = A_{16} = 0 \quad A_{17} = -\frac{\omega_o m_{10} \sin \delta_o}{X_d} \quad A_{18} = A_{19} = A_{1,10} = A_{1,11} = A_{1,12} = 0$$

$$A_{21} = -\frac{\omega_o X_d}{X_q} \quad A_{22} = -\frac{\omega_o R_a}{X_q} \quad A_{23} = \frac{\omega_o m_{10} V_{co} \sin \delta_o}{X_q} \quad A_{24} = \frac{\omega_o (\psi_o - X_d i_{gdo})}{X_q}$$

$$A_{25} = A_{26} = 0 \quad A_{27} = -\frac{\omega_o m_{10} \cos \delta_o}{X_q} \quad A_{28} = A_{29} = A_{2,10} = A_{2,11} = A_{2,12} = 0$$

$$A_{31} = A_{32} = A_{33} = 0 \quad A_{34} = \omega_o \quad A_{35} = A_{36} = A_{37} = A_{38} = A_{39} = A_{3,10} = A_{3,11} = A_{3,12} = 0$$

$$A_{41} = \frac{-(2R_a i_{gdo} + V_{gdo})}{2H_g} \quad A_{42} = \frac{-(2R_a i_{gqo} + V_{gqo})}{2H_g}$$

$$A_{43} = \frac{(V_{gdo} i_{gqo} - V_{gqo} i_{gdo})}{2H_g} \quad A_{44} = \frac{-D_g}{2H_g} \quad A_{45} = \frac{K_s}{2H_g} \quad A_{46} = 0$$

$$A_{47} = \frac{-(V_{gdo} i_{gdo} + V_{gqo} i_{gqo})}{V_{co} 2H_g} \quad A_{48} = A_{49} = A_{4,10} = A_{4,11} = A_{4,12} = 0$$

$$A_{51} = A_{52} = A_{53} = 0 \quad A_{54} = -\omega_o \quad A_{56} = \omega_o \quad A_{55} = A_{57} = A_{58} = A_{59} = A_{5,10} = A_{5,11} = A_{5,12} = 0$$

$$A_{61} = A_{62} = A_{63} = A_{64} = 0 \quad A_{65} = -\frac{K_s}{2H_t} \quad A_{67} = A_{68} = A_{69} = A_{6,10} = A_{6,11} = A_{6,12} = 0$$

$$A_{66} = -\frac{(6C_1 \omega_{to}^5 + 5C_2 \omega_{to}^4 + 4C_3 \omega_{to}^3 + 3C_4 \omega_{to}^2 + 2C_5 \omega_{to}^1 + C_6) + D_t}{2H_t}$$

$$A_{71} = \frac{m_{10} \sin \delta_o}{C} \quad A_{72} = \frac{m_{10} \cos \delta_o}{C} \quad A_{73} = \frac{m_{10} (\cos \delta_o i_{gdo} - \sin \delta_o i_{gqo})}{C}$$

$$A_{74} = A_{75} = A_{76} = A_{77} = A_{7,10} = A_{7,11} = A_{7,12} = 0$$

$$A_{78} = -\frac{m_{20} \cos \alpha_{20}}{C} \quad A_{79} = \frac{m_{20} \sin \alpha_{20}}{C}$$

$$A_{81} = A_{82} = A_{83} = A_{84} = A_{85} = A_{86} = A_{8,12} = 0$$

$$A_{87} = -\frac{\omega_o m_{20} \cos \alpha_{20}}{X_i} \quad A_{88} = -\frac{\omega_o (R_i + K_1)}{X_i} \quad A_{89} = \frac{\omega_o (X_i - K_2)}{X_i}$$

$$A_{8,10} = -\frac{\omega_o K_1}{X_i} \quad A_{8,11} = -\frac{\omega_o K_2}{X_i}$$

$$A_{91} = A_{92} = A_{93} = A_{94} = A_{95} = A_{96} = A_{9,12} = 0$$

$$A_{97} = -\frac{\omega_o m_{20} \sin \alpha_{20}}{X_i} \quad A_{98} = -\frac{\omega_o (X_i + K_3)}{X_i} \quad A_{99} = \frac{\omega_o (R_i + K_4)}{X_i}$$

$$A_{9,10} = -\frac{\omega_o K_3}{X_i} \quad A_{9,11} = -\frac{\omega_o K_4}{X_i}$$

$$A_{10,1} = A_{10,2} = A_{10,4} = A_{10,5} = A_{10,6} = A_{10,8} = A_{10,9} = 0$$

$$A_{10,3} = \frac{-\omega_o V_{gqo}}{L_{st}} \quad A_{10,7} = \frac{-\omega_o m_{10} \sin \delta_o}{L_{st}}$$

$$A_{10,10} = \frac{-\omega_o R_{st}}{L_{st}} \quad A_{10,11} = \omega_o \quad A_{10,12} = \frac{\omega_o m_{sto} \cos \psi_{sto}}{L_{st}}$$

$$A_{11,1} = A_{11,2} = A_{11,4} = A_{11,5} = A_{11,6} = A_{11,8} = A_{11,9} = 0$$

$$A_{11,3} = \frac{\omega_o V_{gdo}}{L_{st}} \quad A_{11,7} = \frac{-\omega_o m_{1o} \cos \delta_o}{L_{st}}$$

$$A_{11,10} = -\omega_o \quad A_{11,11} = \frac{-\omega_o R_{st}}{L_{st}} \quad A_{11,12} = \frac{\omega_o m_{sto} \sin \psi_{sto}}{L_{st}}$$

$$A_{12,1} = A_{12,2} = A_{12,3} = A_{12,4} = A_{12,5} = A_{12,6} = A_{12,8} = A_{12,9} = 0$$

$$A_{12,10} = \frac{-m_{sto} \cos \psi_{sto}}{C_{dc}} \quad A_{12,11} = \frac{-m_{sto} \sin \psi_{sto}}{C_{dc}} \quad A_{12,12} = 0$$

The matrix elements of [ B ] are as given below;

$$B_{11} = -\frac{\omega_o V_{co} \sin \delta_o}{X_d} \quad B_{12} = B_{13} = B_{14} = B_{15} = 0$$

$$B_{21} = -\frac{\omega_o V_{co} \cos \delta_o}{X_q} \quad B_{22} = B_{23} = B_{24} = B_{25} = 0$$

$$B_{31} = B_{32} = B_{33} = B_{34} = B_{35} = 0$$

$$B_{41} = -\frac{V_{co} (\sin \delta_o i_{gdo} + \cos \delta_o i_{gqo})}{2H_g} \quad B_{42} = B_{43} = B_{44} = B_{45} = 0$$

$$B_{51} = B_{52} = B_{53} = B_{54} = B_{55} = 0 \quad B_{61} = B_{62} = B_{63} = B_{64} = B_{65} = 0$$

$$B_{71} = \frac{(\sin \delta_o i_{gdo} + \cos \delta_o i_{gqo})}{C} \quad B_{72} = \frac{(\sin \alpha_{2o} i_{iqo} - \cos \alpha_{2o} i_{ido})}{C}$$

$$B_{73} = \frac{m_{2o} (\sin \alpha_{2o} i_{ido} + \cos \alpha_{2o} i_{iqo})}{C} \quad B_{74} = B_{75} = 0$$

$$B_{81} = 0 \quad B_{82} = -\frac{\omega_o V_{co} \cos \alpha_{2o}}{X_i} \quad B_{83} = \frac{\omega_o m_{2o} V_{co} \sin \alpha_{2o}}{X_i} \quad B_{84} = B_{85} = 0$$

$$B_{91} = 0 \quad B_{92} = \frac{\omega_o V_{co} \sin \alpha_{2o}}{X_i} \quad B_{93} = \frac{\omega_o m_{2o} V_{co} \cos \alpha_{2o}}{X_i} \quad B_{94} = B_{95} = 0$$

$$B_{10,1} = B_{10,2} = B_{10,3} = 0 \quad B_{10,4} = \frac{\omega_o V_{dco} \cos \psi_{sto}}{L_{st}} \quad B_{10,5} = \frac{-\omega_o V_{stqo}}{L_{st}}$$

$$B_{11,1} = B_{11,2} = B_{11,3} = 0 \quad B_{11,4} = \frac{\omega_o V_{dco} \sin \psi_{sto}}{L_{st}} \quad B_{11,5} = \frac{\omega_o V_{stdo}}{L_{st}}$$

$$B_{12,1} = B_{12,2} = B_{12,3} = B_{12,4} = B_{12,5} = 0$$

## REFERENCES

- [1] A. Pullen, "Global wind energy markets continue to boom–2006 another record year," *Global wind energy council press release, Brussels, Belgium*, 2007.
- [2] A. D. Hansen and L. H. Hansen, "Wind turbine concept market penetration over 10 years (1995–2004)," *Wind energy*, vol. 10, pp. 81-97, 2007.
- [3] H. Lund, "Large-scale integration of wind power into different energy systems," *Energy*, vol. 30, pp. 2402-2412, 2005.
- [4] E. W. E. Association, *Large Scale Integration of Wind Energy in the European Power Supply: Analysis, Issues and Recommendations: a Report*: European Wind Energy Association, 2005.
- [5] T. Ackermann, "Wind power in power systems," *Wind Engineering*, vol. 30, pp. 447-449, 2006.
- [6] F. González-Longatt, O. Amaya, M. Cooz, and L. Duran, "Dynamic Behavior of Constant Speed WT based on Induction Generator Directly connect to Grid," 2007.
- [7] A. Grauers, "Efficiency of three wind energy generator systems," *Energy Conversion, IEEE Transactions on*, vol. 11, pp. 650-657, 1996.
- [8] M. Chinchilla, S. Arnaltes, and J. C. Burgos, "Control of permanent-magnet generators applied to variable-speed wind-energy systems connected to the grid," *Energy Conversion, IEEE Transactions on*, vol. 21, pp. 130-135, 2006.



- [9] D. Qiu-ling, L. Gou-rong, and X. Feng, "Control of variable-speed permanent magnet synchronous generators wind generation system," 2008, pp. 2454-2458.
- [10] Y. Errami, M. Maaroufi, and M. Ouassaid, "Modelling and control strategy of PMSG based variable speed wind energy conversion system," 2011, pp. 1-6.
- [11] S. Muyeen, R. Takahashi, T. Murata, J. Tamura, and M. Ali, "Transient stability analysis of permanent magnet variable speed synchronous wind generator," 2007, pp. 288-293.
- [12] H. Wang, W. Ma, F. Xiao, M. Cheng, and Y. Liu, "Control strategy of permanent magnet synchronous generator of directly driven wind turbine," 2009, pp. 320-323.
- [13] V. Akhmatov, *Analysis of dynamic behaviour of electric power systems with large amount of wind power*: Electric Power Engineering, Ørsted-DTU, Technical University of Denmark, 2003.
- [14] T. Senjyu, R. Sakamoto, N. Urasaki, T. Funabashi, H. Fujita, and H. Sekine, "Output power leveling of wind turbine generator for all operating regions by pitch angle control," *Energy Conversion, IEEE Transactions on*, vol. 21, pp. 467-475, 2006.
- [15] S. Muyeen, M. Ali, R. Takahashi, T. Murata, and J. Tamura, "Wind generator output power smoothing and terminal voltage regulation by using STATCOM/ESS," 2007, pp. 1232-1237.
- [16] M. Singh and A. Chandra, "Control of PMSG based variable speed wind-battery hybrid system in an isolated network," 2009, pp. 1-6.

- [17] M. Okamura, "A basic study on power storage capacitor systems," *TRANSACTIONS-INSTITUTE OF ELECTRICAL ENGINEERS OF JAPAN B*, vol. 115, pp. 504-510, 1995.
- [18] Z. Chen, F. Blaabjerg, and Y. Hu, "Stability improvement of wind turbine systems by STATCOM," 2006, pp. 4213-4218.
- [19] C. Han, A. Q. Huang, M. E. Baran, S. Bhattacharya, W. Litzemberger, L. Anderson, A. L. Johnson, and A. A. Edris, "STATCOM impact study on the integration of a large wind farm into a weak loop power system," *Energy Conversion, IEEE Transactions on*, vol. 23, pp. 226-233, 2008.
- [20] A. Westlake, J. Bumby, and E. Spooner, "Damping the power-angle oscillations of a permanent-magnet synchronous generator with particular reference to wind turbine applications," 1996, pp. 269-280.
- [21] P. W. Carlin, A. S. Laxson, and E. Muljadi, "The history and state of the art of variable-speed wind turbine technology," *Wind energy*, vol. 6, pp. 129-159, 2003.
- [22] P. Ledesma, J. Usaola, and J. Rodriguez, "Transient stability of a fixed speed wind farm," *Renewable energy*, vol. 28, pp. 1341-1355, 2003.
- [23] L. M. Fernández, J. R. Saenz, and F. Jurado, "Dynamic models of wind farms with fixed speed wind turbines," *Renewable energy*, vol. 31, pp. 1203-1230, 2006.
- [24] W. Qiao, R. G. Harley, and G. K. Venayagamoorthy, "Dynamic modeling of wind farms with fixed-speed wind turbine generators," 2007, pp. 1-8.

- [25] L. Mihet-Popa and I. Filip, "Modeling and simulation of a soft-starter for large wind turbine induction generators," in *Computational Cybernetics and Technical Informatics (ICCC-CONTI), 2010 International Joint Conference on*, 2010, pp. 465-470.
- [26] L. Holdsworth, X. Wu, J. Ekanayake, and N. Jenkins, "Comparison of fixed speed and doubly-fed induction wind turbines during power system disturbances," 2003, pp. 343-352.
- [27] J. Slootweg, H. Polinder, and W. Kling, "Dynamic modelling of a wind turbine with doubly fed induction generator," 2001, pp. 644-649 vol. 1.
- [28] F. Mei and B. Pal, "Modal analysis of grid-connected doubly fed induction generators," *Energy Conversion, IEEE Transactions on*, vol. 22, pp. 728-736, 2007.
- [29] F. Wu, X. P. Zhang, K. Godfrey, and P. Ju, "Small signal stability analysis and optimal control of a wind turbine with doubly fed induction generator," *Generation, Transmission & Distribution, IET*, vol. 1, pp. 751-760, 2007.
- [30] J. Slootweg and W. Kling, "The impact of large scale wind power generation on power system oscillations," *Electric power systems research*, vol. 67, pp. 9-20, 2003.
- [31] R. Pena, J. Clare, and G. Asher, "Doubly fed induction generator using back-to-back PWM converters and its application to variable-speed wind-energy generation," 1996, pp. 231-241.
- [32] I. Margaritis and N. Hatziaargyriou, "Direct drive synchronous generator wind turbine models for power system studies," 2011, pp. 1-7.

- [33] H. Polinder, S. W. H. de Haan, M. R. Dubois, and J. G. Slootweg, "Basic operation principles and electrical conversion systems of wind turbines," *EPE JOURNAL*, vol. 15, p. 43, 2005.
- [34] P. Vas, *Electrical machines and drives: a space-vector theory approach* vol. 25: Oxford University Press, USA, 1992.
- [35] M. Mansour, M. Mansouri, and M. Mimouni, "Comparative study of fixed speed and variable speed wind generator with pitch angle control," 2011, pp. 1-7.
- [36] K. Tan and S. Islam, "Optimum control strategies in energy conversion of PMSG wind turbine system without mechanical sensors," *Energy Conversion, IEEE Transactions on*, vol. 19, pp. 392-399, 2004.
- [37] M. U. Guide, "The MathWorks," *Inc., Natick, MA*, vol. 5, 1998.
- [38] M. E. Haque, M. Negnevitsky, and K. Muttaqi, "A novel control strategy for a variable speed wind turbine with a permanent magnet synchronous generator," 2008, pp. 1-8.
- [39] S. Morimoto, T. Nakamura, and Y. Takeda, "Power maximization control of variable speed wind generation system using permanent magnet synchronous generator," *IEEJ Transactions on Power and Energy*, vol. 123, pp. 1573-1579, 2003.
- [40] S. Muyeen, R. Takahashi, T. Murata, J. Tamura, M. Ali, Y. Matsumura, A. Kuwayama, and T. Matsumoto, "Low voltage ride through capability enhancement of wind turbine generator system during network disturbance," *Renewable Power Generation, IET*, vol. 3, pp. 65-74, 2009.

- [41] J. Conroy and R. Watson, "Low-voltage ride-through of a full converter wind turbine with permanent magnet generator," *Renewable Power Generation, IET*, vol. 1, pp. 182-189, 2007.
- [42] F. Deng and Z. Chen, "Low-voltage ride-through of variable speed wind turbines with permanent magnet synchronous generator," 2009, pp. 621-626.
- [43] S. W. Saylor, "Wind parks as power plants," 2006, p. 9 pp.
- [44] L. Gyugyi, "Converter-based FACTS controllers," 1998, pp. 1/1-111.
- [45] L. Qi, J. Langston, and M. Steurer, "Applying a STATCOM for stability improvement to an existing wind farm with fixed-speed induction generators," 2008, pp. 1-6.
- [46] S. Mueen, M. A. Mannan, H. Ali, R. Takahashi, T. Murata, and J. Tamura, "Stabilization of grid connected wind generator by STATCOM," 2005, pp. 1584-1589.
- [47] A. Hamdan, "An investigation of the significance of singular value decomposition in power system dynamics," *International Journal of Electrical Power & Energy Systems*, vol. 21, pp. 417-424, 1999.
- [48] M. El-Sherbiny, M. Hasan, G. El-Saady, and A. M. Yousef, "Optimal pole shifting for power system stabilization," *Electric power systems research*, vol. 66, pp. 253-258, 2003.
- [49] A. M. Yousef and A. M. Kassem, "Optimal pole shifting controller for interconnected power system," *Energy Conversion and Management*, vol. 52, pp. 2227-2234, 2011.

- [50] W. Shepherd and L. Zhang, "Electricity generation using wind power," *Recherche*, vol. 67, p. 02, 2011.
- [51] N. Mithulanathan, C. A. Canizares, J. Reeve, and G. J. Rogers, "Comparison of PSS, SVC, and STATCOM controllers for damping power system oscillations," *Power Systems, IEEE Transactions on*, vol. 18, pp. 786-792, 2003.
- [52] M. Kandlawala and A. Rahim, "Power system dynamic performance with STATCOM controller," 2001.
- [53] M. F. Kandlawala, "Investigation of dynamic behavior of power system installed with STATCOM," King Fahd University of Petroleum and Minerals, 2001.
- [54] G. H. Golub and C. Reinsch, "Singular value decomposition and least squares solutions," *Numerische Mathematik*, vol. 14, pp. 403-420, 1970.
- [55] M. Farsangi, Y. Song, and K. Y. Lee, "Choice of FACTS device control inputs for damping interarea oscillations," *Power Systems, IEEE Transactions on*, vol. 19, pp. 1135-1143, 2004.
- [56] J. Hahn and T. F. Edgar, "An improved method for nonlinear model reduction using balancing of empirical gramians," *Computers & chemical engineering*, vol. 26, pp. 1379-1397, 2002.
- [57] M. E. Aboul-Ela, A. Sallam, J. D. McCalley, and A. Fouad, "Damping controller design for power system oscillations using global signals," *Power Systems, IEEE Transactions on*, vol. 11, pp. 767-773, 1996.

- [58] A. SIVARAMAKRISHNAN, M. Hariharan, and M. Srisailam, "Design of variable-structure load-frequency controller using pole assignment technique," *International Journal of control*, vol. 40, pp. 487-498, 1984.
- [59] A. O'Dwyer, *Handbook of PI and PID controller tuning rules*: Imperial College Pr, 2009.
- [60] F. Gunnarsson, F. Gustafsson, and J. Blom, "Pole placement design of power control algorithms," 1999, pp. 2149-2153 vol. 3.

## VITAE

NAME : MIR SADAT ALI

DATER OF BIRTH : 23<sup>rd</sup> NOVEMBER, 1984

NATIONALITY : INDIAN



PRESENT ADDRESS : PRINCE SULTAN BIN ABDULAZIZ ROAD, RAKAH,  
AL-KHOBAR-DAMMAM HIGHWAY, P.O. BOX: 3594,  
AL-KHOBAR 31952, K.SA.

PERMANENT ADDRESS : H.NO: 8-1-351/12, RAHUL COLONY NEAR GALAXY  
THEATRE, TOLICHOWKI, HYDERABAD, A.P,  
INDIA.

EMAIL ID : [mr.sadat@yahoo.com](mailto:mr.sadat@yahoo.com) / [mir.sadatali@gmail.com](mailto:mir.sadatali@gmail.com)

CONTACT NUMBER : (LANDLINE-INDIA) - +91-040-23564741

(MOBILE-INDIA) - +91-9908786966

(MOBILE-SAUDI ARABIA) - +966-561638157